الجمهورية الجزائرية الديمقراطية الشعبية

People's **D**emocratic **R**epublic of **A**lgeria

وزارة التعليم العالي و البحث العلمي

Ministry of **H**igher **E**ducation and **S**cientific **R**esearch

جامعة الشهيد الشيخ العربي التبسي_تبسة

Echahid **C**heikh **L**arbi **T**ebessi **U**niversity_**T**ebessa

كليه العلوم والتكنولوجيا

Faculty of **S**ciences and **T**echnology

قسم الهندسة الكهربائية

Electrical **E**ngineering **D**epartment

DOCTORAL THESIS

With a view to obtaining the LMD 3rd cycle doctoral degree

Option : Automatic

Speciality: Automatic and systems

LABGET Laboratory

Presented by: Brahim AYEB

Theme

Advanced Control Of a Renewable Energy System

Publicly supported on: 08/01/2025 before the jury composed of:

Jury members	Grade	Designation	University
Pr. Salah CHENIKHER	Professor	Chairman	Echahid Cheikh Larbi Tebessi University- Tebessa
Pr. Youcef SOUFI	Professor	Supervisor	Echahid Cheikh Larbi Tebessi University- Tebessa
Dr. Djamel OUNNAS	MCA	Co-Supervisor	Echahid Cheikh Larbi Tebessi University- Tebessa
Pr. Abderrazak LACHOURI	Professor	Member	University of 20th August 1955 Skikda
Pr. Aziz BOUKADOUM	Professor	Member	Echahid Cheikh Larbi Tebessi University- Tebessa
Dr. Abdelhamid DJARI	MCA	Member	Echahid Cheikh Larbi Tebessi University- Tebessa
Dr. Dhaouadi GUIZA	MCA	Invited	Echahid Cheikh Larbi Tebessi University- Tebessa

Academic Year 2024-2025

TABLE OF CONTENT

TABLE OF CONTENT I
ACKNOLEDGEMENT VI
DEDICATION VII
ABSTRACT VIII
RESUME IX
الملخص X
TABLE OF FIGURES XI
LISTE OF TABLES XVI
SYMBOLS XVII
ABREVIATIONS XVIII
GENERAL INTRODUCTION 1

CHAPTER I: OVERVIEW OF PV GENERATOR

I.1. Introduction 7
I.2. Solar energy 7
I.3. PV system 8
I.3.1. PV generator 9
I.3.1.1. PV effect 9
I.3.1.2. Solar radiation 9
I.3.2. PV cell 10
I.3.2.1. Single/ Mono-crystalline silicon solar cell 10
I.3.2.2. Polycrystalline silicon solar cell 11
I.3.2.3. Amorphous Silicon Thin Film (a-Si) Solar Cell 11
I.3.2.4. Cadmium Telluride (CdTe) Thin Film Solar Cell 12
I.3.2.5. Copper Indium Gallium Di –Selenide (CIGS) solar cells 12
I.3.2.6. Nano crystal based solar cells 13
I.3.2.7. Polymer based solar cells 13
I.3.2.8. Dye sensitized solar cells (DSCC) 14
I.3.2.9. Concentrated solar cells 15

I.3.3. PV cell electrical modeling 15
I.3.3.1. Ideal model 16
I.3.3.2. PV cell modeling with ohmic losses 17
I.3.4. PV module 19
I.3.4.1. Mathematical modeling of PV module 21
I.3.4.2. Effect of solar radiation and temperature 21
I.3.5. PV panel 21
I.3.5.1. Effect of series connection 24
I.3.5.2. Effect of parallel connection 25
I.4. PSC effect 25
I.5. Fault effect 25
I.5.1. Line-to-line/ground fault (LLF⁄LLG) 26
I.5.2. Mismatch fault (MF) 27
I.6. Stand alone system 27
I.7. Grid connected 28
I.8. Conclusion 29

CHAPTER II: POWER ELECTRONICS DESIGN

II.1. Introduction 31
II.2. DC/DC converter 31
II.2.1. Boost converter 32
II.2.1.1. Inductor 32
II.2.1.2. Output Capacitor 33
II.2.1.3. Diode 33
II.2.1.4. Switching transistor 33
II.2.1.5. Control circuitry 33
II.2.1.6. Mathematical modeling of boost converter at “Sw” closes 35
II.2.1.7. Mathematical modeling of boost converter at “Sw” opens 36
II.2.2. Buck converter 38
II.2.1.1. Mathematical modeling of buck converter at “Sw” closes 39
II.2.1.2. Mathematical modeling of buck converter at “Sw” opens 40

II.2.3. Buck-boost converter 43
II.2.3.1. Mathematical modeling of buck-boost converter at “Sw” closes 43
II.2.3.2. Mathematical modeling of buck-boost converter at “Sw” opens 44
II.3. PV system connectivity to grid 46
II.3.1. PV inverter 47
II.3.1.1. Inverter control 48
II.3.1.2. Phase locking loop (PLL) 48
II.3.2. Filter topologies 51
II.3.2.1. L filter 51
II.3.2.2. LC filter 51
II.3.2.3. LCL filter 52
II.4. Conclusion 53

CHAPTER III: INTELLIGENT CONTROLS OF A PV SYSTEM

III.1. Introduction 55
III.2. Perturb and observation (P&O) 56
III.3. Incremental Conductance (IC) 58
III.4. Fuzzy logic controller (FLC) 58
III.4.1. Fuzzification 59
III.4.2. Inference 60
III.4.3. Defuzzification 61
III.4.4. MPPT based FLC 61
III.5. Artificial neural network (ANN) 61
III.6. Adaptive neural fuzzy inference system (ANFIS) 63
III.7. Result and discussion 65
III.7.1. Simulation with stand-alone PV system 65
III.7.2. Simulation with PV system connectivity to grid 74
III.8. Conclusion 82

CHAPTER IV: METAHEURISTIC ALGORITHMS BASED MPPT OF A PV SYSTEM UNDER PSC AND MALFUNCTION CONDITIONS

IV.1. Introduction 84
IV.2. Diagnosis method 84
IV.2.1. Collection of data 85
IV.2.2. Feature selection 85
IV.2.2. Locate of fault 87
IV.3. Metaheuristic method based MPPT 87
IV.3.1. Grey wolf optimization (GWO) 88
IV.3.1.1. Encircling 88
IV.3.1.2. Haunting 89
IV.3.1.3. Attacking 90
IV.3.2. Particle swarm optimization (PSO) 91
IV.3.3. Adaptive particle swarm optimization (APSO) 93
IV.3.3.1. Adaptive inertia weight 94
IV.3.3.2. Adaptive acceleration coefficients 94
IV.4. Simulation results of studied metaheuristic method 95
IV.4.1. Simulation under different fault system 95
IV.4.1.1. Without faults 96
IV.4.1.2. Shade fault (SF) 96
IV.4.1.3. Open circuit fault (OCF) 97
IV.4.1.4. Line to line fault (LLF) 98
IV.4.1.5. Line to ground fault (LGF) 99
IV.4.2. Simulation under PSC 100
IV.4.2.1. Normal condition 101
IV.4.2.2. Partial shading condition 1 (PSC1) 102
IV.4.2.3. Partial shading condition 2 (PSC2) 103
IV.4.2.4. Completely shading condition (CSC) 104
IV.4. Conclusion 106
GENERAL CONCLUSION AND PERSPECTIVE 107
REFERENCES 111

ACKNOLEDGEMENT

My sincere gratitude goes to Allah for providing me with the unwavering support, courage, perseverance, determination and fortitude I needed to see this project through to its successful conclusion. I almost failed to achieve my goals because of all the difficulties I faced while working on this project. But with God's help and grace, I was able to overcome these obstacles and move forward with optimism and perseverance.

I want to express my heartfelt thanks to my supervisor, Pr. Youcef SOUFI for the invaluable support provided throughout this work. I also wish to express my heartfelt appreciation to the President of the jury, Pr. Salah CHENIKHER and each member of the esteemed jury, Pr. Abderrazak LACHOURI, Pr. Aziz BOUKADOUM, Dr. Abdelhamid DJARI, Dr. Dhouadi GUIZA for generously investing their time in engaging discussions about our thesis, and finally, I deeply appreciate the steadfast support from all contributors to this project.

DEDICATION

With profound gratitude and sincere appreciation, I am honored to dedicate this humble work to all my family, my colleagues and friends.

Brahim AYEB

ABSTRACT

This thesis investigates advanced control strategies for photovoltaic (PV) systems to address challenges arising from climate variations and operational conditions in both stand-alone and grid-connected configurations. The research is divided into four main chapters: an overview of PV generators, power electronics design, intelligent control techniques, and metaheuristic algorithms for maximum power point tracking (MPPT) under partial shading conditions (PSC). The study begins by analyzing the behavior of PV generators and their integration with DC/DC converters. Intelligent control methods, including Perturb and Observe (P&O) and Adaptive Neuro-Fuzzy Inference System (ANFIS), are employed to enhance MPPT efficiency under varying irradiance levels, with ANFIS demonstrating superior performance. Hybrid approaches combining Fuzzy Logic Control (FLC) and Artificial Neural Networks (ANN) are compared against Incremental Conductance (IC) methods for grid-connected systems, highlighting the hybrid controller's ability to track maximum power dynamically without prior PV system information. For fault diagnosis, a neural network (NN) model achieves high accuracy in detecting PV faults. Lastly, metaheuristic MPPT controllers—Grey Wolf Optimization (GWO), PSO, and Adaptive PSO (APSO)—are evaluated under PSC. The APSO algorithm excels in achieving fast and efficient MPPT. Simulations conducted using MATLAB/Simulink validate the effectiveness of the proposed methods, showcasing their potential for real-world applications in renewable energy systems.

Keywords: PV system, MPPT, partial shading condition , P&O algorithm, IC algorithm, FLC, ANN, ANFIS, APSO, GWO.

RESUME

Cette thèse examine les stratégies de contrôle avancées pour les systèmes photovoltaïques (PV) afin de relever les défis liés aux variations climatiques et aux conditions opérationnelles, en configurations autonomes et connectées au réseau. Les recherches sont divisées en quatre chapitres principaux : une vue d'ensemble des générateurs PV, la conception de l'électronique de puissance, les techniques de contrôle intelligent et les algorithmes métaheuristiques pour le suivi du point de puissance maximale (MPPT) sous conditions de partielle ombre (PSC). L'étude débute par l'analyse du comportement des générateurs PV et leur intégration avec des convertisseurs DC/DC. Des méthodes de contrôle intelligent, notamment Perturb and Observe (P&O) et Adaptive Neuro-Fuzzy Inference System (ANFIS), sont appliquées pour améliorer l'efficacité du MPPT sous des niveaux d'irradiance variables, ANFIS montrant une performance supérieure. Des approches hybrides combinant le contrôle logique flou (FLC) et les réseaux neuronaux artificiels (ANN) sont comparées aux méthodes de conductance incrémentale (IC) pour les systèmes connectés au réseau, mettant en évidence la capacité du contrôleur hybride à suivre dynamiquement la puissance maximale sans informations préalables sur le système PV. Pour le diagnostic des pannes, un modèle basé sur les réseaux neuronaux (NN) atteint une précision élevée. Enfin, des contrôleurs MPPT métaheuristiques—Optimisation par Loup Gris (GWO), PSO et APSO—sont évalués sous PSC. L'algorithme APSO se distingue par sa rapidité et son efficacité. Les simulations effectuées avec MATLAB/Simulink valident l'efficacité des méthodes proposées, démontrant leur potentiel pour des applications concrètes dans les systèmes d'énergie renouvelable.

Mots-clés : Système PV, MPPT, condition d'ombrage partiel, perturbation et observation, conductance incrémentale, contrôleur à logique floue, réseau neuronal artificiel, système d'inférence floue neuronal adaptatif, optimisation adaptative des essaims de particules, optimisation du loup gris.

الملخص

تتناول هذه الأطروحة استراتيجيات التحكم المتقدمة لأنظمة الطاقة الكهروضوئية (PV) لمعالجة التحديات الناجمة عن التغيرات المناخية وظروف التشغيل، سواء في الوضع المستقل أو المتصل بالشبكة. تنقسم الدراسة إلى أربعة فصول رئيسية: نظرة عامة على المولدات الكهروضوئية، تصميم إلكترونيات الطاقة، تقنيات التحكم الذكية، والخوارزميات الميتاheuristic لتتبع نقطة الطاقة القصوى (MPPT) تحت ظروف التظليل الجزئي (PSC). تبدأ الدراسة بتحليل سلوك المولدات الكهروضوئية ودمجها مع المحولات DC/DC. يتم استخدام تقنيات التحكم الذكية، بما في ذلك خوارزمية التذبذب والمراقبة (P&O) ونظام الاستدلال العصبي الضبابي التكيفي (ANFIS)، لتحسين كفاءة MPPT تحت مستويات إشعاعية متغيرة، حيث تظهر تقنية ANFIS أداءً متفوقًا. يتم مقارنة منهجيات هجينة تجمع بين التحكم المنطقي الضبابي (FLC) والشبكات العصبية الاصطناعية (ANN) مع طريقة الموصلية المتزايدة (IC) لأنظمة PV المتصلة بالشبكة، مما يبرز قدرة المتحكم الهجين على تتبع الطاقة القصوى ديناميكيًا دون الحاجة إلى معلومات مسبقة عن النظام PV. في تشخيص الأعطال، يحقق نموذج الشبكة العصبية (NN) دقة عالية. أخيرًا، يتم تقييم خوارزميات MPPT الميتاheuristic—تحسين الذئب الرمادي ((GWO، PSO وAPSO—تحت PSC. يبرز خوارزمية APSO بسرعة وكفاءة عالية. تؤكد المحاكاة التي أجريت باستخدام MATLAB/Simulink فعالية الطرق المقترحة وإمكاناتها للتطبيقات العملية في أنظمة الطاقة المتجددة.

الكلمات المفتاحية: النظام الكهروضوئي، MPPT، حالة التظليل الجزئي، الاضطراب والملاحظة، التوصيل المتزايد، التحكم المنطقي المضبب، الشبكة العصبية الاصطناعية، نظام الاستدلال العصبي المضبب التكيفي، تحسين سرب الجسيمات التكيفي، تحسين الذئب الرمادي.

TABLE OF FIGURES

Figure I.1: Spectral distribution of radiation 8
Figure I.2: Radiation ways 9
Figure I.3: PV cell structure 10
Figure I.4: Mono crystalline silicon solar cell 11
Figure I.5: Polycrystalline solar cell 12
Figure I.6: Amorphous silicon solar cell. 13
Figure I.7: CdTe solar cell 14
Figure I.8: CIGS cells 15
Figure I.9: Polymer solar cell 16
Figure I.10: Ideal model of PV cell 17
Figure I.11: Single diode model 17
Figure I.12: PV module 19
Figure I.13: Solar cell array with parallel and series connected 20
Figure I.14: Radiation effect 20
Figure I.15: Temperature effect 22
Figure I.16: Series connected of PV panel 23
Figure I.17: Parallel connection of PV panel 23
Figure I.18 : Hybrid series and parallel connection of PV panel 24
Figure I.19: Series connection effect 24
Figure I.20: Parallel connection effect. 25
Figure I.21: PSC on PV panel 26
Figure I.22: PSC effect in PV array 26
Figure I.23: PV panel fault locate 27
Figure I.24: Stand alone PV system 28
Figure I.25 : PV system connectivity to grid 28
Figure II.1: DC/DC converter 31
Figure II.2: Boost converter 32
Figure II.3: Input and output voltages and currents in dc and Ts for a Boost 34
Figure II.4: Boost converter “Sw” closes 34

Figure II.5: Boost converter “Sw” opens 36
Figure II.6: Buck converter. 39
Figure II.7: Buck converter voltages and currents 41
Figure II.8: Buck converter “SW” closes 41
Figure II.9: Buck converter “Sw” opens 42
Figure II.10: Buck-boost converter 43
Figure II.11: Tensions and currents of buck-boost converter 44
Figure II.12: Buck-boost converter “Sw” closes 45
Figure II.13: Buck-boost converter “Sw” opens 46
Figure II.14: Grid components 47
Figure II.15: PV inverter topologies 48
Figure II.16: Control block diagram for centralized inverter using DQ current control 49
Figure II.17: Structure of Basic PLL structure 50
Figure II.18 : Stationary and rotating references frames 51
Figure II.19: LC filter 52
Figure II.20: LCL filter. 53
Figure III.1: P&O algorithm 56
Figure III.2: IC approach 57
Figure III.3: FLC generality 59
Figure III.4: Membership function 60
Figure III.5: ANN architecture 62
Figure III.6: ANN-MPPT. 64
Figure III.7: ANFIS-MPPT 65
Figure III.8: Stand-alone PV system with MATLAB/Simulink 67
Figure III.9: PV voltage in stand-alone system with fixed radiation 67
Figure III.10: PV power in stand-alone system with fixed radiation 68
Figure III.11: PV power in stand-alone system with fixed radiation 68
Figure III.12: Output voltage in stand-alone system with fixed radiation 69
Figure III.13: Output current in stand-alone system with fixed radiation 69
Figure III.14: Output power in stand-alone system with fixed radiation 70
Figure III.15: Solar irradiance profile in stand-alone system 70

Figure III.16: PV voltage in stand-alone system with variable radiation. 71
Figure III.17: PV current in stand-alone system with variable radiation..... 71
Figure III.18 : PV power in stand-alone system with variable radiation 72
Figure III.19: Output voltage in stand-alone system with variable radiation 72
Figure III.20: Output current in stand-alone system with variable radiation..... 73
Figure III.21: Output power in stand-alone system with variable radiation 73
Figure III.22: Grid connected PV system employing MATLAB/Simulink..... 75
Figure III.23: PV power in PV system connectivity to grid at fixed radiation 75
Figure III.24: Output boost voltage at fixed radiation 76
Figure III.25 : Grid voltage at fixed radiation..... 76
Figure III.26: Grid current at fixed radiation 77
Figure III.27: Active power at fixed radiation 77
Figure III.28 : Reactive power at fixed radiation..... 78
Figure III.29: Solar radiation profile in grid connected PV system..... 78
Figure III.30: PV power in PV system connectivity to grid at variable radiation 79
Figure III.31 : Output boost voltage at variable radiation..... 79
Figure III.32: Grid voltage at variable radiation 80
Figure III.33: Grid current at variable radiation..... 80
Figure III.34: Active power at fixed radiation 81
Figure III.35: Reactive power at fixed radiation..... 81
Figure IV.1: Different faults occurring in PV System..... 84
Figure IV.2: Proposed diagnosis method of PV system..... 85
Figure IV.3: NN performance 87
Figure IV.4: Confusion maatrix..... 88
Figure IV.5 : Grey wolf's hierarchy (dominance increasing from down 89
Figure IV.6: Position updating in GWO..... 90
Figure IV.7: Particle motion while optimization..... 92
Figure IV.8: PSO flowchart..... 93
Figure IV.9: Output power without faults 96
Figure IV.10: Output power under SF..... 97
Figure IV.11: Output power under OCF..... 98

Figure IV.12: Output power under LLF 99
Figure IV.13: Output power under LGF 100
Figure IV.14: State of PV system (a) NC, (b) PSC1, (c) PSC2, (d) CSC 101
Figure IV.15: Output power under NC 102
Figure IV.16: Output power under PSC1 103
Figure IV.17: Output power under PSC2 104
Figure IV.18: Output power under CSC 105

LISTE OF TABLES

Table III.1: Fuzzy rule base 58
Table III.2: Components of considered stand-alone PV system 66
Table. III.3: PV system connectivity to grid parameters..... 74
Table IV.1: Characteristics of PV cell and boost converter 95
Table IV.2: Efficiency of different MPPT studied 105

SYMBOLS

h: Planck constant

c: Propagation speed

ג: Light wavelength

n: Ideality factor

K: Boltzmann constant

T: Ambient temperature

q: Electron's charge

$\tilde{y}_{\mathbf{Vo}}$: Output current ripple

$\tilde{y}_{\mathbf{Vmp}}$: Input voltage ripple

$\boldsymbol{w}$**:** Inertia weight

(C_1, C_2): Cognitive and social constants

$(r_1, r_2) \in [0\ 1]$: Random numbers

ABREVIATIONS

IEA:	International Energy Agency
PV:	Photovoltaic
MPPT:	Maximum power point tracking
PCA:	principle component analysis
SCF:	Short current fault
PSC:	Partial shading condition
CSC:	Completely shading condition
PLL:	Phase locking loop
HC:	Hill climbing
IC:	Incremental conductance
P&O:	Perturb and observe
FLC:	Fuzzy logic controller
ANN:	Artificial neural network
ANFIS:	Adaptive neural fuzzy inference system
GWO:	Grey wolf optimization
PSO:	Particle swarm optimization
APSO:	Adaptive particle swarm optimization
HANN-FLC:	Hybrid artificial neural network -fuzzy logic controller
AI:	Artificial intelligence
BNNs:	Biological neural networks
DC:	Direct current

BP:	Back propagation
MLP:	Multi layer perceptron
MSE:	Mean square error
dc:	Duty cycle
OCF:	Open circuit fault
SF:	Shade fault
NC:	Normal condition
LLF:	Line to line fault
LGF:	Line to ground fault
CSF:	Converter switch fault
ZER:	Zero
PBIG:	Positive big
NBIG:	Negative big
PSHO:	Positive short
NSHO:	Negative short

GENERAL INTRODUCTION

GENERAL INTRODUCTION

Various institutions and industrial facilities rely on diverse energy sources to meet their growing power demands [1]. Non-renewable energy sources such as oil, petroleum, gas, and uranium dominate energy markets [2]. However, several challenges arise with these sources, including limited availability, high costs driven by global demand, and uncertainties linked to geopolitical and technical factors [3-5]. Additionally, the extraction and use of fossil fuels release significant quantities of greenhouse gases, contributing to environmental degradation, affecting plant and animal ecosystems, and increasing respiratory diseases among humans, particularly those near industrial zones [6][7].

The shift from traditional energy sources to renewable energy is driven by rising costs, environmental concerns, and the need for sustainable solutions. Renewable energy, being environmentally friendly and diverse, offers alternatives like solar, wind, and biomass energy [8][9]. Regions with warm climates and abundant sunlight benefit significantly from solar energy, which is highly efficient, reliable, and requires minimal maintenance [10][11].

The solar energy is an important renewable energy when the principle of utilizing this energy type is the convert of received light from the sun into electrical energy using photovoltaic (PV) cells by a conversion phenomenon called the PV effect [12]. A group of cells connected in series forms an array and this provides more energy [13]. The values of PV cell effect of generate the maximum power, this parameters also effect of power in the load of PV system [14]. The PV array can be connected to an electrical grid, or isolated from the grid and connected to a direct current load [15].

PV arrays often experience voltage mismatches with connected loads, necessitating DC-DC converters to regulate voltage and current levels. Climatic factors such as temperature and shading significantly impact PV cell efficiency, requiring advanced converter designs [16-19]. Boost converters, built primarily with passive components, are among the most commonly used [20].

The normal condition (NC) can't give the advantages and disadvantages of various controls where all methods select optimal duty cycle (dc) without problems. In other hand, the partial shading condition (PSC) is the right test for evaluate any approach based on MPPT when the MPP divide into local and global values. The PSC affect to generate the needed peak power by the decreasing of its value [21]. In addition, there are many electrical faults that interfere with the performance of the PV system and lead to decreased power supply, as well as to decreased system integrity [22].

The first part of this work focuses on the maximum power point tracking (MPPT) of a PV system in stand-alone and connected to grid.

This thesis emphasizes MPPT techniques for standalone and grid-connected PV systems. Raiker et al. (2021) introduced a P&O controller combined with current regulation [23]. Gupta et al. (2021) compared incremental conductance (IC) methods, validated through hardware tests, highlighting their effectiveness in fast MPP tracking [24]. Yilmaz et al. (2018) implemented an FLC-based system combined with a PI controller for battery charge management [25]. Bisht and Sikander (2022) proposed a novel FLC technique coupled with beta algorithms [26]. Ahmed and Nasserdine (2019) developed a hybrid ANN and sliding mode control method for grid-connected systems [27]. Brahim et al. (2022) integrated ANN-FLC methods to optimize PV voltage and

duty cycles [29]. Numerous studies, including Aldair et al. (2016), demonstrated the efficacy of ANFIS-based controllers, which outperform traditional approaches under varying irradiance conditions [30].

The obtained results were shown in [25-30] proved the effectiveness of intelligent controllers for choice the required dc of PV system in grid-connected and stand-alone system under fast variation in irradiance compared to traditional approaches which have big oscillations and bad performances. In our thesis, the ANFIS controller is proposed to follow the MPP under various irradiance degrees and a combined ANN-FLC with the connectivity to electrical grid.

In the second work part, three approaches based on metaheuristic algorithms are applied to choice dc under PSC and abnormal conditions. D. S. Pillai et al. (2019) described the most fault whuich faces the PV system under PSC [31]. The fault diagnosis is divided into three main steps: select data, feature selection, and classification stage. Z. Chen et al. (2018) suggested a method based on random forest for select data and feature selection stages [32]. F. Harrou et al. (2019) gave a monitoring schemes based on k-NN algorithm to classify if PV system in normal or malfunction conditions [33]. Numerous MPPT approaches of PV system under PSC have been described in detail in literature [34-36]. H. Chaieb and A. Sakly proposed a new MPPT based on PSO controller, this obtained results of PSO method justified the effect of PSO based MPPT in atmospheric variations [37]. N. Priyadarshi et al. (2019) suggested the effectiveness of their used method, where the resolution of PSO problem resolved by ANFIS controller, and the error of ANFIS rectified by PSO method [38]. T. Imtiazet al. (2020) replaced the standard PSO technique by a precious approach fast called fast improved PSO (FIPSO) [39]. S. Mohanty et al. (2016) utilized a MPPT algorithm based on GWO, this algorithm can track the MPP under PSC quickly compared to IPSO technique [40]. Where the PSO controller has the problems in results because

the bad choice of PSO parameters, A. M. Eltamaly et al. (2020) proposed a MPPT based on APSO algorithm of PV system in different irradiation level [41].

The basic objective of this part is the prove the benefits of utilizing evolutionary approaches for select optimal dc to follow MPP under PSC generally and APSO especially.

This present thesis consists of four chapters which are systematically coordinated and organized. In the starting chapter, different components of PV generator will describe. Various PV cells types will present in detail, the mathematical model of PV cell and module and theirs basic elements will depict in this chapter. The PSC and fault effects in PV system will also well describe. Second chapter studies in first point the modeling important DC/DC transformers, the DC/DC boost components will show in detail. Secondly will represent the overview of grid, the role of phase locked loop (PLL) and filter will study.

Third chapter focuses on comparative study between P&O and ANFIS controllers in stand-alone system, and the effectiveness of combined ANN-FLC approach compared to IC controller. In the first part of the end chapter, the fault diagnosis of PV system will applied by three step, the data collect will evaluate by statistical parameters, and the principle component analysis (PCA) reduces the dimension size, the studied fault types will detect by NN type back-propagation (BP), and the PSO controller compared to previous algorithms uses to follow MPP in many fault scenario. The evolutionary technique based on GWO, PSO, and APSO approaches based MPPT utilize for PSC, this work will finish by a general conclusion and some perspectives.

CHAPTER I

OVERVIEW ON PV GENERATOR

I.1. Introduction

There appears to be no longer any room for debate about the critical nature of electricity and water just like basic human necessities. As our technology progresses, so does our demand for power, and the issue becomes ever greater in remote areas where traditional options can be prohibitively expensive [42][43].

We all know that most of the energy we use today comes from burning fossil fuels like coal, oil, or nuclear power. Recent studies and predictions have warned us that massive resource extraction will surely deplete these reserves. Plus, everyone is convinced that this process poses a danger to the environment. Therefore, it has been necessary to seek out renewable energy sources, such as solar power, to replace this. As an added bonus, this energy source is not only free and unstoppable, but also very clean for the planet [44-46].

Solar photovoltaic (PV) is a renewable energy source that might one day replace fossil fuels. Accordingly, academics are thinking about it in the context of satisfying potential energy demands in the future. There has been significant progress in both the reliability and price of PV module production processes recently [47].

Partial shading and electrical faults are defined as the consequences that reduce a system's capabilities and isn't able to reversed by regular operation. In this case, too, the PV systems are involved [48]. In the context of PV module's assurance, any malfunction that happens while the module is normally operating is considered a PV module malfunction. It is believed that instability in the efficiency of certain modules is mostly caused by manufacturing flaws [49].

After reviewing the basics of solar generator theory in present chapter, we dive into the modeling process of PV array characteristics. Additionally, we investigate instances of partial shadowing and problems impacting solar energy generation.

I.2. Solar energy

Considering that the sun and our planet are about 150 million kilometers apart and that light travels at a speed of around 300,000 km/s, it takes approximately eight minutes for the sun's beams to reach Earth [50][51].

When we face the sun directly, value of the solar constant that reaches the outermost regions of atmosphere is often close to 1360W/m2 [52].

The photon energy can be calculated as:

$$E = \frac{h*c}{\lambda} \quad (I.1)$$

With:

$h = 6{,}62.10 - 34\ j.s^{-1}$: Planck constant;

$c = 3.108\ m.s^{-1}$: Propagation speed.

λ: Light wavelength (m).

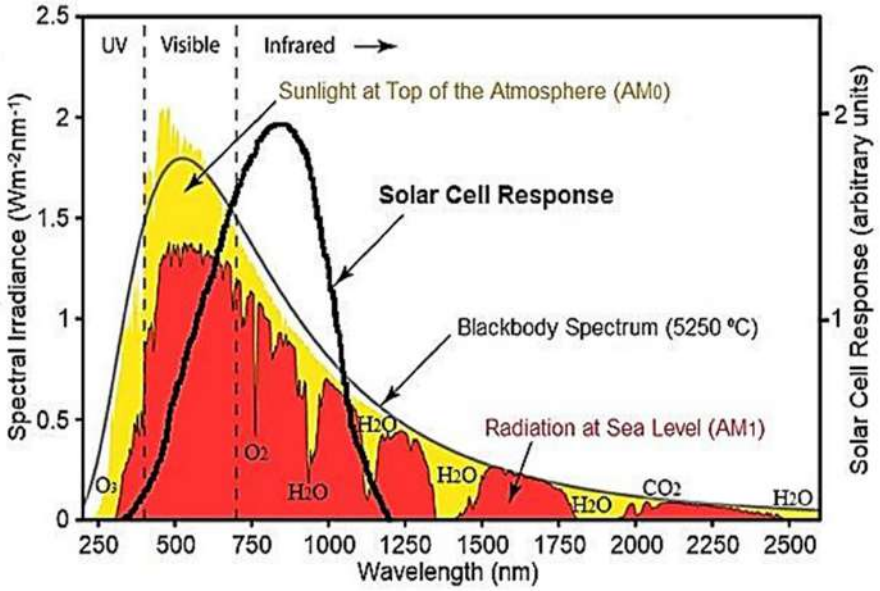


Figure I.1 Spectral distribution of radiation [54].

I.3. PV system

The PV system is the technology that converts the sun power into electricity, the PV system consists of PV panel, boost converter, and control block, this technology using for supplying a DC load or connected to electrical grid.

I.3.1. PV generator

The PV generator is a gadget that utilized in subject to turn solar energy into electrical power. This device is made up of a specific number of modules that are connected in parallel or series, depending on the global power needed [53].

I.3.1.1. PV effect

In a process called the PV effect, PV cells convert the energy from the sun directly into electricity. To build PV modules, a collection of cells must be connected to generate sufficient electricity [53].

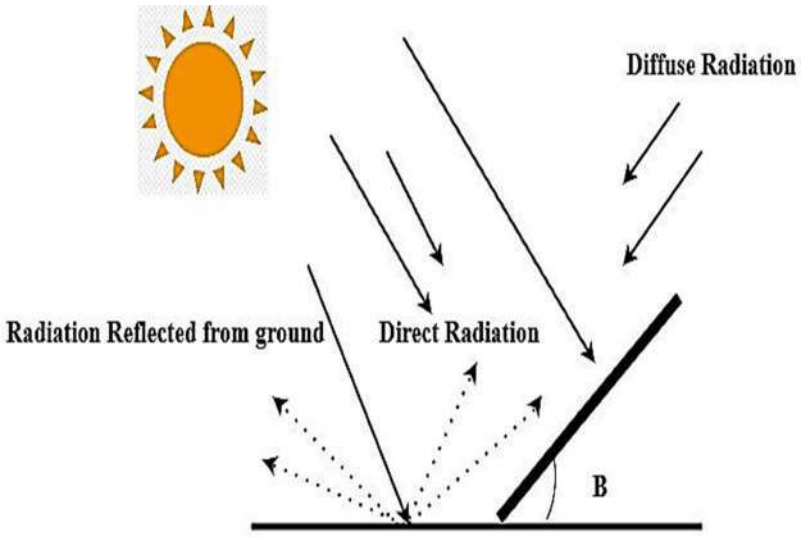


Figure I.2 Radiation ways [56].

I.3.1.2. Solar radiation

The sun generates energy in the form of electromagnetic waves, with 30% of it reflected into space and 47% absorbed. In contrast, 23% of it is retained as an energy source used for the atmospheric evaporation cycle (see Figure I.1) [54] [55].

Radiation from the sun extends across all regions of the electromagnetic spectrum. The most active part, going from the near ultraviolet to the infrared, comes mainly from the photosphere. Ignoring extreme ultraviolet radiation, this radiation can be expressed as a black element rose to

the characteristic temperature of the photosphere, estimated at 5780 Kelvin. Because most of the solar radiation is absorbed as it passes through the atmosphere, not all of it reaches the Earth's surface [56]. The Earth's surface receives radiation from three sides: directly from the sun, scattered from the atmosphere, and reflected from the Earth's interior (Figure I.2) [57][58].

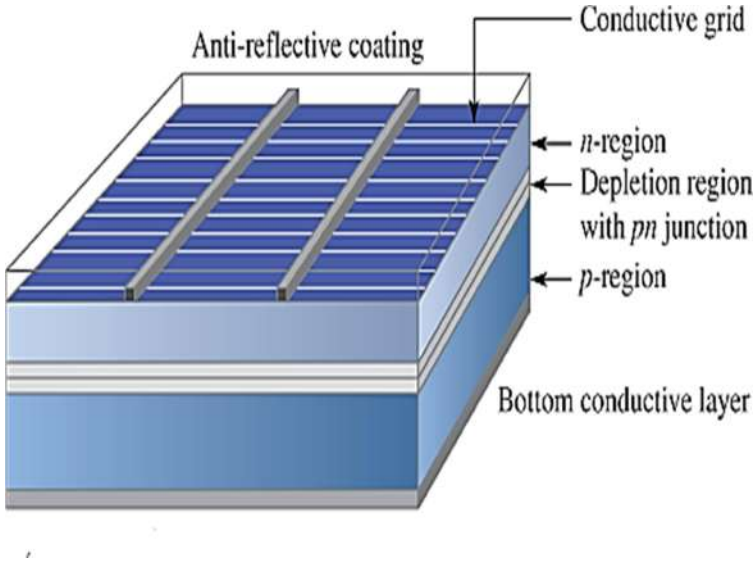


Figure I.3 PV cell structure [61].

I.3.2. PV cell

A PN junction, which is represented in Figure I.3, is the basis of the classic solar cell. Phosphorus diffusion at the surface of a p-type doped silicon substrate causes the PN junction, which in turn produces an n-type doped area, which is essential for the fabrication of solar cells. This junction is important for the right migration of surplus electrons to the P substrate and excess holes to the N area, with positive and negative ions suitably staying on each side of the junction [59][60]. This forms an electric field over the junction, which serves as a barrier to the charges dispersing until equilibrium is established. As a consequence, the charge carriers are kept in the location where they are most prevalent [61]. It exists various types of PV cell:

I.3.2.1. Single/ Mono-crystalline silicon solar cell

Mono crystalline solar cells are manufactured utilizing the Czochralski process. The Czochralski process involves cutting massive ingots of silicon into individual crystals. The

procedure of "recrystallizing" is more expensive as it needs careful processing during manufacture of the enormous single crystal. However, there are a number of issues that constrain the efficiency of solar cells manufactured of mono crystalline silicon. Depending on the wavelength and the kind of semiconductor used, the maximum efficiency of solar cells made of silicon may reach around 23%, while other semiconducting materials can reach up to 30%. The Figure I.4 shows the schema of mono crystalline silicon solar cell [62] [63].

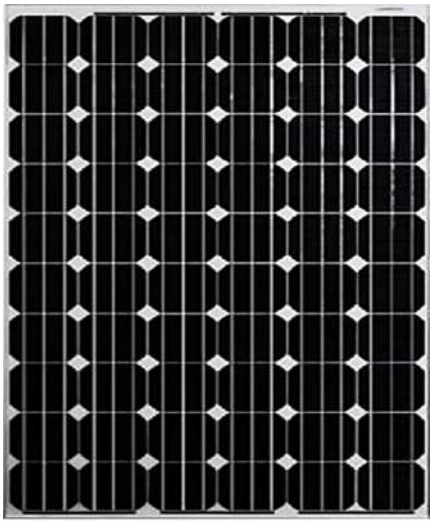


Figure I.4 Mono crystalline silicon solar cell [62].

I.3.2.2. Polycrystalline silicon solar cell

Since the manufacturing cost is cheaper, this is starting to seem more appealing than mono crystalline. Despite its improved aesthetics, it is less efficient and consumes less energy overall. Produced with reduced energy expenditure and no need for an ideal crystal structure (see Figure I.5) [64].

I.3.2.3. Amorphous Silicon Thin Film (a-Si) Solar Cell

These cells may be made at low processing temperatures and hence employ low-cost polymers and other flexible substrates. During the production process, the rear of the substrate is coated with dipped silicon. These solar cell shapes feature dark brown tones on the reflection side and silver hues on the conductivity side. Unsustainable efficiency is a key shortcoming of these cells. Figure I.6 depicts the schematic of an amorphous silicon solar cell [65].



Figure I.5 Polycrystalline solar cell [64].

I.3.2.4. Cadmium Telluride (CdTe) Thin Film Solar Cell

From an economic point of view, cadmium telluride (CdTe) is one of the most essential varieties of thin-film solar cells, affordable and commercially feasible. Ap-n junction diode is created between the layers of cadmium sulfide. The manufacturing processes sectors follow: At first, CdTe-based solar cells are produced from polycrystalline materials and glass is used as the substrate. Secondly, the deposited layer is employed inseveral cheap methods, where the various layers of the CdTe solar cells are coated on the substrate. Its efficacy is normally between 9.5 and 11%. However, owing to the dangerous nature of cadmium in human body, animals, and plants, it produces many environmental concerns. Further recycling and disposal of dangerous CDs also has a detrimental influence on our ecology (Figure I.7) [66] [67].

I.3.2.5. Copper Indium Gallium Di –Selenide (CIGS) solar cells

A kind of thin-film PV cell technology, copper-indium-gallium di-selenide (CIGS) solar cells has garnered significant attention due to its ability to provide cost-effective and very efficient solar energy conversion. Two electrodes and a thin layer of semiconductor material composed of copper, indium, and gallium dieseline make up the conventional structure of CIGS solar cells. As depicted in Figure I.8, the composition of the thin film may be optimized to

improve cell performance by adjusting the ratios of copper, indium, gallium, and selenium. Commercial modules use CIGS solar cells, which are similar to crystalline silicon cells, and attain an efficiency of around 20%, whereas laboratory efficiency approaches 23% [68-70].

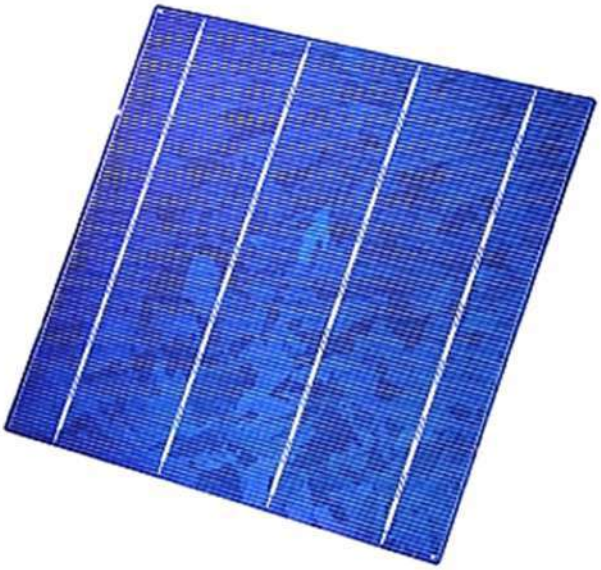


Figure I.6 Amorphous silicon solar cell [65].

I.3.2.6. Nano crystal based solar cells

Next generation PV technology may find hope in Nano crystal based solar cells, often called quantum dot solar cells, due to their many unique benefits. One significant feature is their variable band gap, which enables for effective absorption of a wide variety of wavelengths throughout the solar spectrum [71]. One way to maximize the effectiveness of light absorption and energy conversion is to regulate the size of semiconductor Nano crystals. This allows one to customize the band gap to fit certain areas of the solar spectrum [72].

I.3.2.7. Polymer based solar cells

Solar cells composed of polymers provide numerous benefits and might be a feasible approach for generating energy in the long term. Their intrinsic pliability enables for the construction of lightweight, pliable, and even see-through solar panels, which is a big benefit. Integrating solar energy into curved surfaces, wearable electronics, and portable power devices

are just a few examples of the numerous possible uses for this adaptable energy source. It is feasible to modify device performance by changing the tunable characteristics of organic semiconducting polymers, which in turn increases light absorption, charge transport, and stability. Considering all the criteria, solar cells built of polymers appear to be an effective, low-cost, and eco-friendly alternative for creating renewable energy. Plus, there are continuing trials to make them even better (Figure I.9) [73].

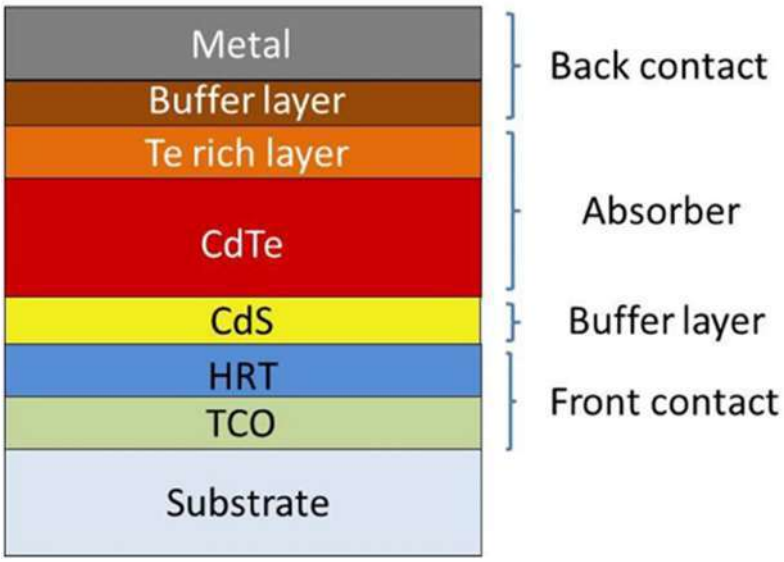


Figure I.7 CdTe solar cell [66].

I.3.2.8. Dye sensitized solar cells (DSCC)

Dye-sensitized solar cells (DSSCs) are considered cost-effective and versatile, collecting sunlight using thin film designs with transparent conductive substrates and coated with thin titanium dioxide nanoparticles (TiO2). The core of their function is a photosensitive dye, usually ruthenium-based or organic, which absorbs photons and triggers the production of pairs of electron holes. Excited electrons are ultimately forced into the TiO2 conductor and holes remain in the dye. External circuits promote electron transmission and generate current. DSSC features characteristics such as low light performance and transparency, enabling them to be used for several applications, including internal settings and building integration. Challenges such as efficiency improvement and stability improvements are abundant, which lead to continued

research to create breakthrough materials and device designs to make the DSSCs commercially viable at scale [74].

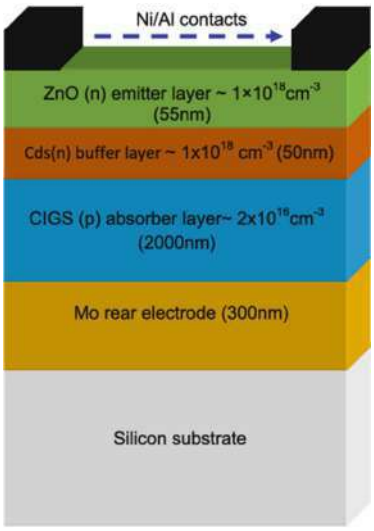


Figure I.8 CIGS cells [68].

I.3.2.9. Concentrated solar cells

The concentrated solar cells (CSCs) use optical devices that concentrate sunlight in compact areas of high-efficiency solar materials and improve the energy output per unit. This method is usually used to concentrate light in narrow regions of receivers such as lenses and mirrors, and high-efficiency solar cells successfully convert the focus light into electricity. Compared to conventional PV systems, CSCs have important efficiency and material costs advantages, making them particularly suitable for large-scale solar power plants and limited-space applications, but problems such as thermal management, optical efficiency and cost-effectiveness remain a research and development area. Efficiency research on concentrator technology and material research on the performance of high-efficiency solar cells on concentrator systems contribute to strengthening technology, ensuring greater use and improved sustainability [75].

I.3.3. PV cell electrical modeling

Several mathematical modeling of PV cell include ideal, with one and two diodes, the current work focuses on PV cell with one diode.

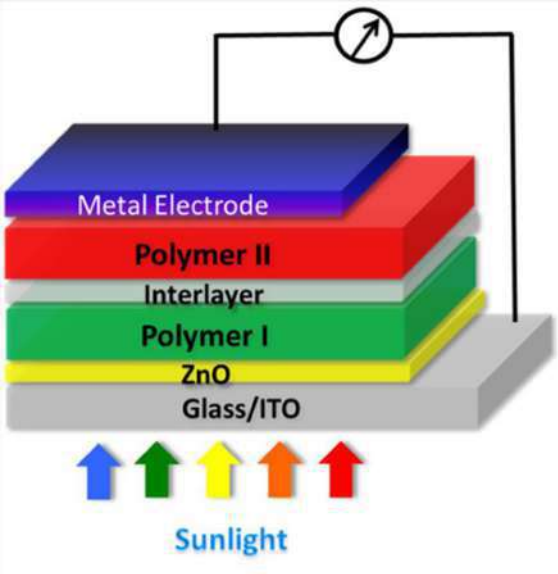


Figure I.9 Polymer solar cell [73].

I.3.3.1. Ideal model

The electronic circuit of P V cell is shown in Figure I.10, the output current of the PV cell is given by [76]:

$$I = I_{ph} - I_d \qquad (I.2)$$

Where

$$I_d = I_s \left[e^{\frac{(V+I*R_S)}{n*N_S*V_S}} - 1 \right] \qquad (I.3)$$

By replacing the equations I.3 in I.2 we find:

$$I = I_{ph} - I_s \left[e^{\frac{(V+I*R_S)}{n*N_S*V}} - 1 \right] \qquad (I.4)$$

With

I_d: Diode current;

I: PV current;

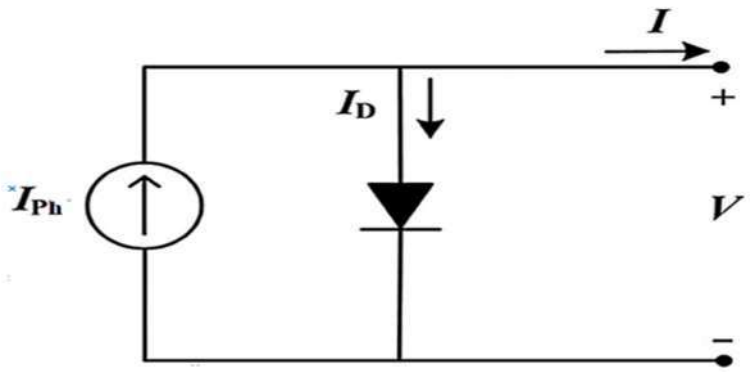


Figure I.10 Ideal model of PV cell [76].

V: PV voltage;

n: Ideality factor;

F: Boltzman constant;

T_a: Ambiant temperature;

q: Electron's charge.

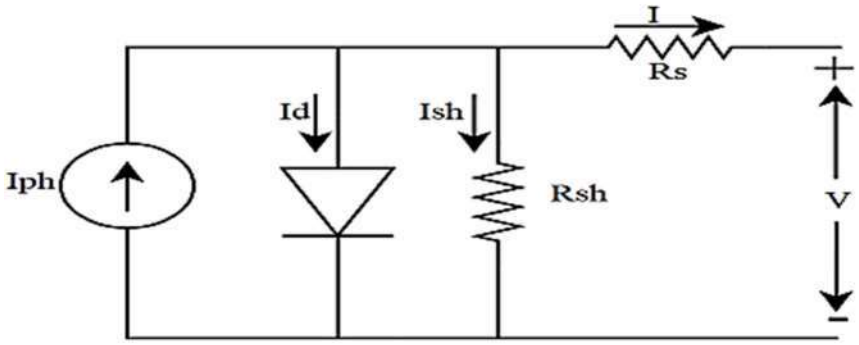


Figure I.11 Single diode model [77].

I.3.3.2. PV cell modeling with ohmic losses

The PV cell is the basic component in PV system, for study the characteristics and performances of PV cell is obligatory its electronic circuit mathematically. For that, several

mathematical models of PV cell have been proposed. The PV cell with ohmic losses is utilized in current work with a single diode is shown in Figure I.11.

The output current of the PV cell is given by [77]:

$$I = I_{ph} - I_s\left[e^{\frac{(V+I*R_S)}{n*N_S*V_S}} - 1\right] - \frac{(V+IR_S)}{R_{sh}} \quad (I.5)$$

With:

$$V_s = \frac{F*T_a}{q} \quad (I.6)$$

$$I_s = I_{sn} * \left(\frac{T_a}{25}\right)^3 * e^{\left[\frac{(qE_g)}{n*F}\left(\frac{1}{25}-\frac{1}{T_a}\right)\right]} \quad (I.7)$$

$$I_{sn} = \frac{I_{sc}}{e^{\frac{V_{oc}}{n*V_S*N_S}} - 1} \quad (I.8)$$

And the photocurrent (I_{ph}) is calculated by equation I.9

$$I_{ph} = \frac{G}{G_{rsc}}\left(I_{sc} + K_l(T_a - T_{rsc})\right) \quad (I.9)$$

I_{sc}: Short circuit current;

R_s: Series resistor;

R_{sh}: Shunt resistor;

T_{rsc}: Standard temperature;

G : Solar radiation;

G_{rsc} : Standard solar radiation;

K_l: Open circuit voltage temperature coefficients;

E_g: Band gap energy.

When measuring cells under controlled circumstances, it's can be defined a filling factor (FF) by:

$$FF = \frac{V_{max} * I_{max}}{V_{oc} * I_{sc}}$$

Where V_{max}, I_{max} are the maximum values of PV cell voltage and current respectively.

I.3.4. PV module

The very low voltage and current produced by PV cells, together with their fragile thinness, make them impractical for use in most electrical applications when used alone (Figure I.12). Can be defined the PV module as the series and parallels communication of many cells [78] [79].

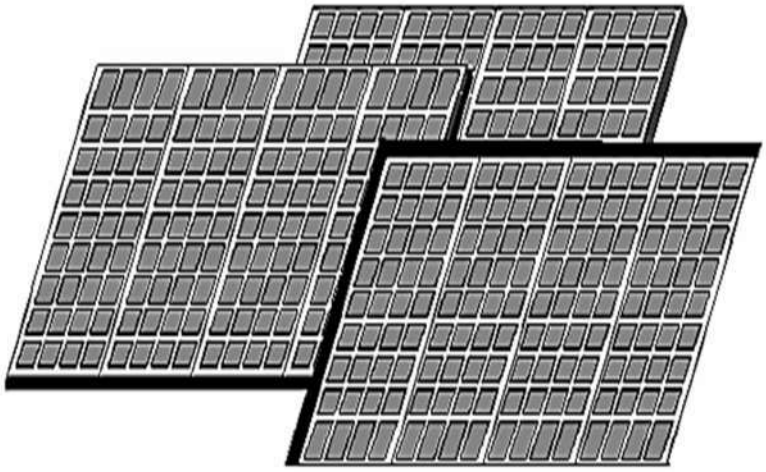


Figure I.12 PV module [78].

Since most electrical appliances have conventional operating voltages (12, 24, 48 V, etc.), it is not possible to directly power them with only one PV cell. Manufacturers construct PV modules by connecting PV cells in parallel as well as series, which increases the power output and available electricity (see Figure I.13) [80].

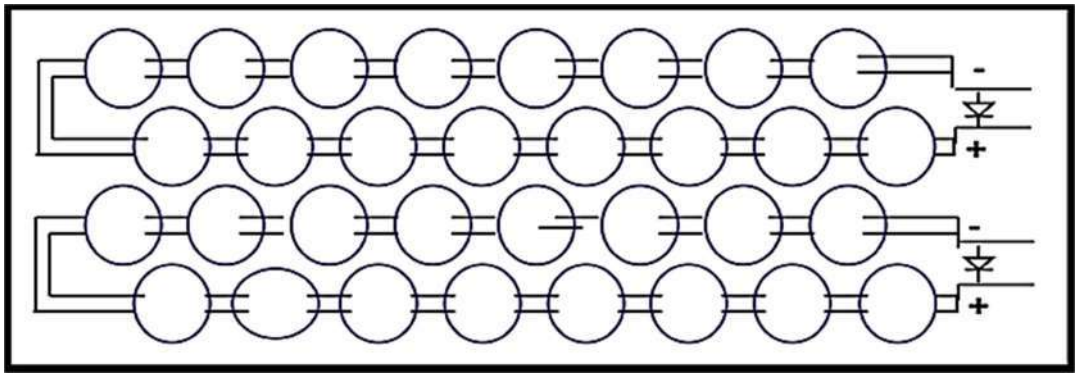


Figure I.13 Solar cell array with parallel and series connected [80].

The electrical tension is raised to the required level by connecting the PV cells in series, and connecting them in parallel regularly to ensure the solidity of the cells and protect them from external dangers [80]

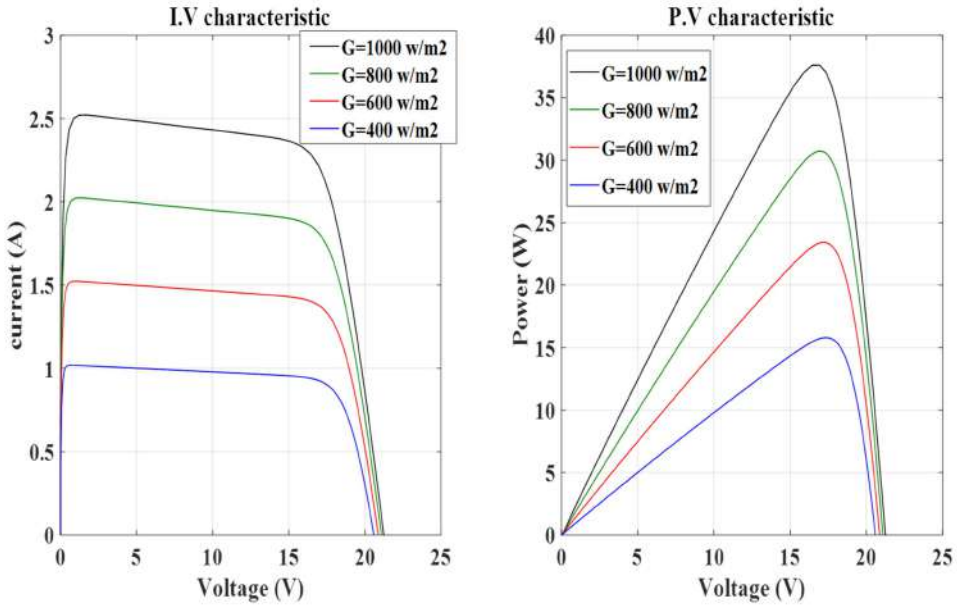


Figure I.14 Radiation effect.

The output power of PV generator is given by:

$$P_{PVG} = V * I \qquad (I.10)$$

$$P_{PVG} = N_{ser} * V * N_{par} * I \quad (I.11)$$

I.3.4.1. Mathematical modeling of PV module

The output of PV module can be calculated as fellow [79] [81]:

$$I_{pv} = N_{par} * I_{ph} - N_{p*} I_0 \left[e^{\frac{\left(V + I * R_s * N_{ser}/N_{par}\right)}{n * V_S * N_S}} - 1 \right] - \frac{\left(V + I * R_s * N_{ser}/N_{par}\right)}{R_{sh} * N_{ser}/N_{par}} \quad (I.12)$$

Where:

N_{par}: Number of parallel string.

N_{ser}: Number of cells connected in series.

I.3.4.2. Effect of solar radiation and temperature

Figure I.14 shows the curves of current-voltage and power-tension changes at standard temperature (25° C) and a study of the effect of solar radiation. The current I_{sc} is directly proportional to the increase in radiation, and thus the maximum power value increases [82]. On the other hand, as shown in Figure I.15, when the radiation value is fixed at $1000\ W/m^2$, as the temperature increases, the open circuit voltage (V_{oc}) decreases with a slight increase in the current I_{sc}. The temperature is inversely proportional to the maximum power value [83].

I.3.5. PV panel

The PV panel can be linked in parallel or series, in series link (Figure I.16) as shown in equations I.11 and I.12 the voltage is increased contrary to the current that stays fixed [84] [85].

$$V_{PV} = V_{PV1} + V_{PV2} + V_{PV3} + \cdots + V_{PVN} = \sum_{1}^{N} V_{PVN} \quad (I.13)$$

$$I_{PV} = I_{PV1} = I_{PV2} = I_{PV3} = \cdots = I_{PVN} \quad (I.14)$$

$$P_{PV} = V_{PV} * I_{PV} = (V_{PV1} + V_{PV2} + V_{PV3} + \cdots + V_{PVN}) * I_{PV} \quad (I.15)$$

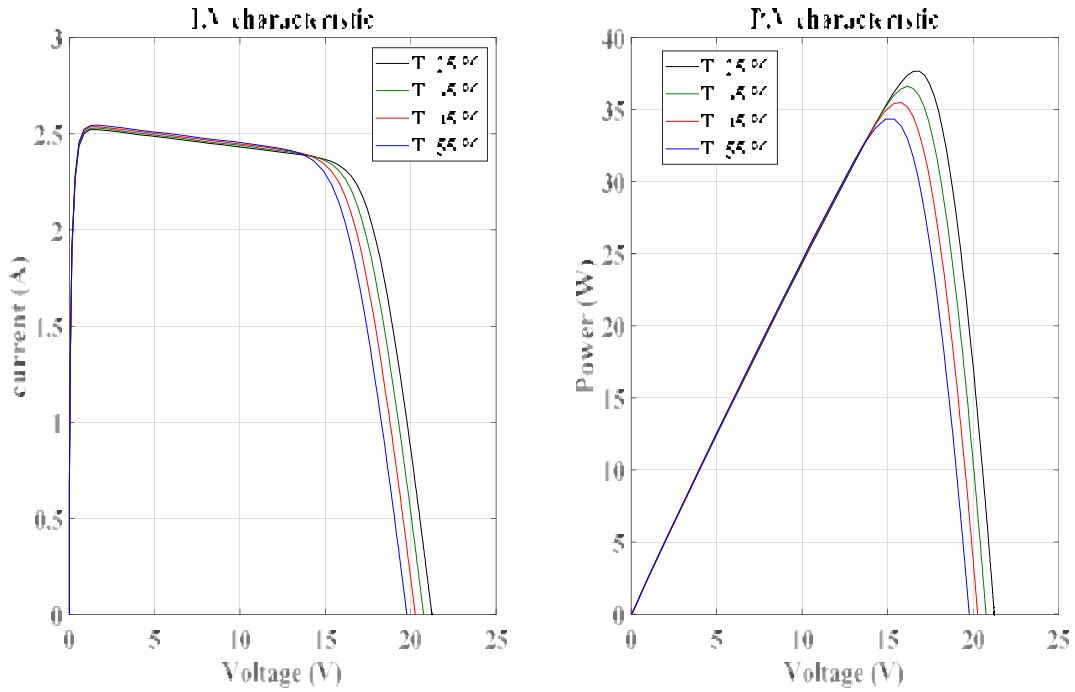


Figure I.15 Temperature effect.

In parallel link (Figure I.17) as shown in equations I.16 and I.17 the voltage is fixed contrary to the current that increases [86].

$$V_{PV} = V_{PV1} = V_{PV2} = V_{PV3} = \cdots = V_{PVN} \quad (I.16)$$

$$I_{PV} = I_{PV1} + I_{PV2} + I_{PV3} + \cdots + I_{PVM} = \sum_{1}^{M} I_{PVM} \quad (I.17)$$

$$P_{PV} = V_{PV} * I_{PV} = V_{PV} * (I_{PV1} + I_{PV2} + I_{PV3} + \cdots + I_{PVM}) \quad (I.18)$$

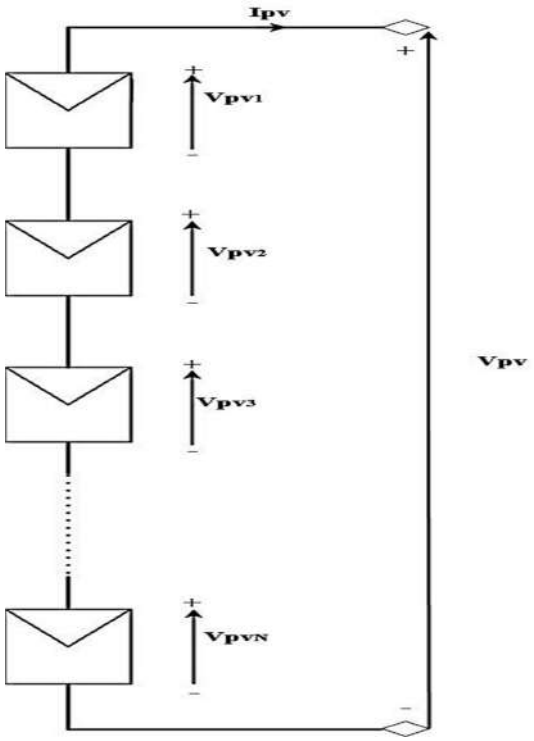


Figure I.16 Series connected of PV panel [84].

The PV panel can be linked in parallel and series, in N series and M parallel link (see Figure I.18), the voltage and current which are calculated in equations I.13 and I.17 and are increased. So, the PV power is given in equation I.19 [86].

$$P_{PV} = V_{PV} * I_{PV} = \sum_{1}^{N} V_{PVN} * \sum_{1}^{M} I_{PVM} \qquad (I.19)$$

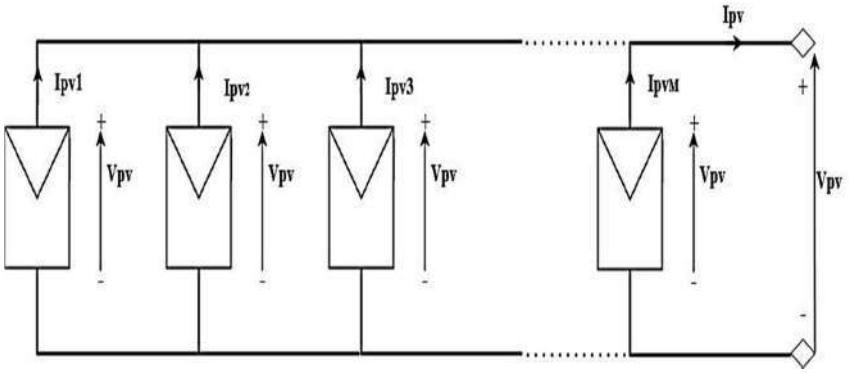


Figure I.17 Parallel connection of PV panel [86].

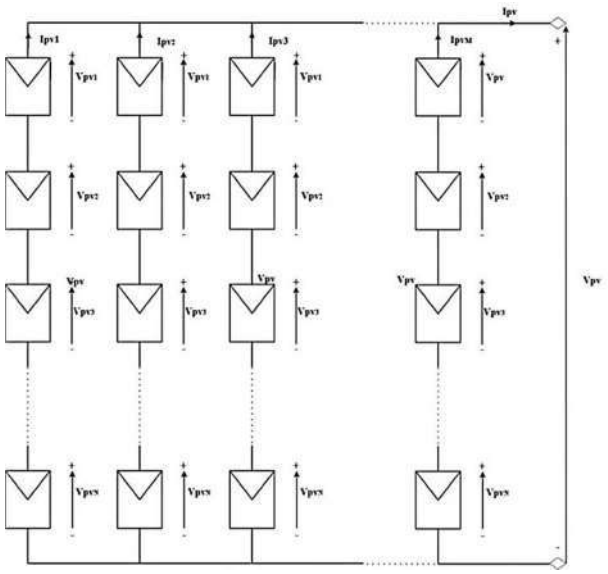


Figure I.18 Hybrid series and parallel connection of PV panel [86].

I.3.5.1. Effect of series connection

The number of N_{ser} is increased when a larger voltage difference is needed. The current remains constant at different values of N_{ser}. This increase affects the amplification of the power generated by PV array (Figure I.19) [86] [53].

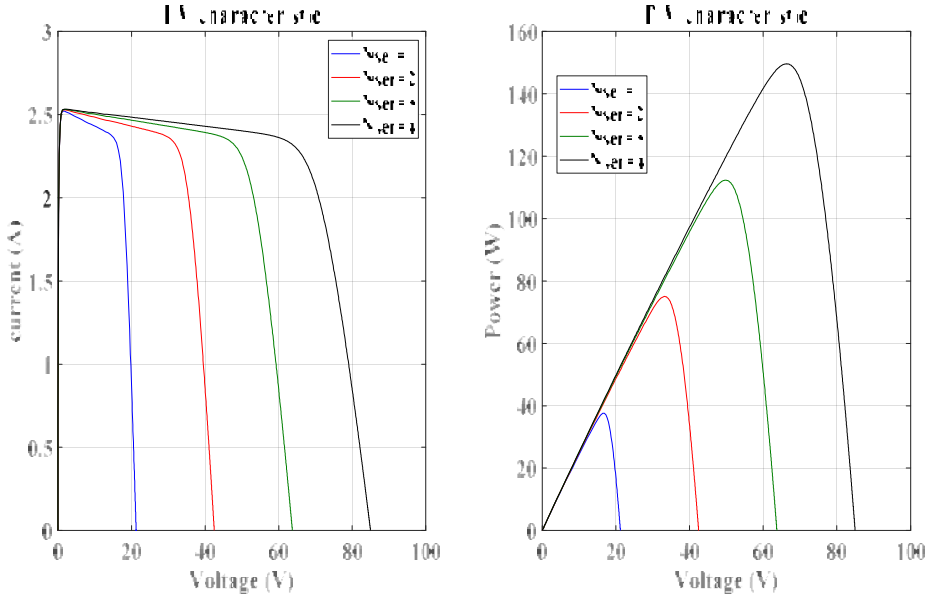


Figure I.19 Series connection effect.

I.3.5.2. Effect of parallel connection

As shown in Figure I.20, the I doubles with an increase in N_{par}, which is automatically increases the power by returning to Equation I.18[53].

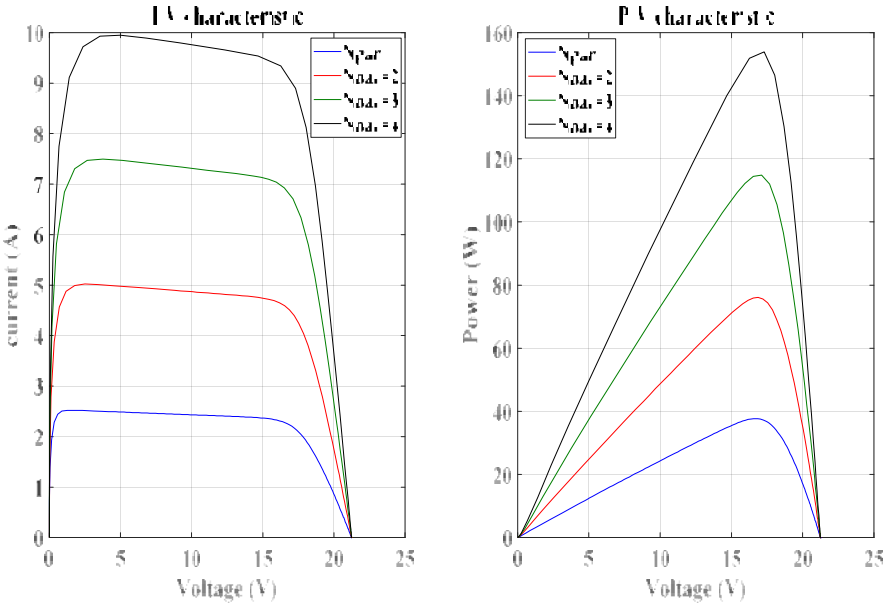


Figure I.20 Parallel connection effect.

I.4. Partial shading condition (PSC) effect

Having constant illumination of PV panels all time isn't always practical due to factors like weather changes, cloud cover, shadows cast by buildings or arbors, and the fact that the trajectory of sun changes daily, as shown in Figure I.21. Shadow is one of main causes of power loss in PV systems. To prevent loss due to inversion bias on partly shaded cells, a regular PV module will include bypass semiconductors (Figure I.22) [87-90].

I.5. Fault effect

As shown in Figure I.23 PV systems are exposed to many errors that reduce their efficiency and productive capacity, the most important of which are electrical faults. Some common types of PV system faults are defined in next points [91-93].



Figure I.21 PSC on PV panel [87].

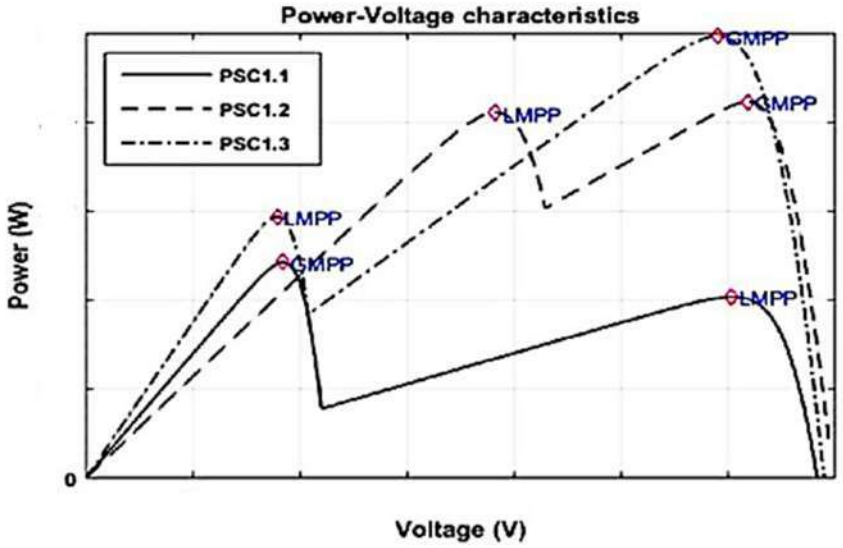


Figure I.22 PSC effect in PV array [88].

I.5.1. Line-to-line/ground fault (LLF/LLG)

The unintentional linking of two distinct areas in PV arrays is known as a LLF and LLG. The most common causes of line-line faults in real-world scenarios are damage to cable isolation, improper maintenance procedures, or damage around PV modules [94].

I.5.2. Mismatch fault (MF)

The MF presents other faults scenario like a shade fault (SF), and open circuit fault (OCF), the OCF can be defined as the disconnection between two or more PV arrays. Arc fault, shading, type and seniority of panels are classified as SF [95] [96].

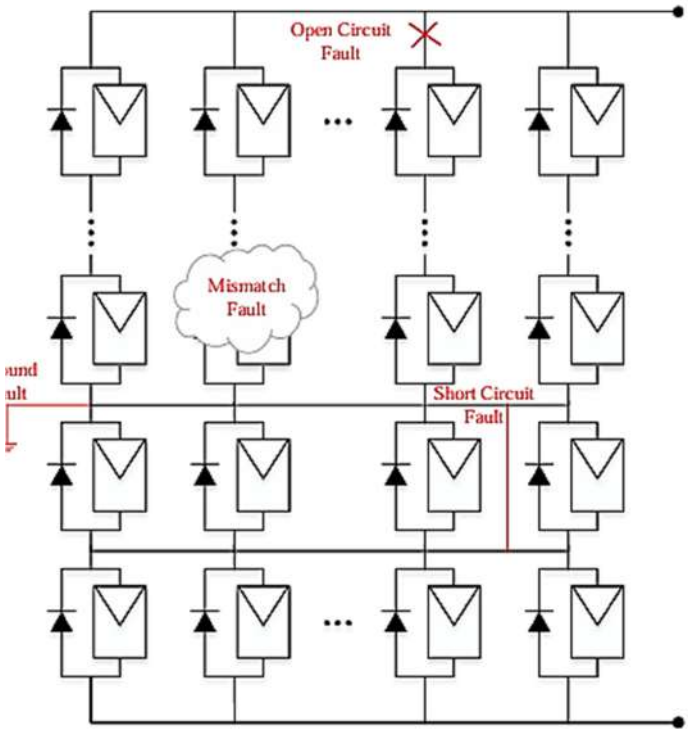


Figure I.23 PV panel fault locate [91].

I.6. Stand alone system

Independent of the electricity grid, independent PV systems are usually built to scale and meet specific DC and/or AC electricity needs. Independent PV systems may be as simple as connecting the DC load to the DC output of a PV module using a direct coupling mechanism [53].

A PV system's key advantages are its extended lifespan, continuous power delivery to the load while operating, and the minimal maintenance cost over the system's lifetime (see Figure I.24) [53].

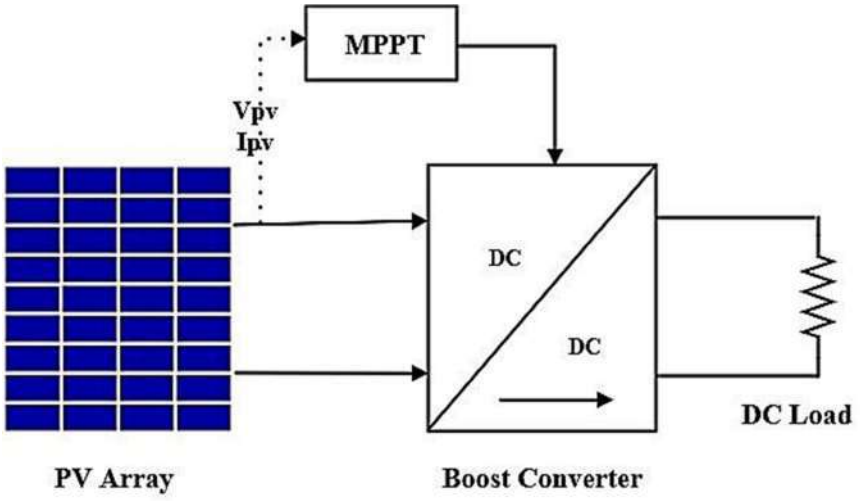


Figure I.24 Stand alone PV system [53].

I.7. Grid connected

Installed on both business and residential structures, utility-interactive PV power systems have the potential to become a significant contributor to the nation's electrical generation. By connecting to the grid, PV systems may produce large amounts of high-quality electricity close to the point of consumption, cutting out transmission and distribution losses. These networks function in conjunction with the existing electrical infrastructure to facilitate the transfer of electricity into and out of the grid (Figure I.25) [97][98].

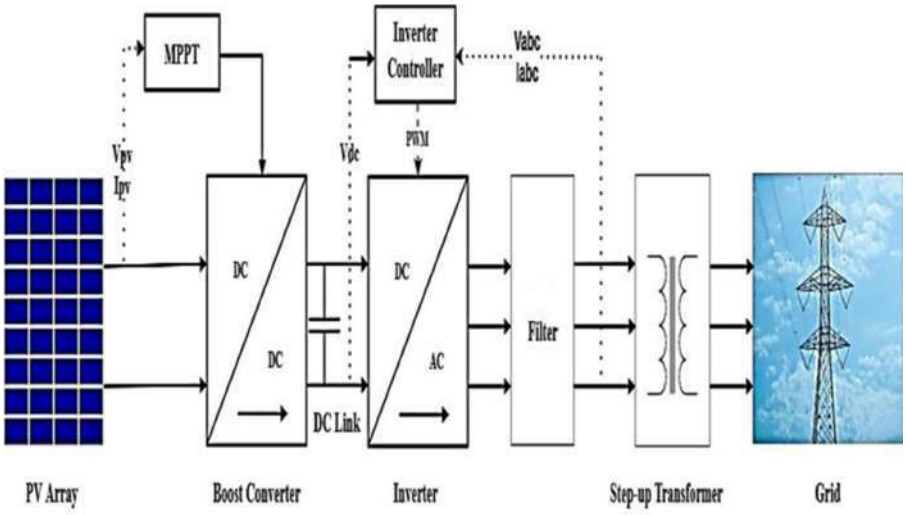


Figure I.25 PV system connectivity to grid [97].

I.8. Conclusion

In conclusion, the different PV cell types have been studied and described, the PV cell and varying in radiation and ambient temperature have shown and proved, the mathematical modeling of PV array has been done with the influence of connection series and parallels. The needed power has decreased and affected a causing of changing climatic and malfunctions in the PV panel when it may be augmented using several controls.

[

CHAPTER II

POWER ELECTRONICS DESIGN

II.1. Introduction

The previous chapter focused on the study of PV generator influence, where the power that supplies from PV array is related with solar radiation and temperature. Usually, the voltage and current of DC load aren't disproportionate with PV voltage and current [99]. The boost converter can augment the first voltage with height efficiency and security a causing o its compact design [100] [101]. Secondly, for assure the no loss in power is necessary to adding a grid, the grid consists needs a inverter control has the Phase locking loop (PLL) for regulated of frequency and in order to eliminate the harmonics from grid voltage it's necessary to added a LCL filter [102] [103]. For that, this chapter focuses on study many DC/DC converters and grid components.

II.2. DC/DC converter

The DC/DC converter is a device that converts direct voltage (DC) from one level to another (Figure II.1). DC/DC converters play an important role in controlling solar power generation, and these converters are needed to convert solar panel DC voltages into sufficient voltages to supply local load or the injection into the electricity network, the DC/DC converters is divided into boost, buck and buck-boost converters [99].

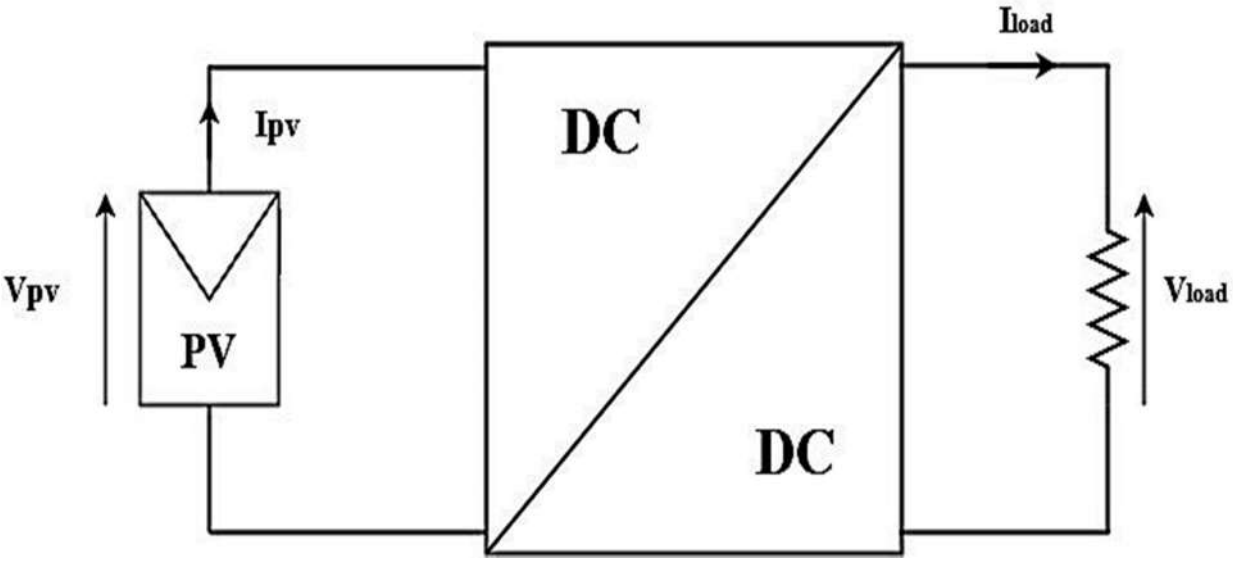


Figure II.1 DC/DC converter [99].

II.2.1. Boost converter

Usually, the electrical grid or DC load needs a voltage higher than the output values of PV array. For that, it's necessary to add a DC/DC boost converter in the object to maximize the value of voltage from the PV array into the load. The boost converter provides higher power output, improves overall system performance, and ensures optimal utilization of solar energy resources. It also facilitates flexible handling of different types of loads, increasing PV systems' reliability. As shown in Figure II.2 this converter consists of an inductor, two capacitors, diode, switching transistor, and control circuitry [104-106].

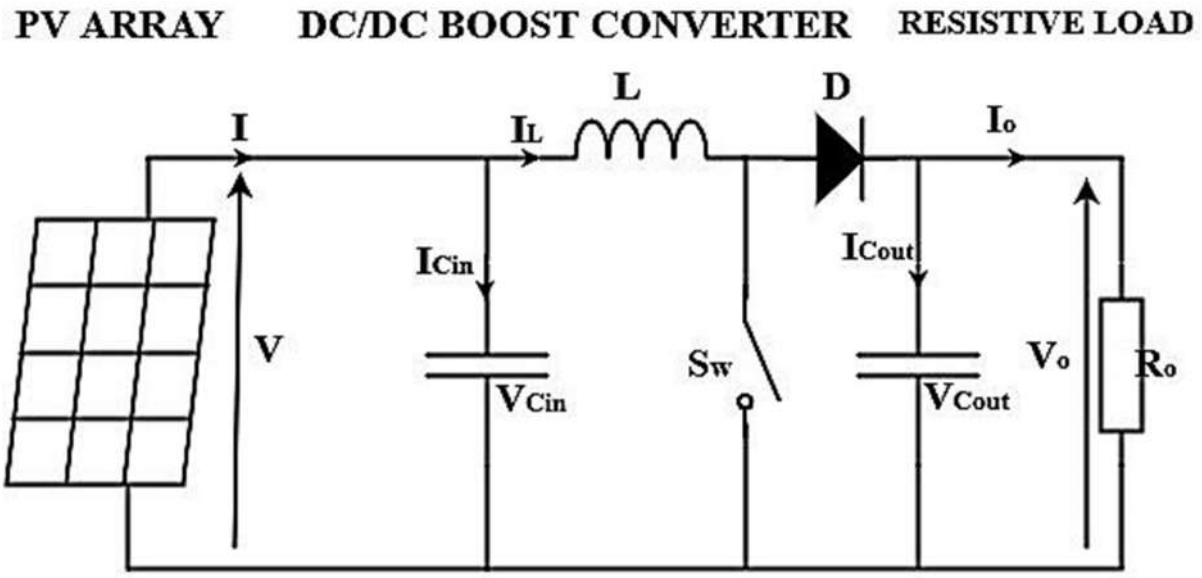


Figure II.2 Boost converter [107].

II.2.1.1. Inductor

Although inductors are often linked to alternating current (AC) circuits, they really serve an essential function in direct DC/DC boost converters. A boost converter uses an inductor to store energy while the switching transistor is ON and release it when it is OFF. In a DC/DC boost converter, energy is stored in the magnetic field when the inductor current increases while the switching transistor is active. On the other hand, when turned off, the inductor current keeps flowing to generate a voltage across its polarity-reversed terminals, which raises the voltage at the output. Furthermore, inductance impacts the boost converter's efficiency. The larger its value,

the lower the peak currents and the lower the switching losses, without forgetting its help in regulating the output voltage and facilitating the ripple of the current flowing through the output capacitor, provided that its value is chosen well [53].

II.2.1.2. Output Capacitor

The output capacitor is a main component in the boost chopper, which plays a principal role in smoothing the output voltage by filtering out any change during the switching between ON-OFF, and the regulate the output voltage by reducing the ripple in voltage [53].

II.2.1.3. Diode

When the transistor is OFF, the diode provides a path for current flow. If the transistor is disconnected, the current of the inductor continues to circulate through the circuit, thus preventing the reverse voltage through the transistor [53].

II.2.1.4. Switching transistor

Essential for adjusting the duty cycle, raising voltage, and switching power, the switching transistor is a key component of a DC/DC boost converter. In its "on" state, energy is stored when current flows from the input source to the inductor; in its "off" state, the output voltage is increased by releasing the stored energy. You may control the transistor's output voltage by fine-tuning the duty cycle, which is the ratio of on-time to total switching length. The efficiency of the converter may be influenced by the attributes and selection of the transistor, which in turn impact switching losses and conduction losses. The switching transistor is a crucial part of the boost converter since it regulates the voltage in conjunction with the control circuitry [53].

II.2.1.5. Control circuitry

The control circuit can be considered to be the brain of the boost converter, as it is considered the fundamental element in controlling the circuits of transistors to achieve the necessary output voltage level, and to adapt the appropriate value of the transistor duty cycle through the implementing control algorithms (the various control algorithms will be discussed in this third chapter of the thesis) [53].

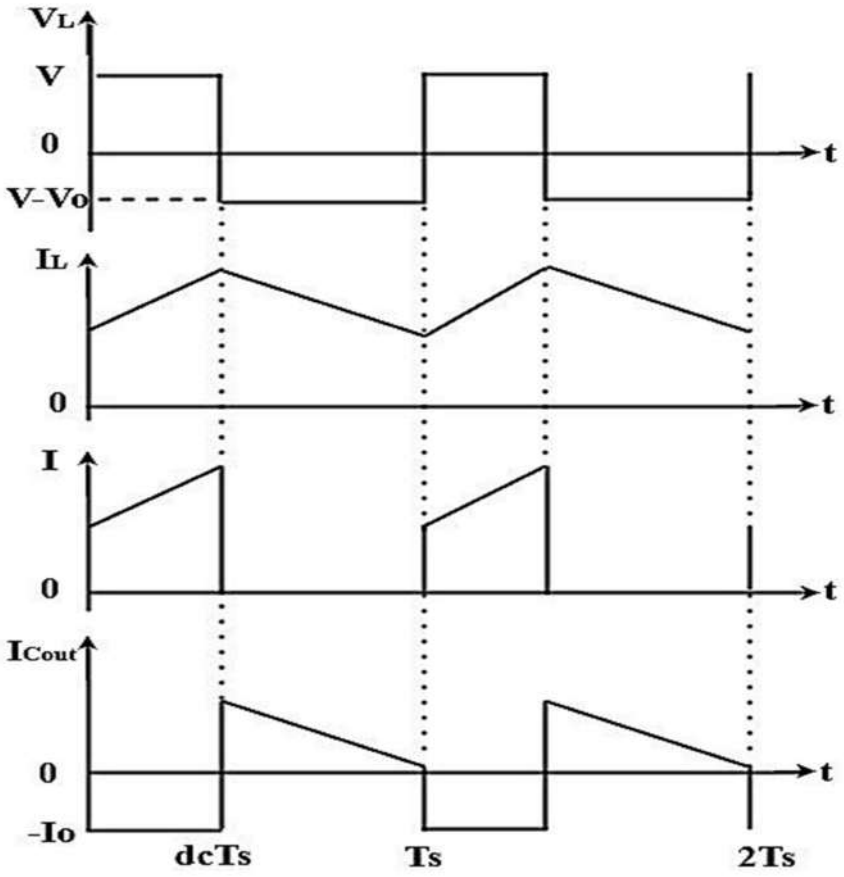


Figure II.3 Input and output voltages and currents in dc and Ts for a Boost [107].

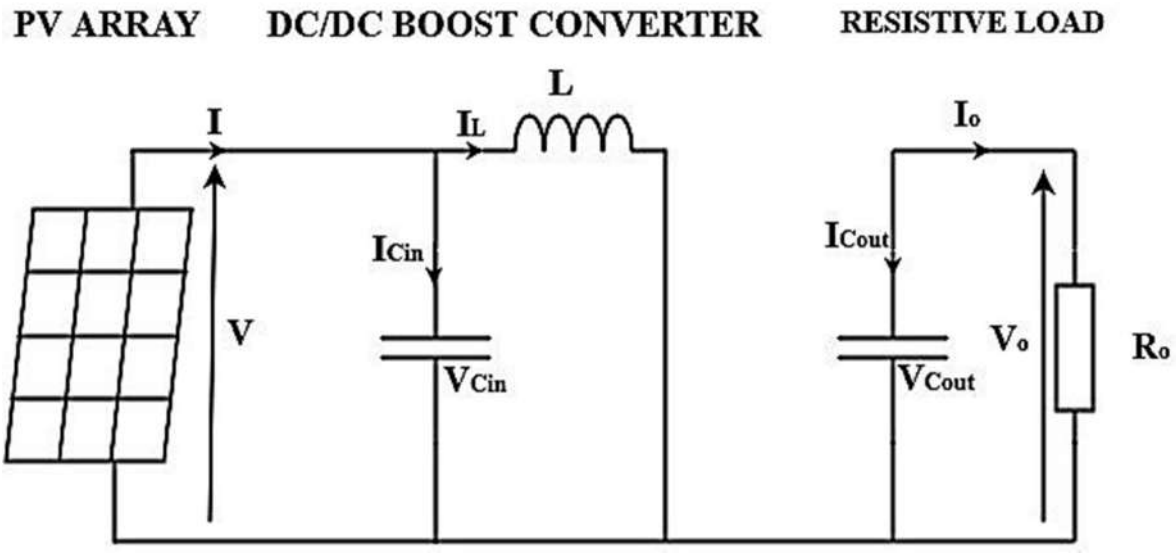


Figure II.4 Boost converter "Sw" closes [107].

II.2.1.6. Mathematical modeling of boost converter at "Sw" closes

According to Figure II.3, the diode becomes reversely biased in $t \in [0, dcTs]$ when Sw shuts. As shown in Figure II.4. L recharges and its current source starts to rise steadily. Throughout this period, we experience [107]:

$$\begin{cases} I_{Cin} = C_{in}\dfrac{dVc_{in}}{dt} = (I - I_L) \\ I_{Cout} = C_{out}\dfrac{dVc_{out}}{dt} = -I_o \\ V_L = L\dfrac{dI_L}{dt} = V \end{cases} \quad (II.1)$$

And for:

$$\begin{cases} V_o = Vc_{out} \\ I_o = \dfrac{V_o}{R_o} \\ I = \dfrac{V}{R_{mp}} \end{cases} \Rightarrow \begin{cases} \dfrac{dVc_{in}}{dt} = \dfrac{1}{C_{in}}\left(\dfrac{V}{R_{mp}} - I_L\right) \\ \dfrac{dV_o}{dt} = -\dfrac{V_o}{R_o.C_{out}} \\ \dfrac{dI_L}{dt} = \dfrac{1}{L}V \end{cases} \quad (II.2)$$

For modeling in state space: $\begin{cases} \dot{x}(t) = A.x(t) + B.U(t) \\ y(t) = C.x(t) + D.U(t) \end{cases}$ (II.3)

With U is the input $[V(t)]$ and y presents the output $[V_o(t)]$ and:

$$x(t) = \begin{bmatrix} x_1(t) \\ x_2(t) \\ x_3(t) \end{bmatrix} = \begin{bmatrix} Vc_{in}(t) \\ Vc_{out}(t) \\ I_L(t) \end{bmatrix} \Rightarrow \dot{x}(t) = \begin{bmatrix} \dot{x_1}(t) \\ \dot{x_2}(t) \\ \dot{x_3}(t) \end{bmatrix} = \begin{bmatrix} \dot{V}c_{in}(t) \\ \dot{V}c_{out}(t) \\ \dot{I}_L(t) \end{bmatrix} \quad (II.4)$$

And

$$\begin{cases} \dot{x}(t) = \begin{bmatrix} 0 & 0 & -\dfrac{1}{C_1} \\ 0 & -\dfrac{1}{R_o.C_{out}} & 0 \\ 0 & 0 & 0 \end{bmatrix}.\begin{bmatrix} x_1(t) \\ x_2(t) \\ x_3(t) \end{bmatrix} + \begin{bmatrix} \dfrac{1}{R_{mp}.C_1} \\ 0 \\ \dfrac{1}{L} \end{bmatrix} U(t) \\ y(t) = [0 \quad 1 \quad 0].\begin{bmatrix} x_1(t) \\ x_2(t) \\ x_3(t) \end{bmatrix} \end{cases} \quad (II.5)$$

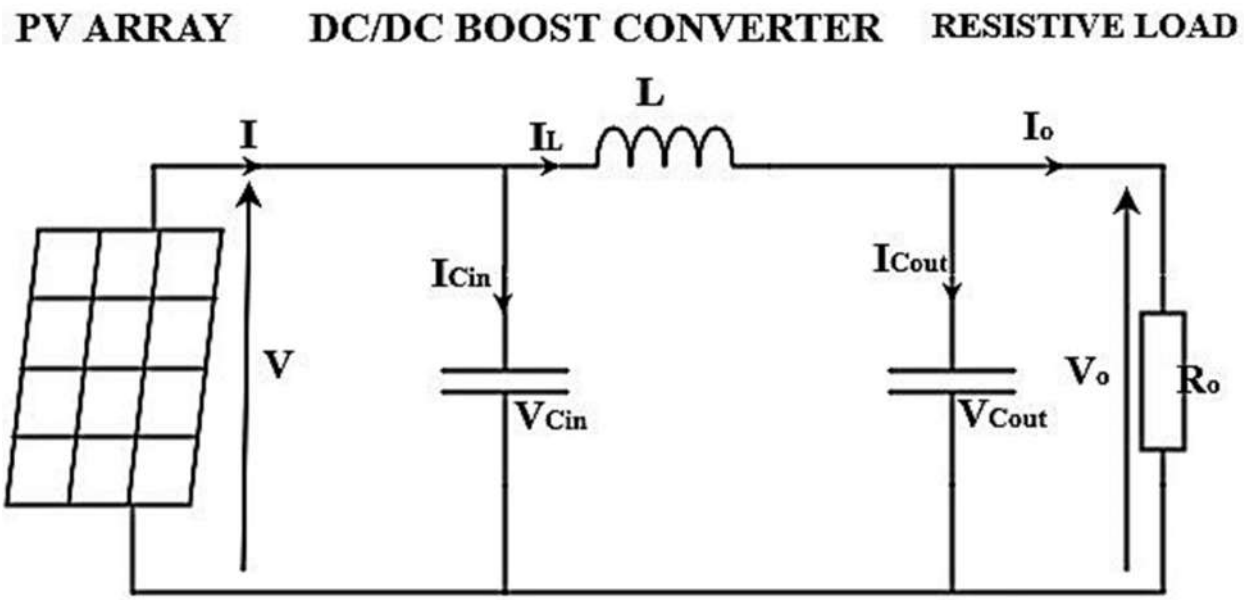


Figure II.5 Boost converter "Sw" opens [107].

II.2.1.7. Mathematical modeling of boost converter at "Sw" opens

According to Figure II.5 when "Sw" is open during t∈ [DT, T], the saved voltage is released via L, which is then combined with the voltage from the supply to supply electricity to load. From this, we derive the following formulas [107]:

$$\begin{cases} I_{Cout} = C_{in}\dfrac{dV}{dt} = \left(\dfrac{V}{R_{mp}} - I_L\right) \\ I_{Cout} = C_{out}\dfrac{dV_0}{dt} = (I_L - I_o) \\ V_L = L\dfrac{dI_L}{dt} = (V - V_0) \end{cases} \quad (II.6)$$

And

$$\begin{cases} \dfrac{dV}{dt} = \dfrac{1}{C_{in}}\left(\dfrac{V}{R_{mp}} - I_L\right) \\ \dfrac{dV_0}{dt} = \dfrac{1}{C_{out}}(I_L - I_o) \\ \dfrac{dI_L}{dt} = \dfrac{1}{L}(V - V_0) \end{cases} \quad (II.7)$$

In state space

$$\begin{cases} \dot{x}(t) = \begin{bmatrix} 0 & 0 & -\frac{1}{C_{in}} \\ 0 & -\frac{1}{R_o.C_{out}} & \frac{1}{C_{out}} \\ 0 & -\frac{1}{L} & 0 \end{bmatrix} . \begin{bmatrix} x_1(t) \\ x_2(t) \\ x_3(t) \end{bmatrix} + \begin{bmatrix} \frac{1}{R_{mp}.C_{in}} \\ 0 \\ \frac{1}{L} \end{bmatrix} U(t) \\ y(t) = [0 \quad 1 \quad 0] . \begin{bmatrix} x_1(t) \\ x_2(t) \\ x_3(t) \end{bmatrix} \end{cases} \quad (II.8)$$

A new equation may be derived from equations II.7 and II.8 [108] [109]:

$$V * dc * T_s = (V_o - V) * (1 - dc) * T_s \quad (II.9)$$

A formula expressing conversion ratio M(dc) looks like this:

$$M(dc) = \frac{V_o}{V} = \frac{1}{1 - dc} \quad (II.10)$$

For calculate the inductor and capacitors values of boost converter necessary to track next steps:

$$R_{mp} = \frac{V_{max}}{I_{max}} \quad (II.11)$$

Output resistance Assume the system is ideal and the input power is equal to output power:

$$\frac{V^2}{R_{mp}} = \frac{{V_o}^2}{R_o} = \frac{\left[\frac{V}{(1 - dc)}\right]^2}{R_o} \quad (II.12)$$

$$R_o = \frac{R_{mp}}{(1 - dc)^2} \quad (II.13)$$

$$dc = 1 - \sqrt{\frac{R_{mp}}{R_o}} \quad (II.14)$$

$$V_o = V_{mp} \sqrt{\frac{R_o}{R_{mp}}} \quad (II.15)$$

$$V_{o_max} = \frac{V_{mp_s}}{(1 - dc_{max})} \quad (II.16)$$

Inductor:

$$L = \left(\frac{V*dc}{(fs_boost*Di_l)}\right) \quad (II.17)$$

$$Di_l = \tilde{y}_{IL}.I_L \quad (II.18)$$

$$Q = \left(\frac{1}{2}\right)\left(\frac{1}{2fs_boost}\right)\left(\frac{Di_l}{2}\right) \quad (II.19)$$

$$Di_l = \frac{V_{mp} * dc}{L * fs_boost} \quad (II.20)$$

$$Dv_{mp} = \tilde{y}_{Vmp} * V = \frac{Q}{C_i} \quad (II.21)$$

Input capacitor:

$$C_{in} = \frac{dc}{8.L.\tilde{y}_{Vmp}fs_boost^2} \quad (II.22)$$

Output capacitor:

$$C_{out} = \frac{dc}{R_o * \tilde{y}_{Vo} * f} \quad (II.23)$$

$$C_{out} = \frac{dc(1-dc)^2}{R_{mp}*\tilde{y}_{Vo}*fs_boost} \quad (II.24)$$

Where dc is the duty cycle, Delta i_l and Delta v_o present Inductor current ripple and Output voltage ripple respectively.

II.2.2. Buck converter

In PV systems, the DC/DC buck converter is widely used, especially in the implementation of storage systems. This enhances the efficiency of the considered system and regulates the voltage into the load or battery needed (Figure II.6) [110-112].

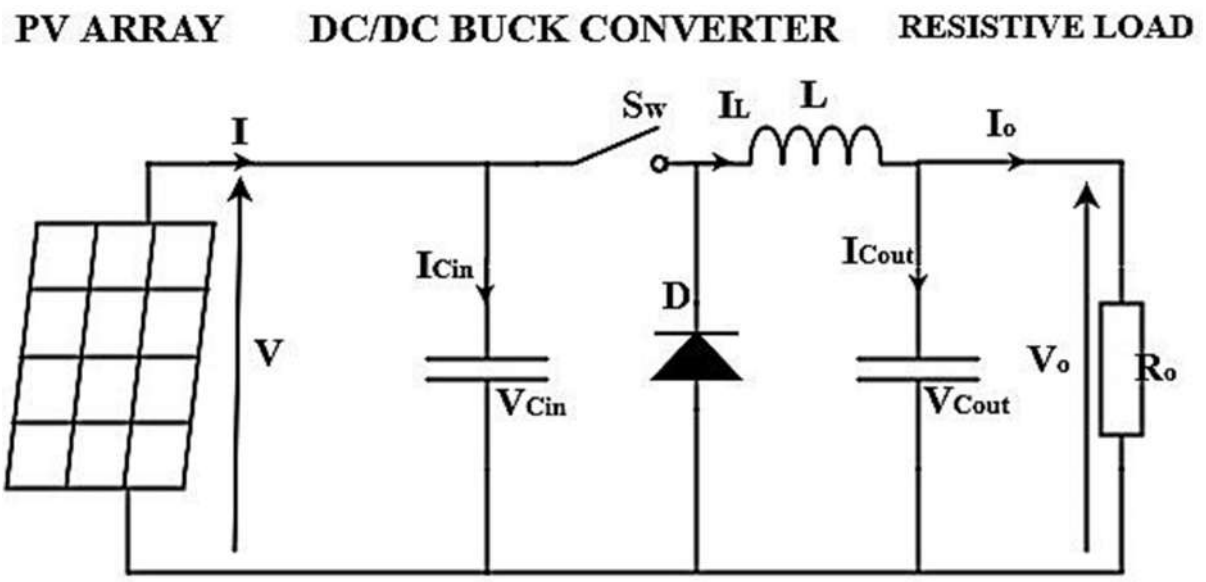


Figure II.6 Buck converter [107].

II.2.2.1. Mathematical modeling of buck converter at "Sw" closes

In order to learn about buck converter and derive its mathematical modeling (Figure II.7), we look at how the analogous circuit works for both Sw states. As shown in Figure II.8 "Sw" is closed for $t \in [0, dc]$ [107]:

$$\begin{cases} I_{Cin} = C_{in}.\dfrac{dVc_{in}}{dt} = \left(\dfrac{V}{R_{mp}} - I_L\right) \\ I_{Cout} = C_{out}.\dfrac{dV_o}{dt} = (I_L - I_o) \\ L.\dfrac{di_L}{dt} = (V - V_o) \end{cases} \quad (II.25)$$

And

$$\begin{cases} \dfrac{dVc_{in}}{dt} = \dfrac{1}{C_{in}}\left(\dfrac{V}{R_{mp}} - I_L\right) \\ \dfrac{dV_o}{dt} = \dfrac{1}{C_{out}}(I_L - I_o) \\ \dfrac{dI_L}{dt} = \dfrac{1}{L}(V - V_o) \end{cases} \quad (II.26)$$

In state space

$$\begin{cases} \dot{x}(t) = \begin{bmatrix} 0 & 0 & -\frac{1}{C_{in}} \\ 0 & -\frac{1}{R_o.C_{out}} & \frac{1}{C_{out}} \\ 0 & -\frac{1}{L} & 0 \end{bmatrix}.\begin{bmatrix} x_1(t) \\ x_2(t) \\ x_3(t) \end{bmatrix} + \begin{bmatrix} \frac{1}{R_{mp}.C_{in}} \\ 0 \\ \frac{1}{L} \end{bmatrix} U(t) \\ y(t) = [0 \quad 1 \quad 0].\begin{bmatrix} x_1(t) \\ x_2(t) \\ x_3(t) \end{bmatrix} \end{cases} \quad (II.27)$$

II.2.2.2. Mathematical modeling of buck converter at "Sw" opens

In tt $\in [dcTS, T]$, the equivalent circuit of buck converter where Sw open is shown in Figure II.9 [107]:

$$\begin{cases} I_{Cin} = C_{in}.\frac{dVc_{in}}{dt} = \frac{V}{R_{mp}} \\ I_{Cout} = C_{out}.\frac{dV_o}{dt} = (I_L - I_o) \\ L.\frac{dI_L}{dt} = -V_o \end{cases} \quad (II.28)$$

And

$$\begin{cases} \frac{dVc_{in}}{dt} = \frac{V}{C_{in}.R_{mp}} \\ \frac{dV_o}{dt} = \frac{1}{C_{out}}(I_L - I_o) \\ \frac{dI_L}{dt} = -\frac{1}{L}V_o \end{cases} \quad (II.29)$$

In state space

$$\begin{cases} \dot{x}(t) = \begin{bmatrix} 0 & 0 & 0 \\ 0 & -\frac{1}{R_o.C_{out}} & \frac{1}{C_{out}} \\ 0 & -\frac{1}{L} & 0 \end{bmatrix}.\begin{bmatrix} x_1(t) \\ x_2(t) \\ x_3(t) \end{bmatrix} + \begin{bmatrix} \frac{1}{R_{mp}.C_{in}} \\ 0 \\ 0 \end{bmatrix} U(t) \\ y(t) = [0 \quad 1 \quad 0].\begin{bmatrix} x_1(t) \\ x_2(t) \\ x_3(t) \end{bmatrix} \end{cases} \quad (II.30)$$

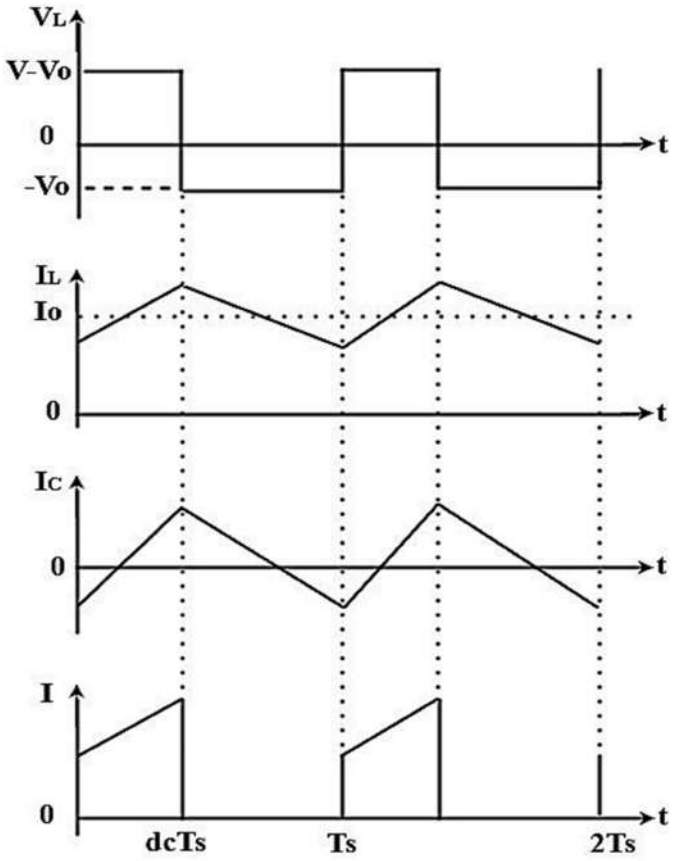


Figure II.7 Buck converter voltages and currents [107].

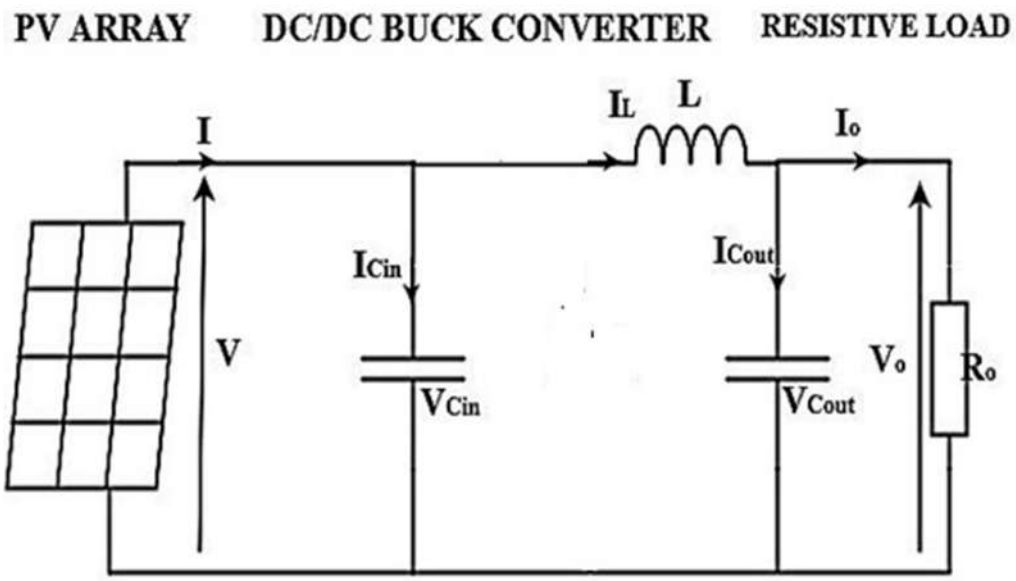


Figure II.8 Buck converter "SW" closes [107].

We can simply extract the formula for the mean inductor voltage. When everything is running well, the average inductor voltage is zero [113]:

$$V_L(t) = dc.(V - V_o) + (1 - dc).(-V_o) = 0 \quad (II.31)$$

The value of V and V_o in respect to the dc may be expressed by the following equation:

$$dc.(V - V_o) = (1 - dc).(V_o) \quad (II.32)$$

The value of V and V_o in respect to the dc may be expressed by the following equation:

$$M(dc) = \frac{V_o}{V} = dc \quad (II.33)$$

The inductance value is given by:

$$L = V_o * \frac{(V - V_{o)}}{DI_L * f_s * V} \quad (II.34)$$

The output capacitor can be calculated as eq.1:

$$C_{out} = \frac{DI_L}{8 * f_s * DV_o} \quad (II.35)$$

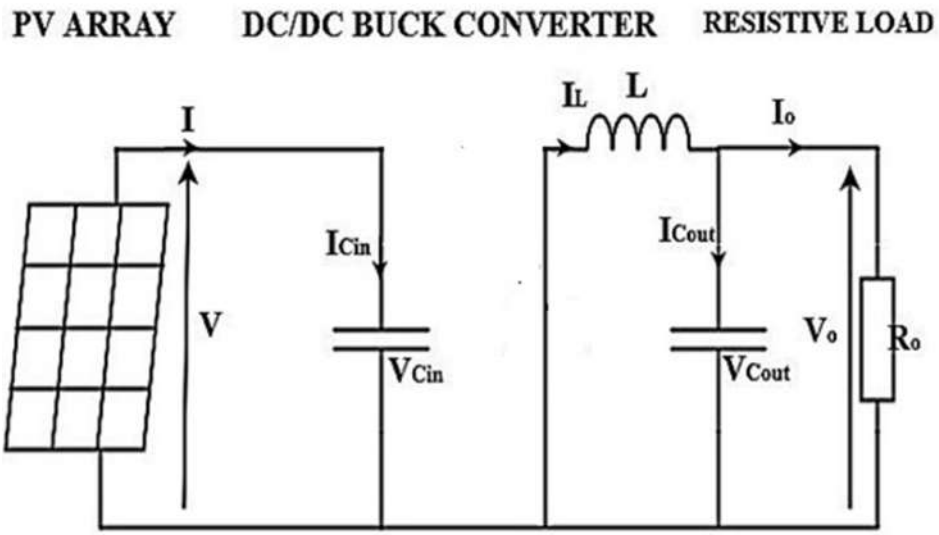


Figure II.9 Buck converter "Sw" open [107].

II.2.3. Buck-boost converter

To maximize efficiency in power transmission from photovoltaic panels to the load or battery bank, the buck-boost converter is an essential component (Figure II.10). The Figure II.11 presents the tensions and currents signals for buck-boost converter [114-117].

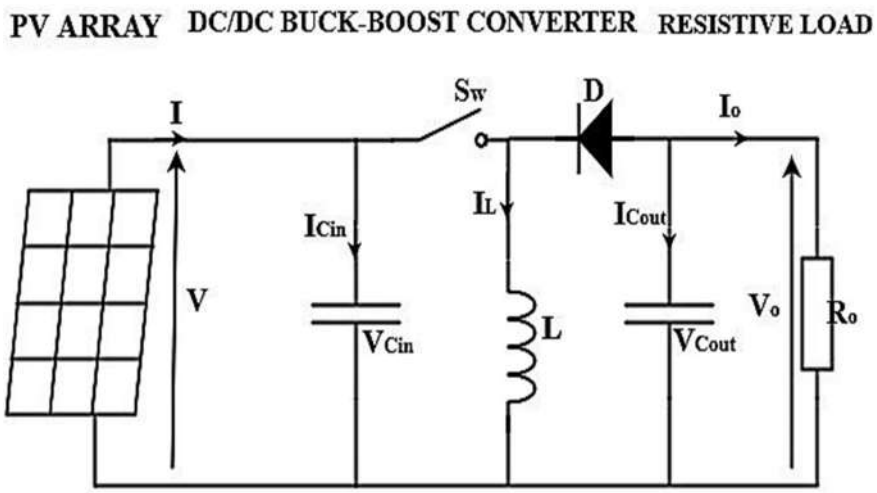


Figure II.10 Buck-boost converter [53].

II.2.3.1. Mathematical modeling of buck-boost converter at "Sw" closes

According to Figure II.12, we can be modeled this converter in the period [0, dcTs] as follow [107] [118] [119]:

$$\begin{cases} I_{Cin} = C_{in}\dfrac{dVc_{in}}{dt} = (i_{pv} - i_L) \\ I_{Cout} = C_{out}\dfrac{dVc_{out}}{dt} = -i_o \\ L.\dfrac{di_L}{dt} = V \end{cases} \quad (II.36)$$

And

$$\begin{cases} \dfrac{dVc_{in}}{dt} = \dfrac{1}{C_{in}}(i_{pv} - i_L) \\ \dfrac{dVc_{out}}{dt} = -\dfrac{1}{C_{out}}i_o \\ \dfrac{di_L}{dt} = \dfrac{1}{L}.V \end{cases} \quad (II.37)$$

In state space,

$$\begin{cases} \dot{x}(t) = \begin{bmatrix} 0 & 0 & -\frac{1}{C_1} \\ 0 & -\frac{1}{R_o.C_2} & 0 \\ 0 & 0 & 0 \end{bmatrix} . \begin{bmatrix} x_1(t) \\ x_2(t) \\ x_3(t) \end{bmatrix} + \begin{bmatrix} \frac{1}{R_{mp}.C_1} \\ 0 \\ \frac{1}{L} \end{bmatrix} U(t) \\ y(t) = [0 \quad 1 \quad 0] . \begin{bmatrix} x_1(t) \\ x_2(t) \\ x_3(t) \end{bmatrix} \end{cases} \quad (II.38)$$

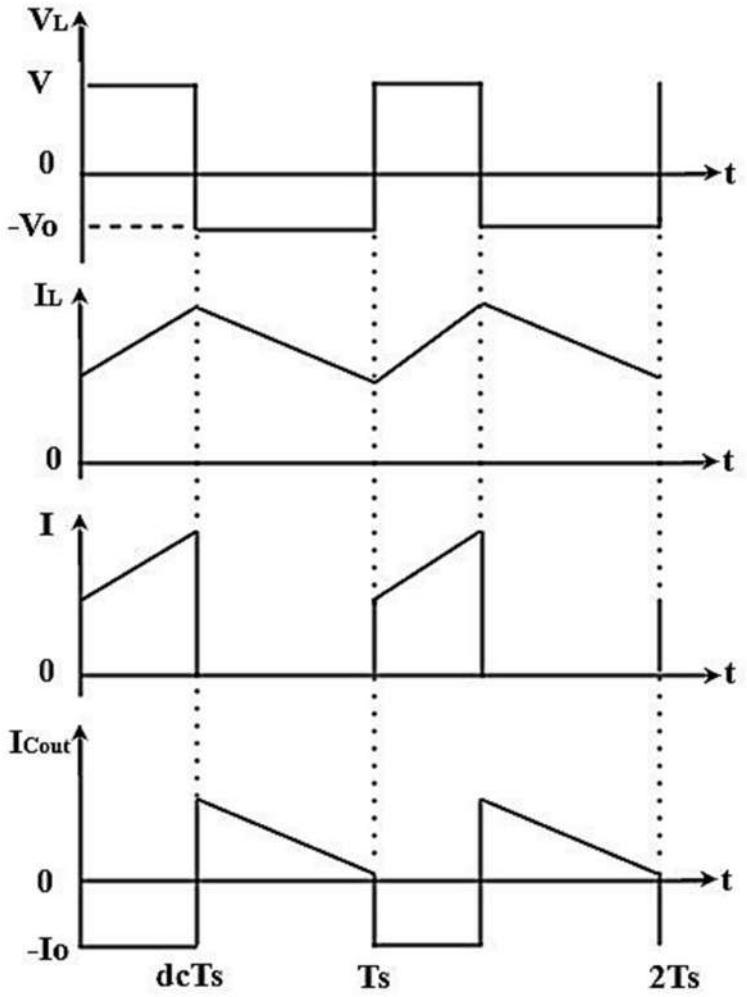


Figure II.11 Tensions and currents of buck-boost converter [53].

II.2.3.2. Mathematical modeling of buck-boost converter at "Sw" opens

According to Figure II.13 For $t \in [dcTs, Ts]$ [107] [118] [119]:

$$\begin{cases} i_{C1} = C_{in}.\dfrac{dVc_{in}}{dt} = i_{pv} \\ i_{C2} = C_{out}.\dfrac{dVc_{out}}{dt} = (i_L - i_o) \\ L.\dfrac{di_L}{dt} = Vc_{out} \end{cases} \quad (II.39)$$

And

$$\begin{cases} \dfrac{dVc_{in}}{dt} = \dfrac{1}{C_{in}}(i_{pv} - i_L) \\ \dfrac{dVc_{out}}{dt} = -\dfrac{1}{C_{out}} i_o \\ \dfrac{di_L}{dt} = \dfrac{1}{L}.V \end{cases} \quad (II.40)$$

In state space,

$$\begin{cases} \dot{x}(t) = \begin{bmatrix} 0 & 0 & 0 \\ 0 & -\dfrac{1}{R_o.C_2} & \dfrac{1}{C_2} \\ 0 & \dfrac{1}{L} & 0 \end{bmatrix}.\begin{bmatrix} x_1(t) \\ x_2(t) \\ x_3(t) \end{bmatrix} + \begin{bmatrix} \dfrac{1}{R_{mp}.C_1} \\ 0 \\ 0 \end{bmatrix} U(t) \\ y(t) = [0 \quad 1 \quad 0].\begin{bmatrix} x_1(t) \\ x_2(t) \\ x_3(t) \end{bmatrix} \end{cases} \quad (II.41)$$

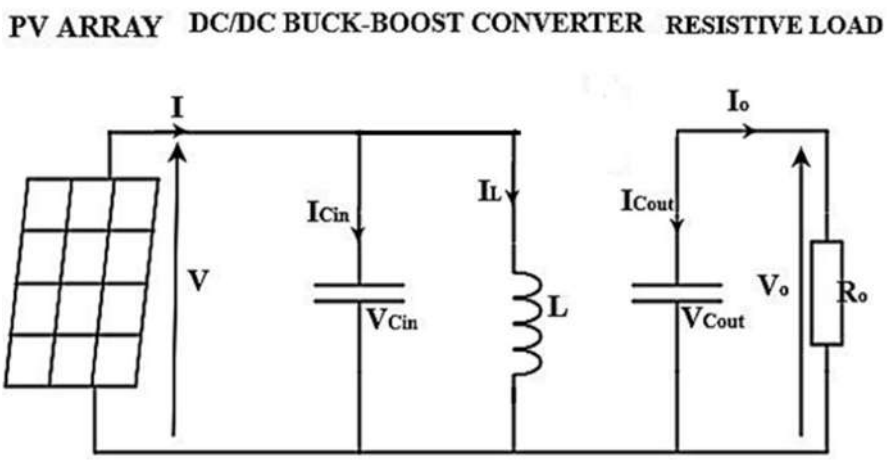


Figure II.12 Buck-boost converter at "Sw" closes [120].

In buck boost converter, M is written as [53] [120] [121]:

$$V * dc * T_s = V_o * (1 - dc) * T_s \quad (II.42)$$

And it's can be given by:

$$M(dc) = \frac{V_o}{V} = \frac{dc}{1 - dc} \quad (II.43)$$

The inductor is calculated by:

$$L = \frac{V * dc}{DI_L * f_s} \quad (II.44)$$

The output capacitor is given by:

$$C_{out} = \frac{V * dc^2}{(1 - dc) * R_o * f_s} \quad (II.45)$$

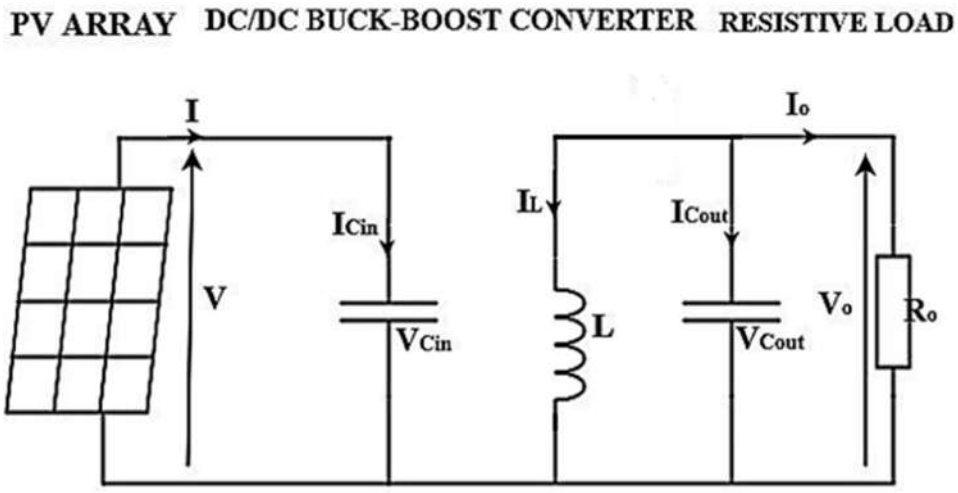


Figure II.13 Buck-boost converter "Sw" open [120].

II.3. PV system connectivity to grid

In order to avoid the loss of electrical power in DC loads it's necessary to link the PV system with grid. For that, as depicted in Figure II.14, it is obligatory to adding following components [122]:

- DC/AC inverter for converting the current into alternative type;
- Inverter control utilizing PLL to regulate the frequency;
- LCL filter for harmonics reduction in grid voltage.

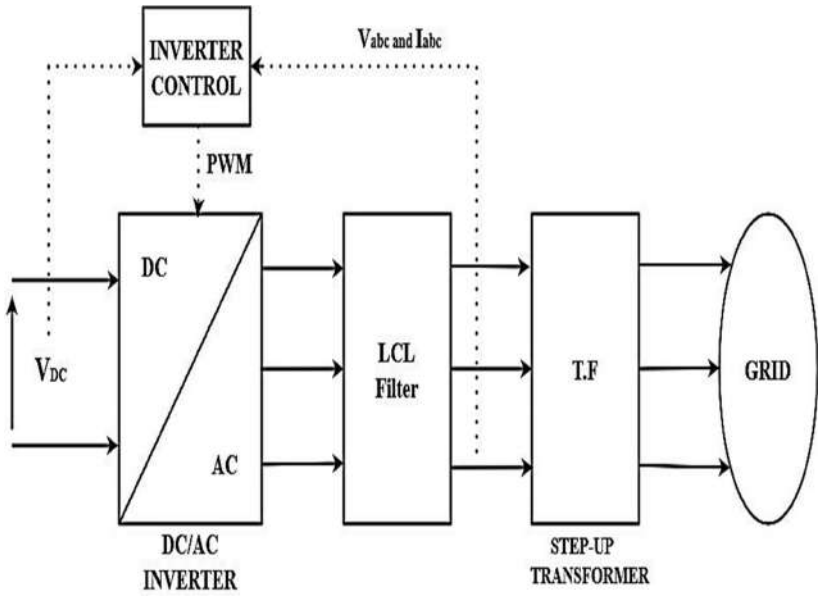
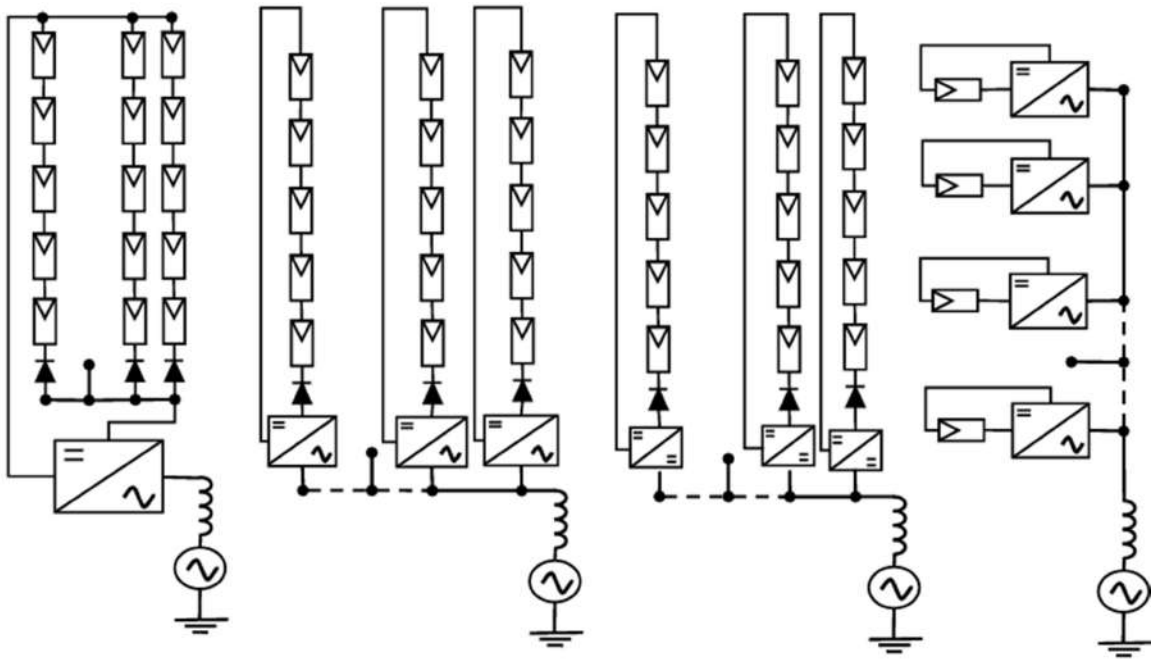


Figure II.14 Grid components [122].

II.3.1. PV inverter

Connectivity to grid, an inverter also known as a DC/AC converter converts the direct current (DC) produced by the PV panel into AC, which may then be sent to the electrical grid. It consists of a transformer, a bridge that converts direct current into alternating current, and an MPPT control that monitors the modules' best working points. You may set the inverter to operate at a certain frequency, whether it's 50 Hz in current thesis [123]. The PV inverter's primary function is to convert a direct current (DC) power source into an alternating current (AC) signal [124].

Figure II.15 shows the topologies of PV inverter where a presents the central inverter, b is the string inverter, c depicts the multi-branch inverter, and the modular inverter is shown in section d [125-127].



(a) (b) (c) (d)

Figure II.15 PV inverter topologies [53].

II.3.1.1. Inverter control

A grid inverter is a device utilized to link the photoelectric power to grid. DC voltage is managed via both reactive and active electrical power commands, which is connected to the electrical grid with the conversion device under altered climatic settings. To accomplish the power factor process, the grid is charged through nil reactive currents by using the vector command. Figure II.16 displays the controlling block design within the control system loops run twin controls of PI to arrange I_q and I_d [128-131].

II.3.1.2. Phase locking loop (PLL)

The phase PLL is used to derive the angle between the inverter's and the voltage across the grid transmissible. In subject to make the feedback variables—the grid's voltages and currents fit the control algorithms' base structure, the phase angle of the voltage generated by the grid is used [132]. To determine the necessary phase angle for the inverter baseline voltage to function, the corresponding reactive and active electrical control signals is put to use. In addition,

the PLL's primary function is to bring the grid and PV systems into harmony with one another. To using this component in considered system, the PLL consists of a phase detector, low-pass filter, and voltage-controlled oscillator [133] [134].

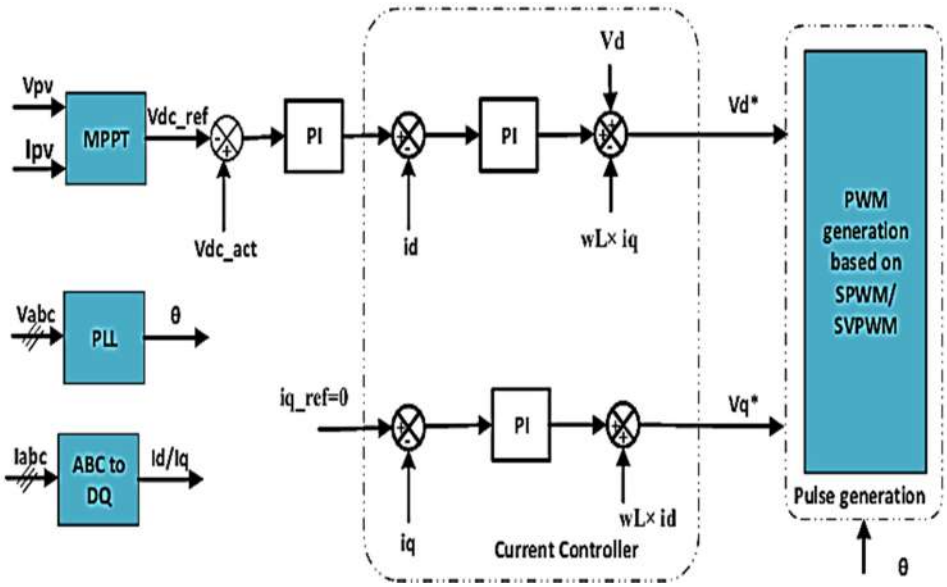


Figure II.16 Control block diagram for centralized inverter using DQ current control [131].

Figure II.17 shows the schematic illustrating an SRF PLL's control scheme. Here, the Q element (V_q) is set to zero so that a triple-phase voltage V_{abc} may be transformed to V_{dq} according to formulas $(II.46)$ to $(II.48)$ [132].

This will bring the voltage into phase via the highest point voltage (V_a).

$$\begin{bmatrix} V_a \\ V_b \\ V_c \end{bmatrix} = \begin{bmatrix} V_m \cos(\theta) \\ V_m \cos(\theta - 120°) \\ V_m \cos(\theta + 120°) \end{bmatrix} \quad (II.46)$$

$$\begin{bmatrix} V_\alpha \\ V_\beta \end{bmatrix} = \frac{2}{3} \begin{bmatrix} 0 & \frac{-1}{2} & -\frac{1}{2} \\ 0 & \frac{\sqrt{3}}{2} & -\frac{\sqrt{3}}{2} \end{bmatrix} \begin{bmatrix} V_a \\ V_b \\ V_c \end{bmatrix} \quad (II.47)$$

$$\begin{bmatrix} V_d \\ V_q \end{bmatrix} = \begin{bmatrix} \cos(\theta') & \sin(\theta') \\ -\sin(\theta') & \cos(\theta') \end{bmatrix} \begin{bmatrix} V_\alpha \\ V_\beta \end{bmatrix} \quad (II.48)$$

While θ and θ' are equal, V_q goes zero, and the system is in synchrony with the grid signals; if (1) is substituted into (3), V_d followed by V_q are determined via equations (II. 49) and (II. 50).

$$V_d = V_m * \sin(\theta - \theta') \quad (II.49)$$

$$V_q = V_m * \cos(\theta - \theta') \quad (II.50)$$

$$V_{ref} = V_d + jV_q \quad (II.51)$$

In addition, Figure II.18 further shows that a concentric extension of V_{ref} upon the q-axis is zero while V_{ref} is in alignment with the d-axis, meaning thus θ and θ' are actually identical. At this point, grid pitch and PLL are synced with one other (Figure II.18) [135].

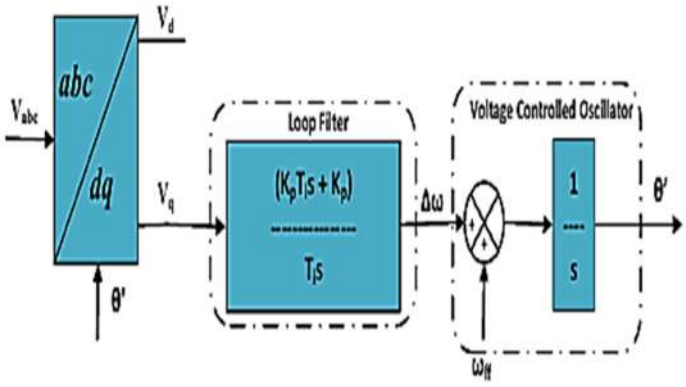


Figure II.17 Structure of Basic PLL structure [132].

For triple-phase, the active power P can be calculated as [97]:

$$P = \frac{3}{2}\left[i_d v_d - i_q v_q\right] \quad (II.52)$$

And the reactive power Q is:

$$Q = \frac{3}{2}\left[i_q v_d - i_d v_q\right] \quad (II.53)$$

With:

V_a, V_b, V_c: Grid voltage;

I_a, I_b, I_c: Grid voltage;

v_q, I_q: Voltage and current in q-axis;

v_d, I_d: Voltage and current in d-axis.

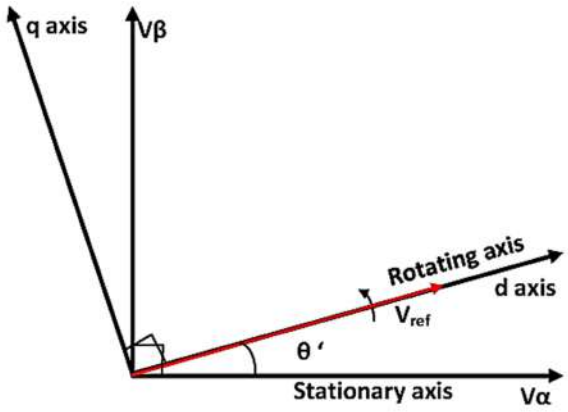


Figure II.18 Stationary and rotating references frames [135].

II.3.2. Filter topologies

Because semiconductor switching introduces harmonics into the produced current, the output filter dampens them. In PV system connectivity to grid, the filter is emplaced in inverter's output and cad divided in to 3 orders [136].

II.3.2.1. L filter

When attenuation is enough for converters operating at high switching frequencies, the L-filter is an appropriate first-order filter. Conversely, the converter-filter technology's dynamics are significantly reduced by inductance [137].

II.3.2.2. LC filter

One second-order structure filter that outperforms the L-filter in terms of dampening is the LC-filter. In most cases, this straightforward topology works as expected and is trivial to implement. This filter's design strikes a balance between inductor and capacity values. When it comes to voltage accuracy, the large capacity is beneficial. A greater inductance value is

necessary to achieve the desired cut-off frequency, however. The grid impedance at the time of system connection determines the resonance rate of this filter (see Figure II.19) [138].

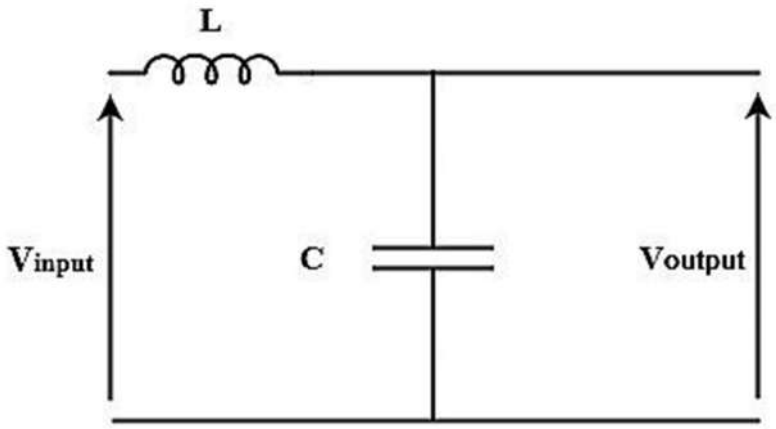


Figure II.19 LC filter [138].

II.3.2.3. LCL filter

Outside of resonate frequency range, the LCL filter attenuates at a rate of 60 dB/decade. Large switching rates converters are therefore compatible with them. For grid-integrated PV applications, an LCL filter is ideal. To a reasonable extent, it may also lessen wave current. Ringing and destabilization in the system might occur if the filter not been carefully constructed according to transformer specifications [139] [140]. Figure depicts electronic schema of LCL filter. The electronic circuit of this filter is shown in Figure II.20, and its components can determine by [141] [142]:

$$L_f = \frac{0.1*U^2}{2*\pi*f*(\frac{R_P}{3})} \quad (II.54)$$

$$C_f = \frac{0.05*(\frac{R_P}{3})}{2*\pi*f*0.1*U^2} \quad (II.55)$$

With:

R_P: Rated power;

U: Output inverter voltage;

f: Grid frequency.

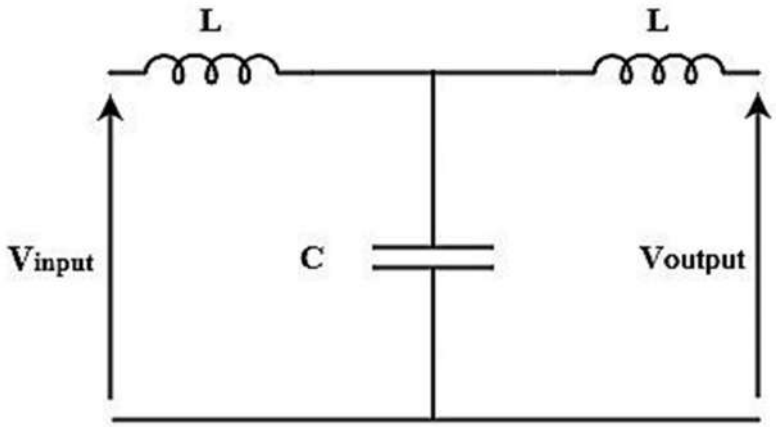


Figure II.20 LCL filter [141].

II.4. Conclusion

Various types of DC/DC converters have been studied and mathematically modeled. For DC/DC boost converter each component that makes this converter is mentioned and detailed. The boost converter is faced two principles problem. In the first, each elements of boost converter is needed to optimal values to its role smoothly. Secondly, the good choice of higher dc is obligatory where the solution of this problem is studied in next chapters. In secondly, we give an overview for role and benefits of various components of utility grid.

CHAPTER III

INTELLIGENT CONTROLS OF A PV SYSTEM

III.1. Introduction

One method to get the most out of a cell in a particular situation is Maximum Power Point Tracking (MPPT). The MPPT has various controls for selecting the required value of dc to follow the MPP [143] [144]. The hill climbing technique has been enhanced and made more efficient by incremental conductance [145]. This technique is built to work with an algorithm for MPPT capable of monitoring the MPP and adjusting the converter's duty cycle accordingly. Although it was the first to be used in an MPPT application, the procedure known as P&O is the most basic of many methods [146]. Altering the panel voltage up or down and then measuring the resulting power usage is how the P&O approach works [147].

The I-V curve that characterizes of the PV cell is not linear. This quality shifts in response to variations in temperature and sunshine intensity, among other environmental variables. That is why the traditional approach has a hard time tracing the MPP. In contrary, the MPPT based on intelligent controls have high benefits compared to conventional approaches that related to mathematical modeling, the intelligent techniques are not interested in mathematical modeling of PV system [144].

The FLC based on P&O or IC techniques relies of if-then rules, this method is not affected to any variation in climate, just need a accurately dataset [147] [148]. The second intelligent control using to track the MPP is the ANN, this approach focuses on collect the data that defined the PV system such as the solar radiation ,temperature, PV voltage and temperature, optimal dc and the training with selected method (in this state the BP algorithm is employed) [149] [150]. For augmenting the performances of FLC and ANN it’s mandatory to utilizing and hybrid techniques called ANFIS algorithm, this approach has higher efficiency and acceptable behavior especially in the changing of the solar radiation [151] [152].

After the study of various MPPT based on traditional and intelligent controls, in second section by employing MATLAB/SIMULINK software we simulate the ANN and FLC as comparative study with IC approach in stand-alone system, and study the comparison result between P&O and ANFIS methods in state of grid connected.

III.2. Perturb and observe (P&O)

Since the P&O algorithm is a genuine MPPT that does not rely on panels, it is being examined. Simple to implement, doesn't need frequent tuning, it relies on adjusting the power converter's duty cycle (the size of a perturbation step) to change the PV array's output voltage, and then monitoring the changes in the array's output power. We are getting close to the maximum panel power when DP is positive, therefore any disturbance must be in the same direction. If the output power drops, on the other hand, you have to do the perturbation in the other way around. If DP=0, then the MPP has been achieved. In Figure III.1, the typical P&O algorithm's flowchart is shown, with k standing for the interval [153] [154].

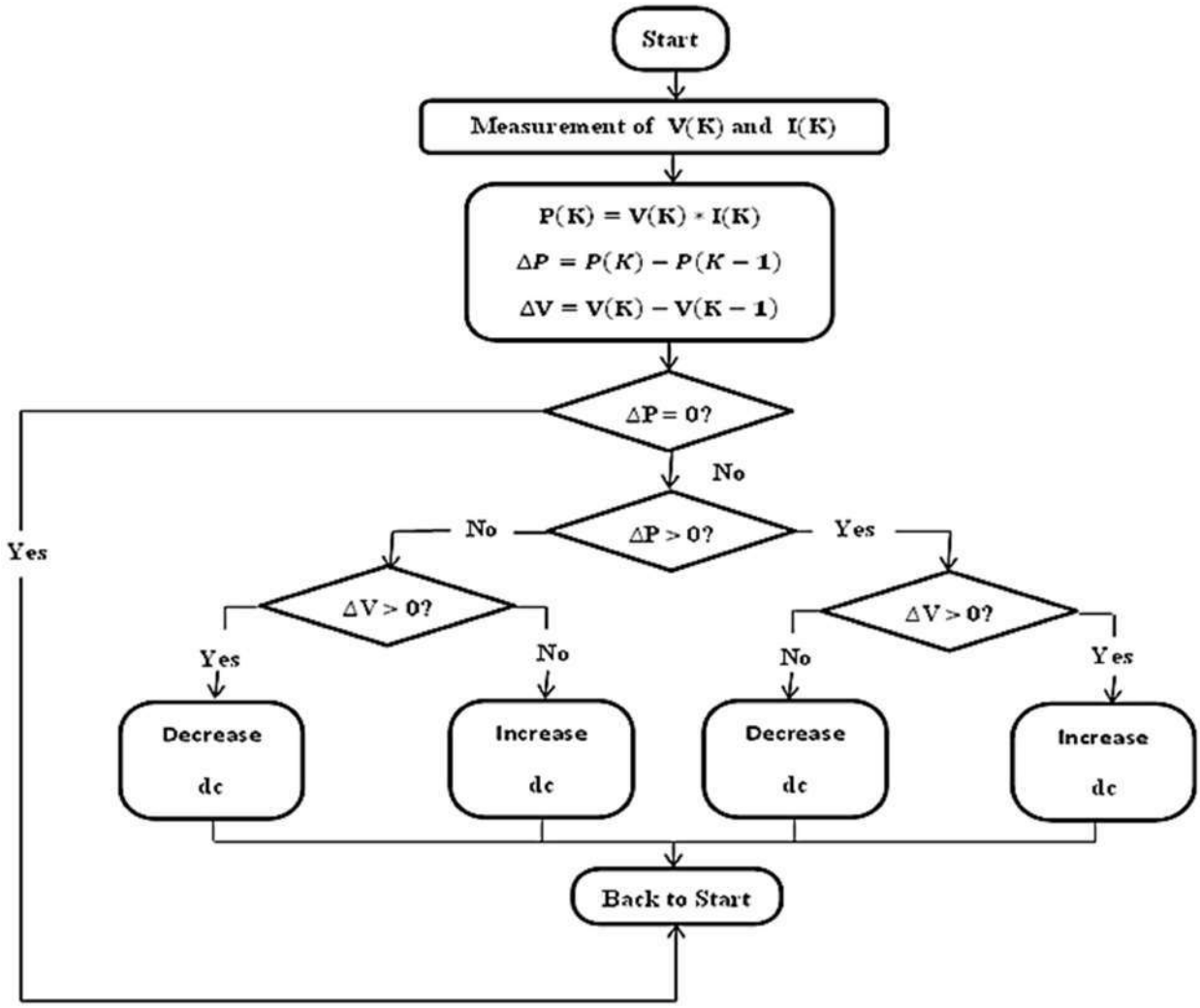


Figure III.1 P&O algorithm [154].

The P&O method can be describe by the following equations [155]:

$$\mathrm{DV} = \mathrm{V(K)} - \mathrm{V(K-1)} \qquad \text{(III. 1)}$$

$$\mathrm{DP} = \mathrm{P(K)} - \mathrm{P(K-1)} \qquad \text{(III. 2)}$$

The dc is incremented when $\mathrm{DP} < 0$ and $\mathrm{DV} < 0$, or when $\mathrm{DP} > 0$ and $\mathrm{DV} > 0$. When $\mathrm{DP} < 0$ and $\mathrm{DV} > 0$, or when $\mathrm{DP} > 0$ and $\mathrm{DV} < 0$), the dc is decremented. (In other sense, the dc is incremented if DP and DV in some sign).

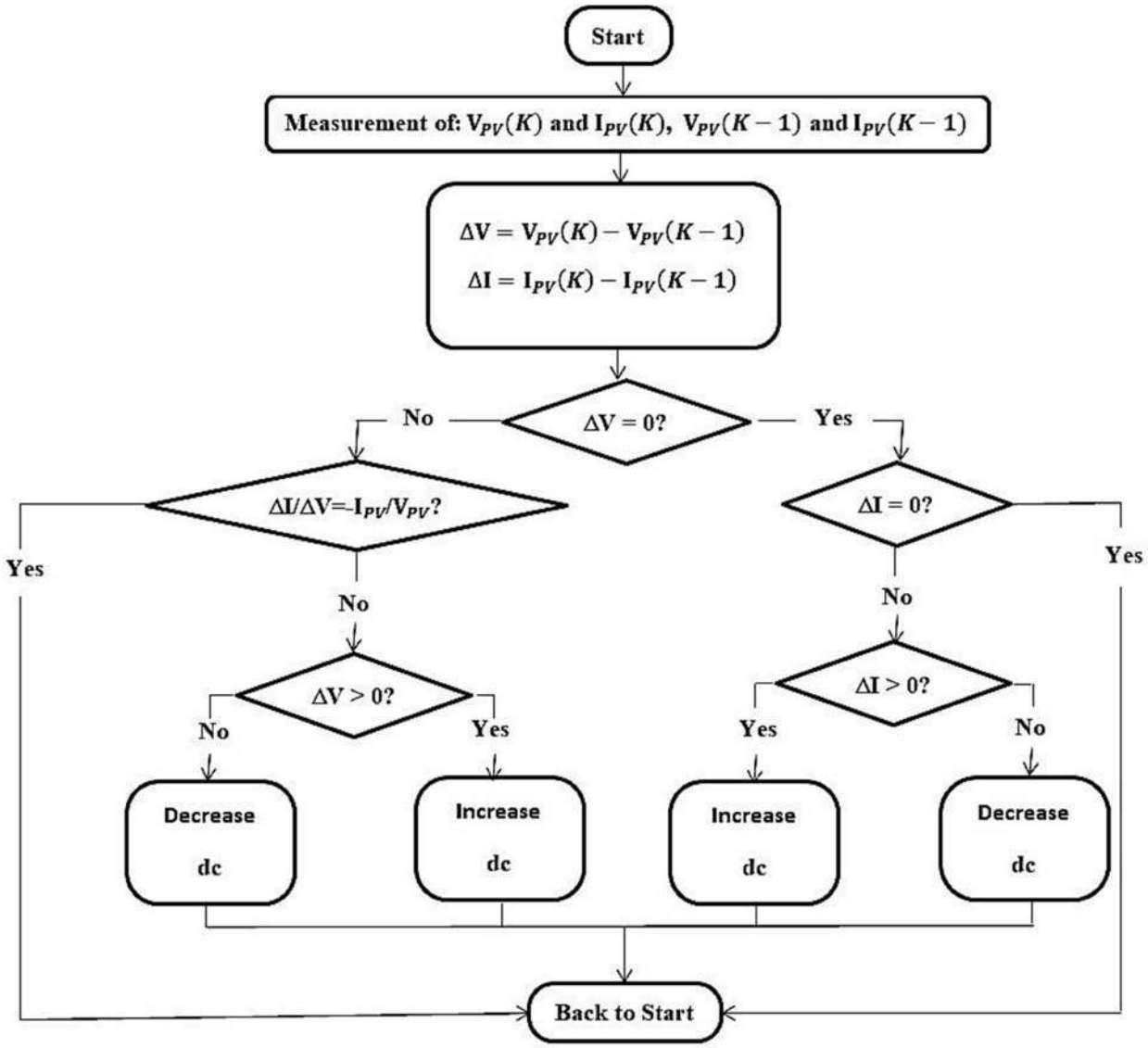


Figure III.2 IC approach [156].

III.3. Incremental Conductance (IC)

Among the several standard MPPT approaches, the IC method is very popular. The power-voltage correlation's gradient provides the basis for this. When the incline is zero, the power output is maximum, when the gradient is negative, the voltage must be decreased, and when the incline is positive, the voltage must be increased, in order to keep the PV array voltage and power at their optimal levels. The following equations describe the IC method [156-159]:

In the MPP:

$$\frac{dP}{dV} = 0 \tag{III. 3}$$

$$\frac{dP}{dV} = \frac{d(V * I)}{dV} = I.\frac{dV}{dV} + V.\frac{dI}{dV} = 0 \tag{III. 4}$$

$$\frac{dI}{dV} = -\frac{I}{V} \tag{III. 5}$$

As shown in the flowchart that described in Figure III.2 when the dc is decremented if $\frac{dP}{dV} > 0$, i.e., $\frac{I}{V} > -\frac{dI}{dV}$. In other hand, where the $\frac{dP}{dV} < 0$, i.e., $\frac{I}{V} < -\frac{dI}{dV}$ the dc is incremented [160].

Table III.1. Fuzzy rule base [170].

ΔE / E	NBIG	NSHO	ZER	PSHO	PBIG
NBIG	ZER	ZER	PBIG	PBIG	PBIG
NSHO	ZER	ZER	PSHO	PSHO	PSHO
ZER	PSHO	ZER	ZER	ZER	NSHO
PSHO	NSHO	NSHO	ZER	ZER	ZER
PBIG	NBIG	NBIG	ZER	ZER	ZER

III.4. Fuzzy logic controller (FLC)

FLC approach often divides challenging systems into many subsystems based on the system's understanding by human experts. In the meantime, a series of basic and easy-to-control

principles have been used to mimic the methods of human management in each local working zone. Afterwards, the global control rules are constructed by integrating all local control actions with the fuzzy membership function, i.e. the weight function. Visually, the conditional statement of "IF-THEN" in the quality language components of human experts associated with the basic models is applied to analysis and synthesis. In recent years, many systems of stability analysis and control synthesis approaches have emerged in fuzzy control theory, in which the Mamdani fuzzy model is commonly used [161-164].

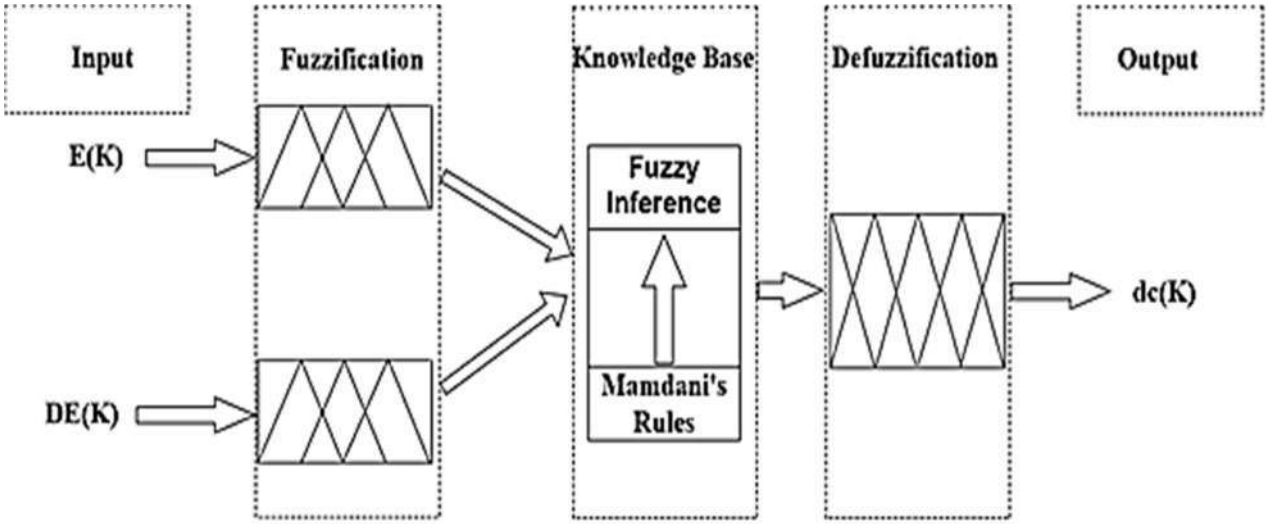
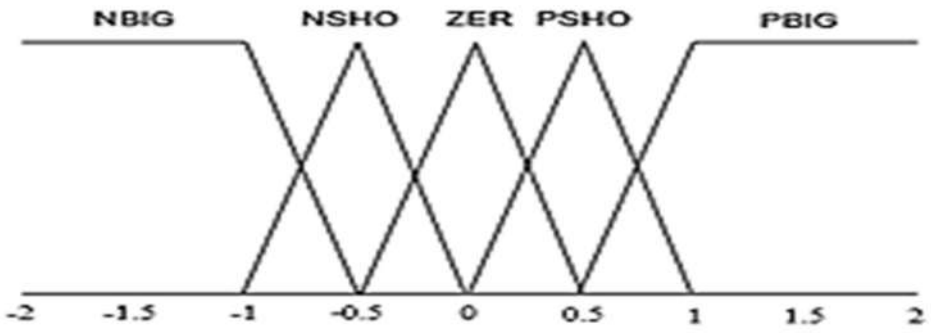


Figure III.3 FLC generality [166].

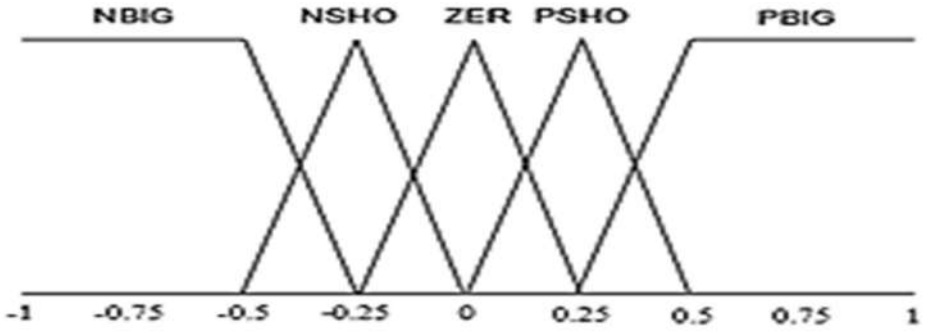
In renewable energy systems in particular, FLC has become a popular AI method for system control. The fact that mathematical modeling is not always necessary to apply FLC to systems is one of its advantages [165]. For PV system MPP monitoring, FLC is a preferred option because to its stability and endurance (Figure III.3) [166].

III.4.1. Fuzzification

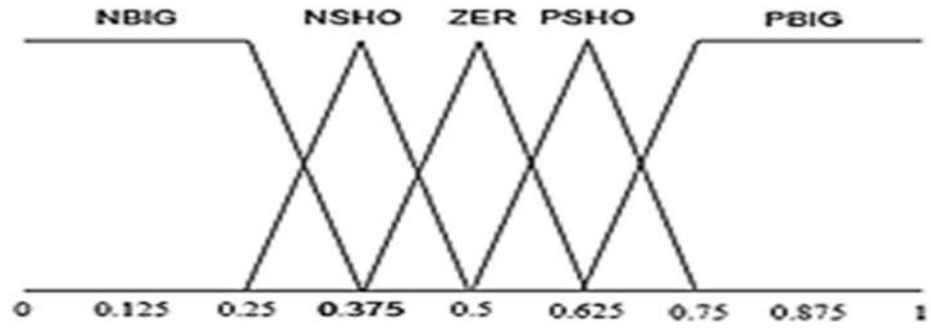
In this context, "fuzzification" refers to the process of giving each variable a degree of uncertainty. Determining the quantity of these fuzzy sets follows an evaluation of the system's behavior. In order to keep select the required dc for the tracking of the MPP when solar irradiance fluctuates rapidly and significantly. For that, this research splits the domain of existence into seven periods for each of the three variables: error (Er), change in error (ΔE), and the output Δdc [167].



(a)



(b)



(c)

Figure III.4 Membership function (a) input Er, (b) input ΔEr and (c) output dc [170].

III.4.2. Inference

The reasoning for our choice to focus on two or more follow-ups ultimately prompted us to form this classification. The fuzzy method includes two phases: the rough phase, where a big search step is used to expedite the search, and the fine phase, where a low search step is used to minimize oscillations and enhance system efficiency [168].

III.4.3. Defuzzification

Defuzzification involves converting linguistic variables into numbers. The fuzzy output of the previous rule is combined with the Max function to form a single fuzzy set. This set is defuzzified and multiplied by the scale factor to obtain a single sequence value. The methodology used for the final stage of the design of the fuzzy controller is the gravity center method. It calculates the growth of the duty cycle [168] [169].

III.4.4. MPPT based FLC

Using two inputs and one output, here are the steps to MPPT based on FLC take in order to employ this technique [170]:

- **Step 1:** Determine the power P by reading $V(K)$ and $I(K)$:

$$P(K) = V(K) * I(K) \quad (III.6)$$

- **Step 2:** Determine the change in voltage (dV) and in power (dP):

$$\begin{cases} dV(K)=V(K)-V(K-1) \\ dP(K)=P(K)-P(K-1) \end{cases} \quad (III.7)$$

- **Step 3:** Calculate:

$$\begin{cases} Er(K)=\frac{dP(K)}{dV(K)} \\ \Delta Er(K)=Er(K)-Er(K-1) \end{cases} \quad (III.8)$$

- **Step 4:** Convert inputs error (Er), error change (ΔEr), and outputs $\Delta dc(i)$ from numerical values to degrees of ambiguity (Figure III.4);
    - **Step 5:** Apply the IF-THEN MAMDANI rules (see Table III.1);
    - **Step 6:** Unify all rule output through a process called grouping;
    - **Step 7:** Convert the aggregated output to numeric values.

III.5. Artificial neural network (ANN)

ANN depicts the reproduction of the biological neural network that fundamentally links many parameters to particular data points. When combining parameters in an ANN model, no complicated mathematical formulae are necessary. As a result, ANN can link several parameters

to large amounts of unknown data points with less theoretical effort than conventional methods. An ANN undergoes supervised learning, also known as training, with the use of imported data. Similar to the human brain, ANN is composed of several types of neurons [171]. The "weight" is a fractional value that connects these neurons. The repercussions are adjusted throughout the training process to forecast the precise outcomes and weight amounts become constant until the mistake surpasses the allowable value [172]. The two-layer ANN model's basic form is shown in Figure III.5 [173]. On the right side of the neural network diagram, you can see how the inputs may be assimilated into the network over time. A larger subset of the total input-output parameter data sets is used to train the neural network; this subset is known as the training data set [172]. On the other hand, validation datasets containing other data points are used to evaluate the trained NN. The NN's input-output parameters and training data points are loaded. Until a satisfactory error occurs, the network is constrained. After the appropriate error occurs, you can verify the qualified network by importing input parameters from the validation data set and predicting the output parameters associated with the input parameters [174-177].

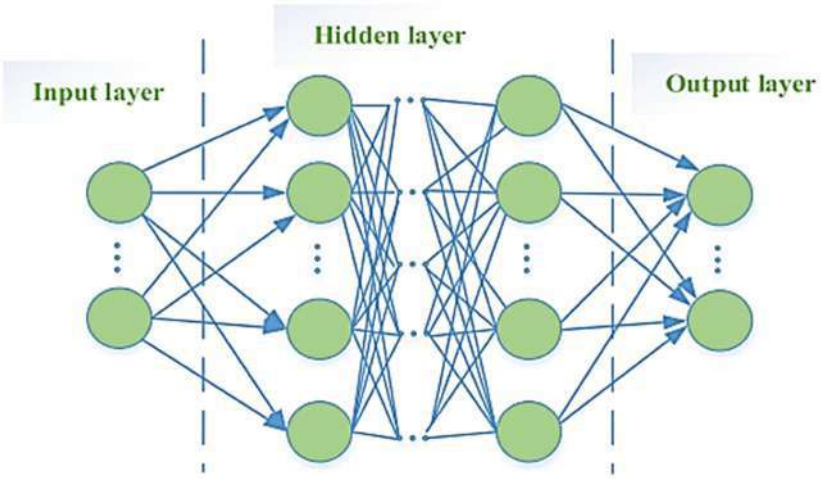


Figure III.5 ANN architecture [173].

The back propagation (BP) approach is used. The dc is computed and ANN is trained for various combinations of PV voltage and current values. To achieve the desired values, the layers weights are adjusted during the NN training. As part of the training process, weights are fine-tuned so that they closely follow the goal values. For evaluate of ANN's performance, is mandatory to employing the MSE, which is calculated as [178][179]:

$$\mathrm{MSE} = \frac{1}{\mathrm{N}}\sum(\mathrm{Target_i} - \mathrm{Output_i})^2 \quad \text{(III. 9)}$$

For applying ANN as a MPPT it may be following steps (Figure III.6):

a) **Data collection:** In considered system for 2 inputs (PV voltage and current) and one output (dc) it's employed 2000 samples for any data. The mathematical relations of inputs and output datas are calculated as [172]:

$$\mathrm{T_{opt}} = (\mathrm{T_{max}} - \mathrm{T_{min}}) * \mathrm{rand} + \mathrm{T_{min}} \quad \text{(III. 10)}$$

$$\mathrm{G_{opt}} = (\mathrm{G_{max}} - \mathrm{G_{min}}) * \mathrm{rand} + \mathrm{G_{min}} \quad \text{(III. 11)}$$

$$\mathrm{I_{opt}} = \frac{\mathrm{G_{opt}}}{1000}\left(\mathrm{I_{mp}} + \mathrm{K_I}(\mathrm{T_{opt}} - 25)\right) \quad \text{(III. 12)}$$

$$\mathrm{V_{opt}} = \left(\mathrm{V_{mp}} + \mathrm{K_{oc}}(\mathrm{T_{opt}} - 25)\right) \quad \text{(III. 13)}$$

$$\mathrm{dc_{opt}} = 1 - \frac{\mathrm{V_{opt}}}{\mathrm{V_{out}}} \quad \text{(III. 14)}$$

b) **Selection of network structure:** In this step, we are utilizing 2 hidden layers, each layer has 10 neurons.

c) **Training and testing the network:** The BP algorithm is applying with 1000 epochs.

III.6. Adaptive neural fuzzy inference system (ANFIS)

Combining ANN and FLC is an ANFIS approach that is used to address the optimization problem. With this method, PV systems and other nonlinear renewable energy applications may be easily managed. All five levels fuzzification, rules, normalization, consequent, and addition are shown in Fig. III.7. It all starts with the two-rule Takagi-Sugeno system. A function z is produced from two parameters, $\mathrm{x_{anf}}$ and $\mathrm{y_{anf}}$ [180] [181].

ANFIS is generally a multilayer back propagation system in which each device plays a specific role in the input signal (node function). In this system, the output z is based on the input $\mathrm{x_{anf}}$ and $\mathrm{y_{anf}}$ of the PV voltage and the PV current. In the rule base there are Takagi and Sugeno

types of unclear rules if-then, in PV system z presents the dc [182] [183][185].

Rule 1: IF x_{anf} = A1, y_{anf}= B1 THEN $z_1 = m_1 x_{anf} + g_1 y_{anf} + u_i$ (III. 15)

Rule 2: IF x_{anf} = A2, y_{anf}= B2 THEN $z_2 = m_2 x_{anf} + g_2 y_{anf} + u_2$ (III. 16)

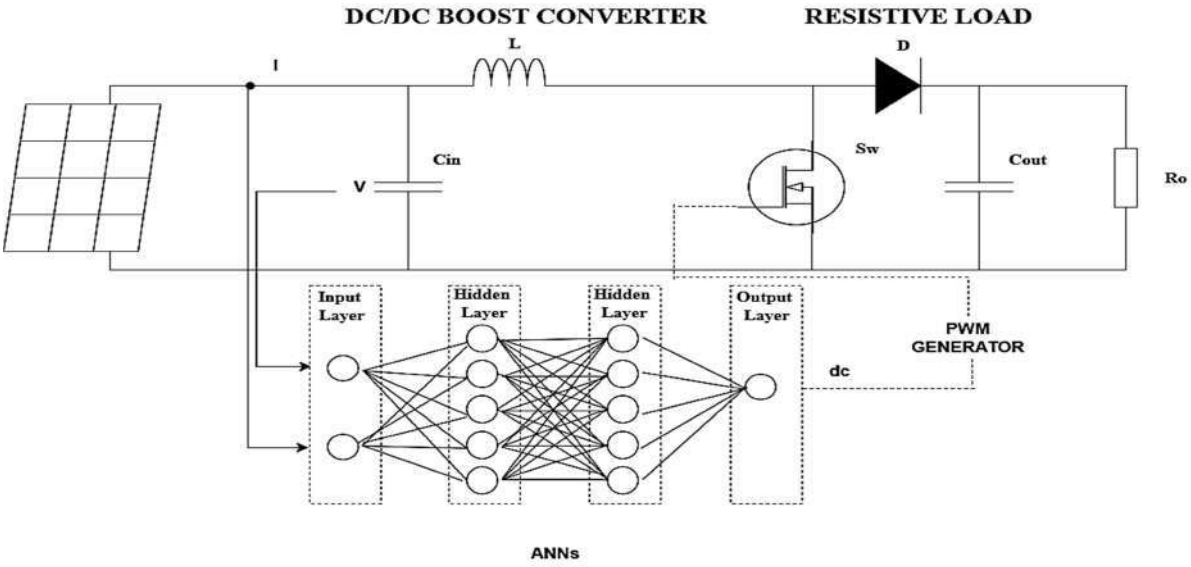


Figure III.6 ANN architecture [172].

The ANFIS control consists of five layers, can describe as follows (Figure III.7) [184] [185]:

- **First layer:** This layer present the fuzzification step, where a group of membership function A_i form a node. The membership of input x_{anf} and output $y_{anf} \in [0\ 1]$ can be calculated:

$$\begin{cases} A_{1,i} = \mu x_i(x_{anf}) & \text{for } i=1,2 \\ A_{1,i} = \mu y_{i-2}(y_{anf}) & \text{for } i=3,4 \end{cases} \quad \text{(III. 17)}$$

- **Second layer:** Can be defined the nodes output in this layer as the product of their inputs:

$$A_{2,i} = w_i = \mu x_{anf_i}(x_{anf}) \mu x_{anf_i}(y_{anf}) \qquad i = 1,2 \quad \text{(III. 18)}$$

- **Third layer:** There is a normalization procedure performed by each fixed node in this layer. It is possible to express the output of every node as:

$$A_{3,i} = s_i = \frac{s_i}{s_1 + s_2} \quad \text{(III. 19)}$$

- **Fourth layer:** Every node is computed and fitted to used rule consequent by:

$$A_{4,i} = s_i z_i = s_i(m_i x_{anf} + g_i y_{anf} + u_i) \quad \text{(III. 20)}$$

where $\{m_i, n_i, u_i\}$ is the collection of parameters calculated by the learning process and s_i is the output of the preceding layer. There are two prevalent learning strategies for ANFIS: the hybrid control technique and the back propagation approach.

- **Last layer:** Only one fixed node, denoted by Σ, exists. This node is responsible for adding up all the signals that come in. From here on, the model's general output may be expressed as:

$$A_{5,1} = \sum_i s_i z_i = \frac{\sum_i s_i z_i}{\sum_i s_i} \qquad \text{(III. 21)}$$

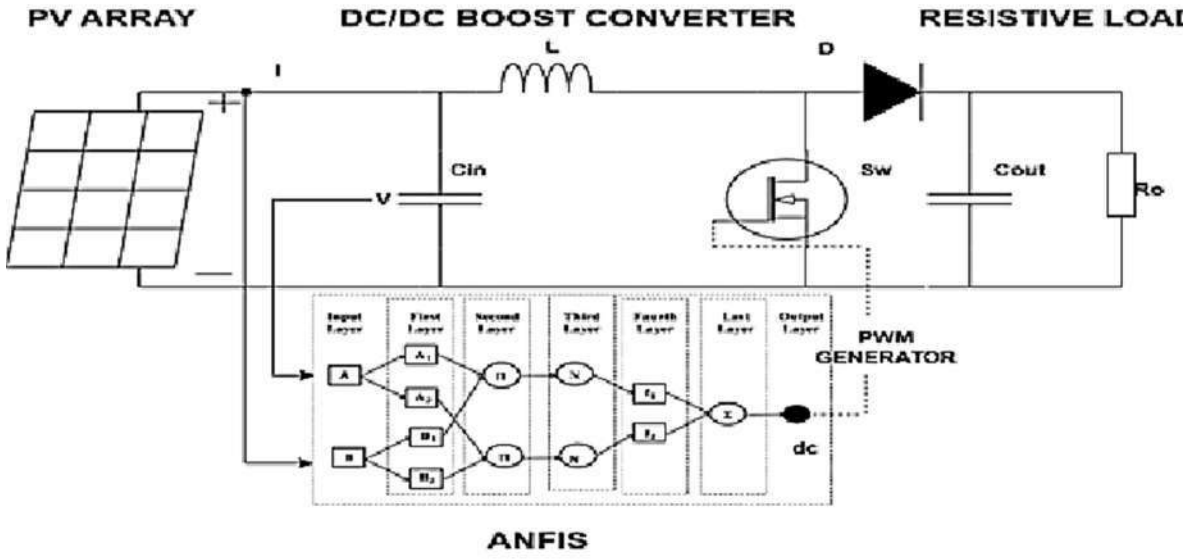


Figure III.7 ANFIS-MPPT [184].

III.7. Result and discussion

In this chapter, we use two types of simulations, stand-alone and grid connected PV system by utilizing four MPPT approaches by employing MATLAB/Simulink software.

III.7.1. Simulation with stand-alone PV system

In this stage, a MPPT based on ANFIS algorithm is simulated and compared to P&O control in fixed and variable solar radiation. To evaluate the effectiveness proposed MPPT under stand-alone system, the Figure III.8 shows the simulation of this technique. The values of PV array and boost converter components is described in Table II.2.

Table III.2 Components of considered stand-alone PV system.

Description	Value
Maximun power (P_{max})	37.26 W
Maximun voltage (V_{max})	16.56 V
Peak current (I_{max})	2.25 A
Voltage of open-circuit (V_{oc})	21.24 V
Current of short-circuit (I_{sc})	2.55 A
Output voltage(V_o)	30 V
Input capacitor (C_{in})	65.3219 µF
Output capacitor (C_{out})	278.228µF
Inductance (L)	1.71438 mH
Switching frequency (fs_boost)	10 kHz

The Figures (III.9 to III.14) show the simulation results under stand-alone system of PV voltage, PV current, and PV power, output voltage, output current, and output power with fixed irradiance. The two methods used (P&O and ANFIS) give an output power of 36.0974 watts and efficiency equals 99.32 %. In standard conditions, we can't prove the benefits of ANFIS based MPPT because the two algorithms have some behavior where follow the MPP.

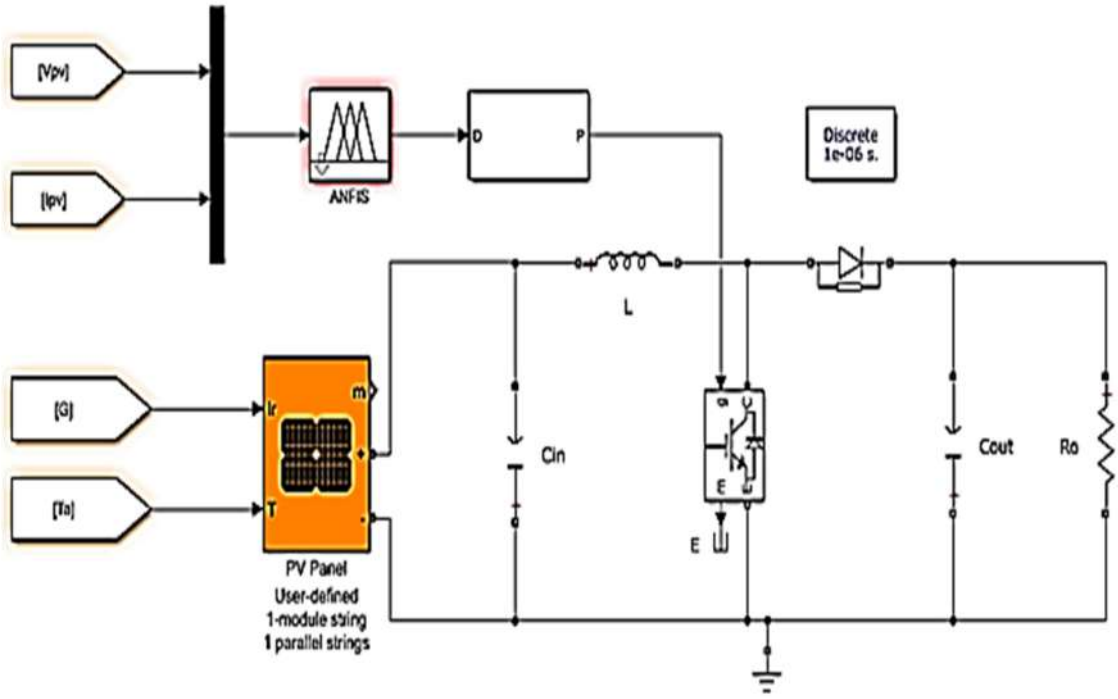


Figure III.8 Stand-alone PV system with MATLAB/Simulink.

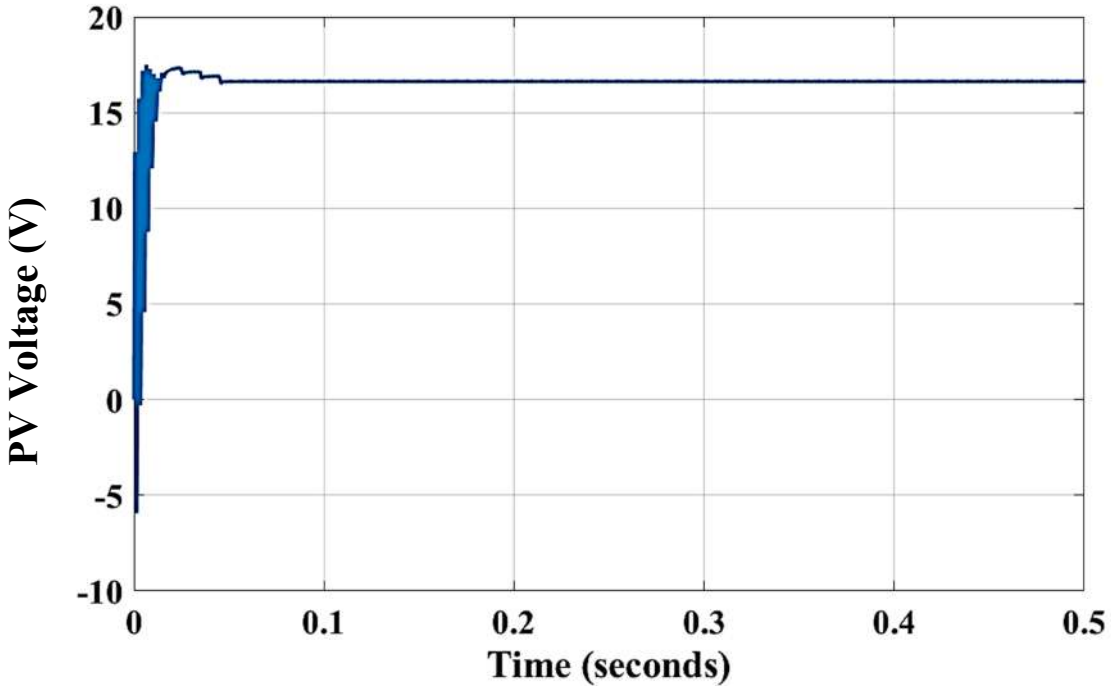


Figure III.9 PV voltage in stand-alone system with fixed radiation.

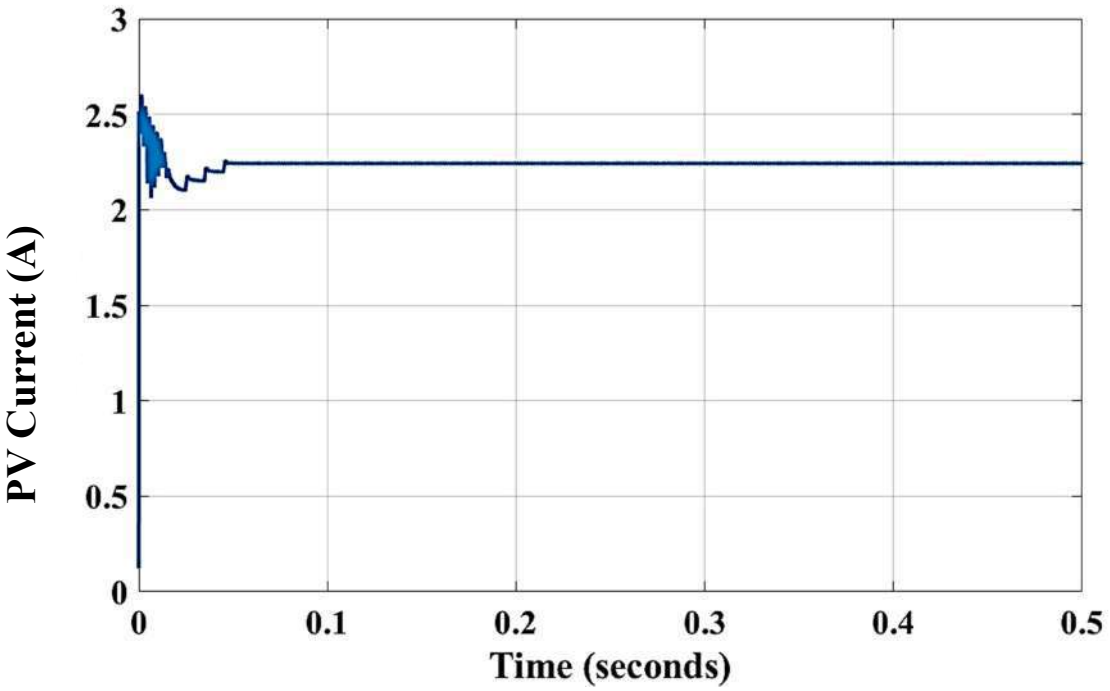


Figure III.10 PV current in stand-alone system with fixed radiation.

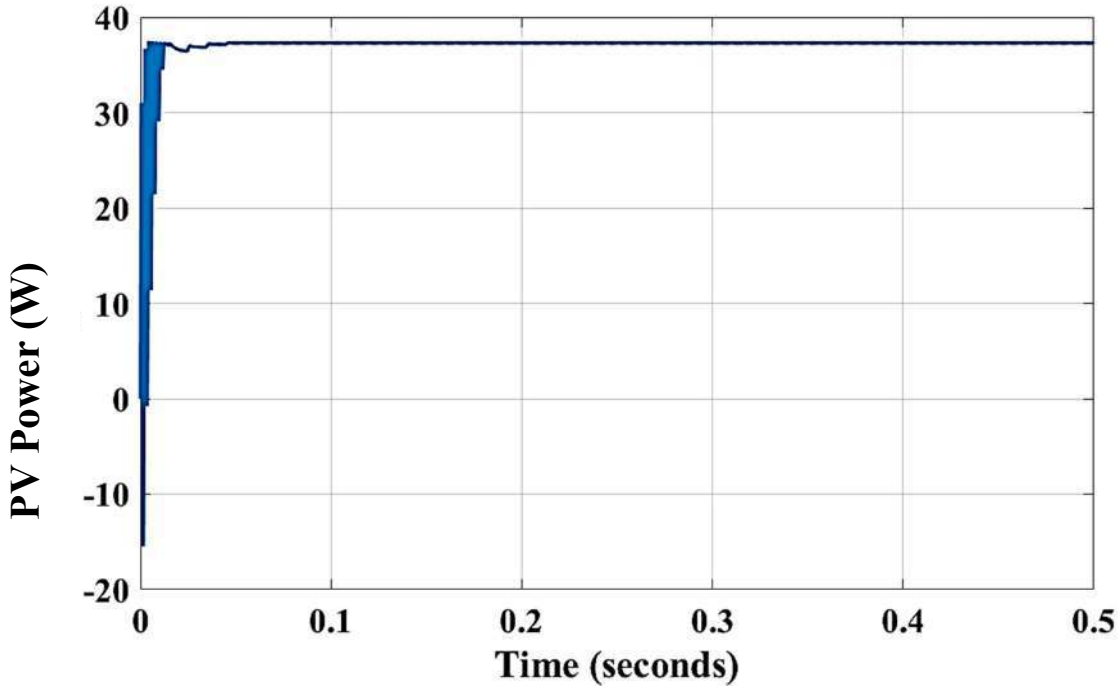


Figure III.11 PV power in stand-alone system with fixed radiation.

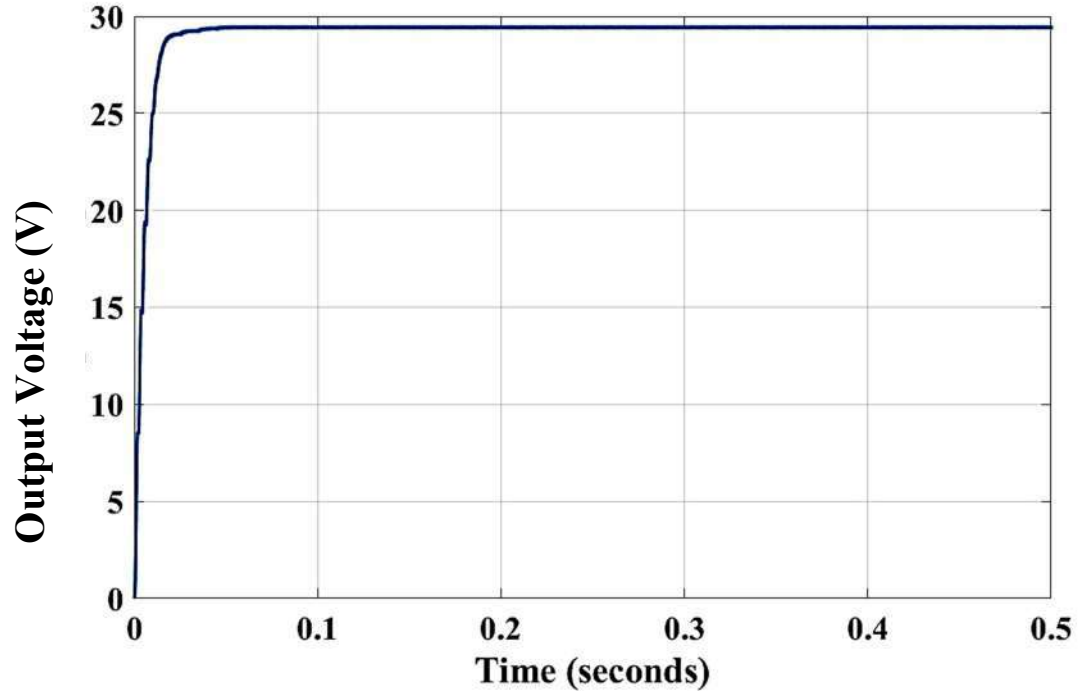


Figure III.12 Output voltage in stand-alone system with fixed radiation.

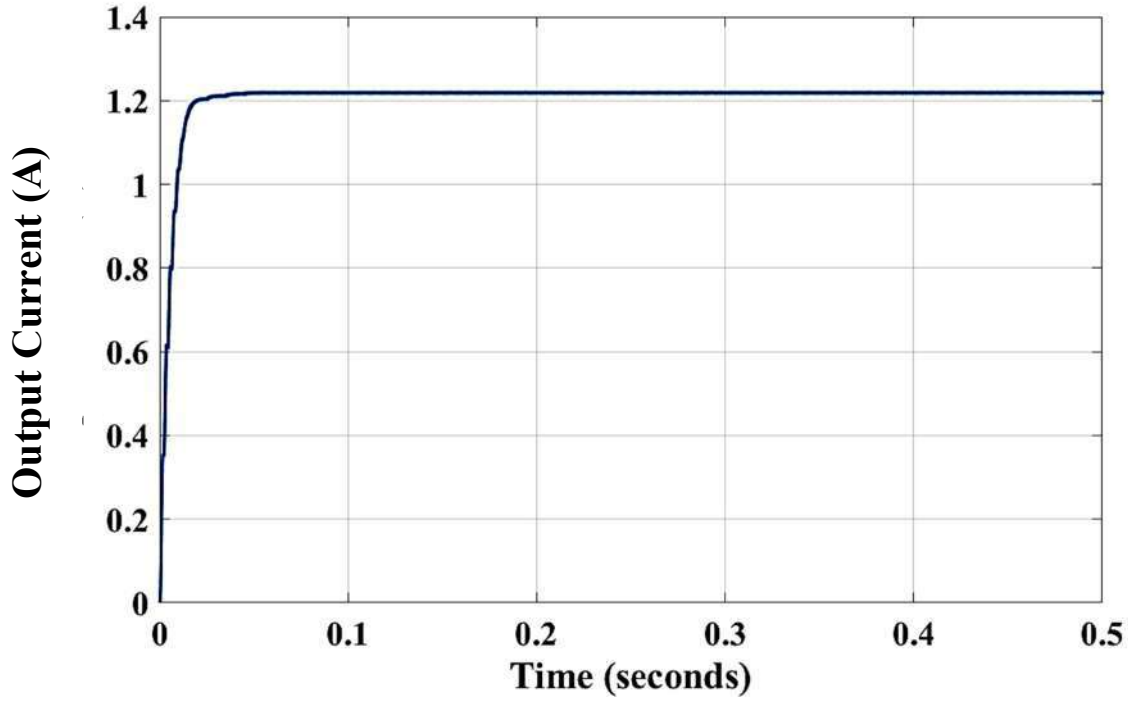


Figure III.13 Output current in stand-alone system with fixed radiation.

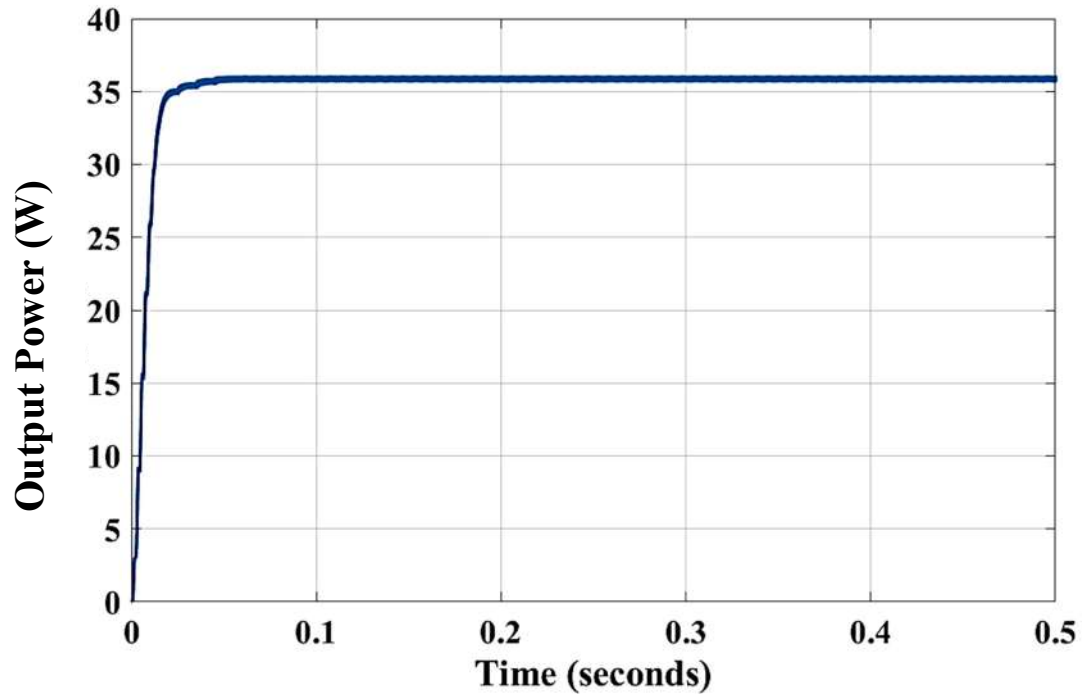


Figure III.14 Output power in stand-alone system with fixed radiation.

Figure III.15 shows the profile of irradiance where its values varies between 600, 800, 950, and 1000 W/m^2.

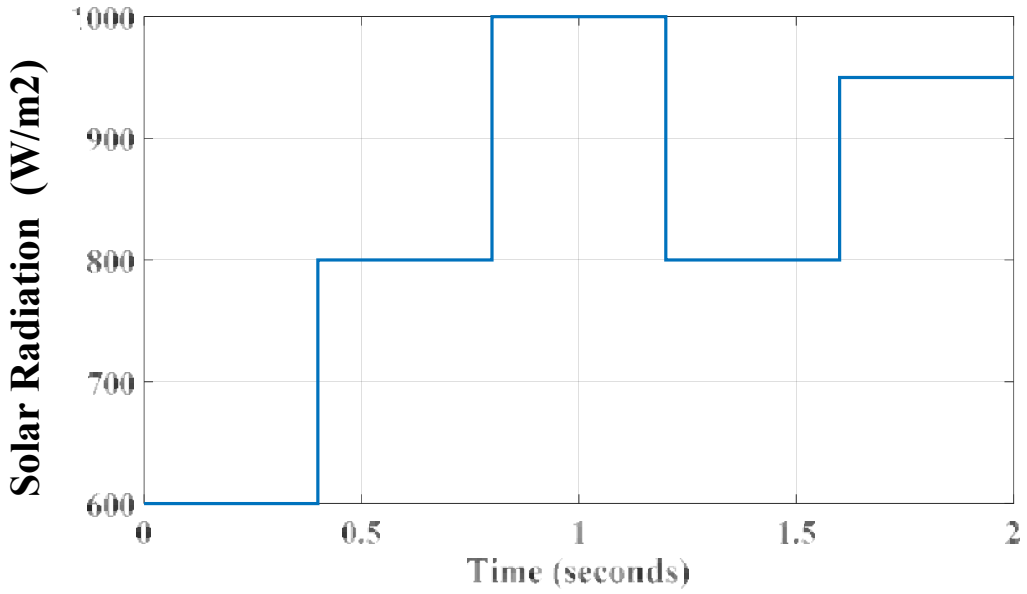


Figure III.15 Solar irradiance profile in stand-alone system.

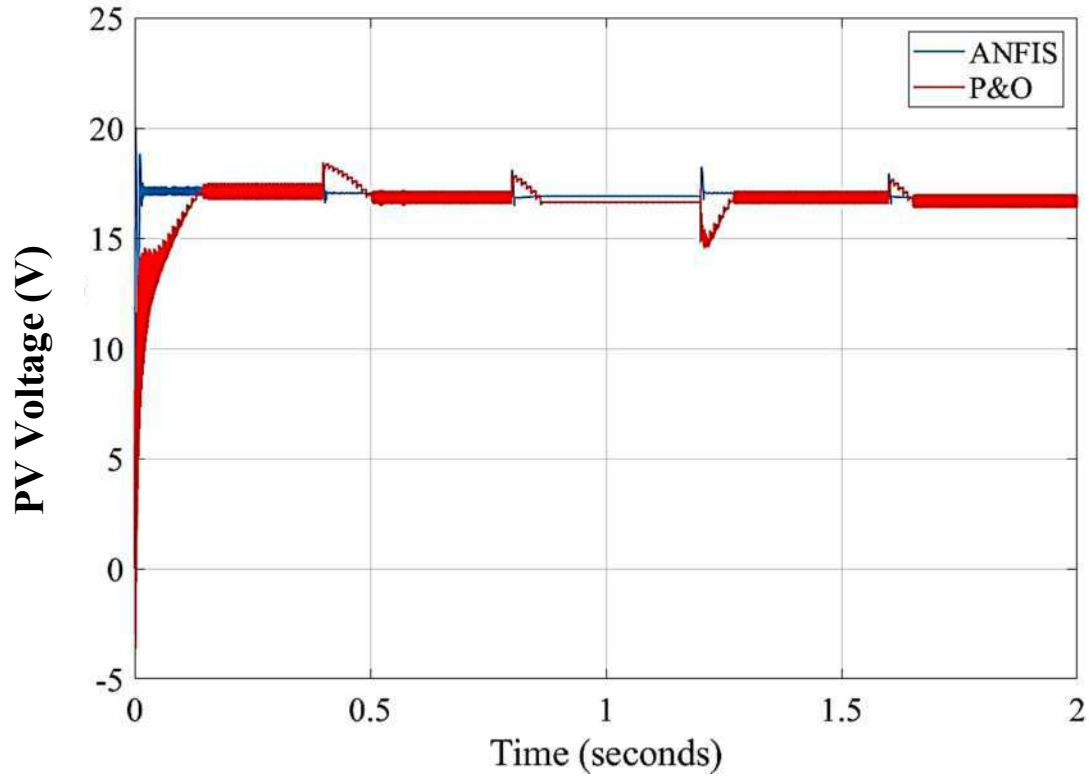


Figure III.16 PV voltage in stand-alone system with variable radiation.

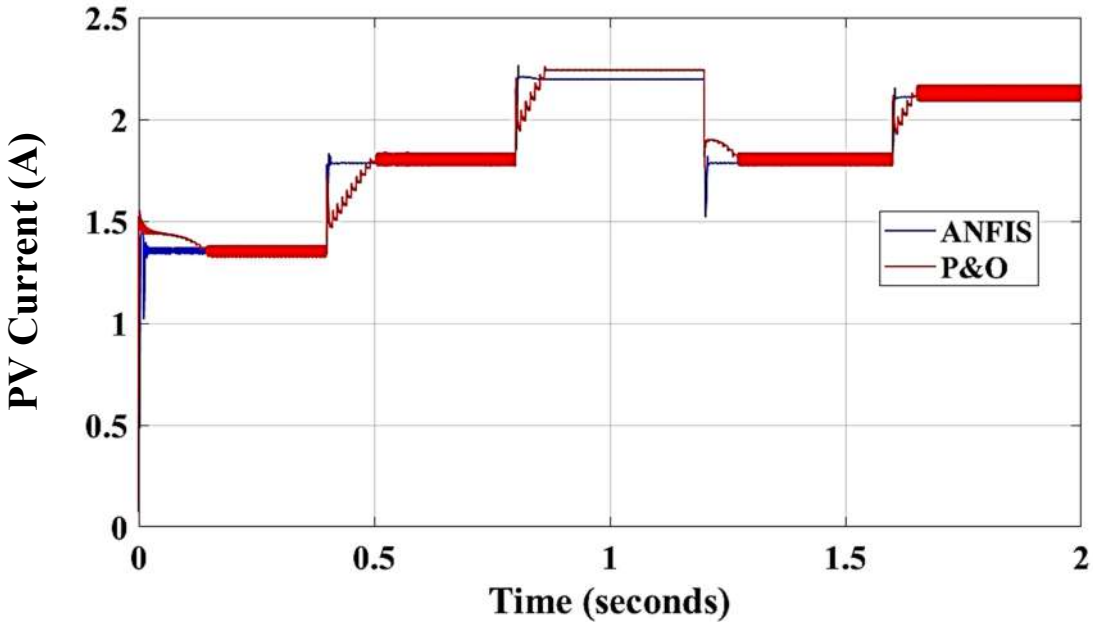


Figure III.17 PV current in stand-alone system with variable radiation.

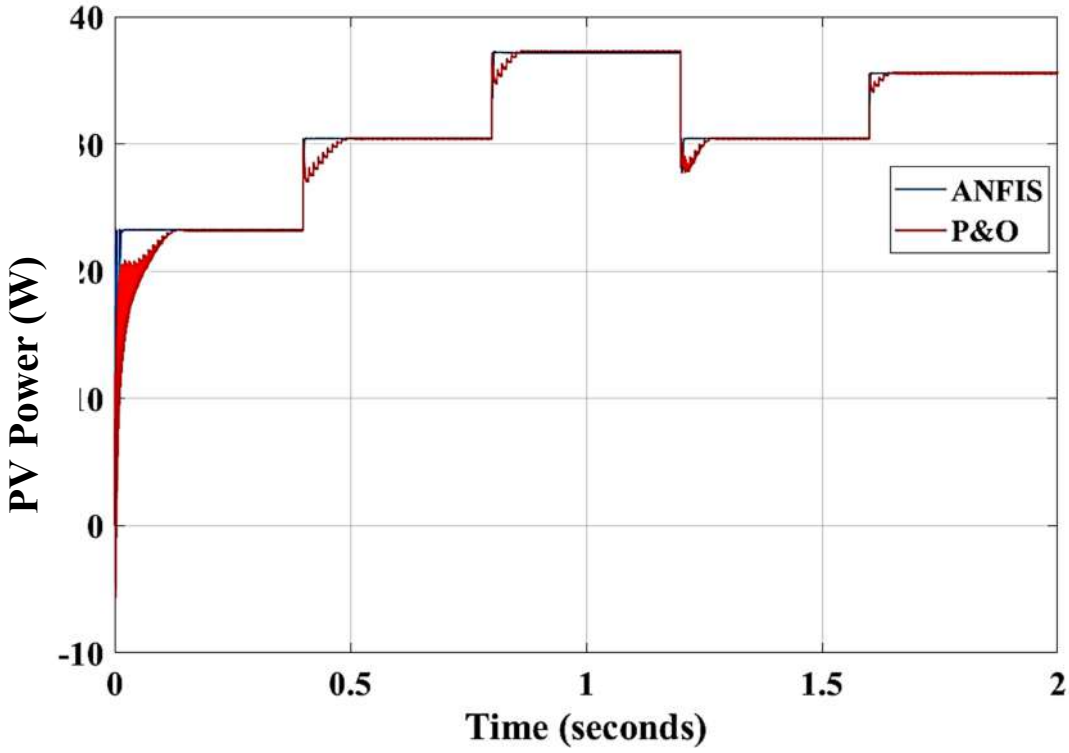


Figure III.18 PV power in stand-alone system with variable radiation.

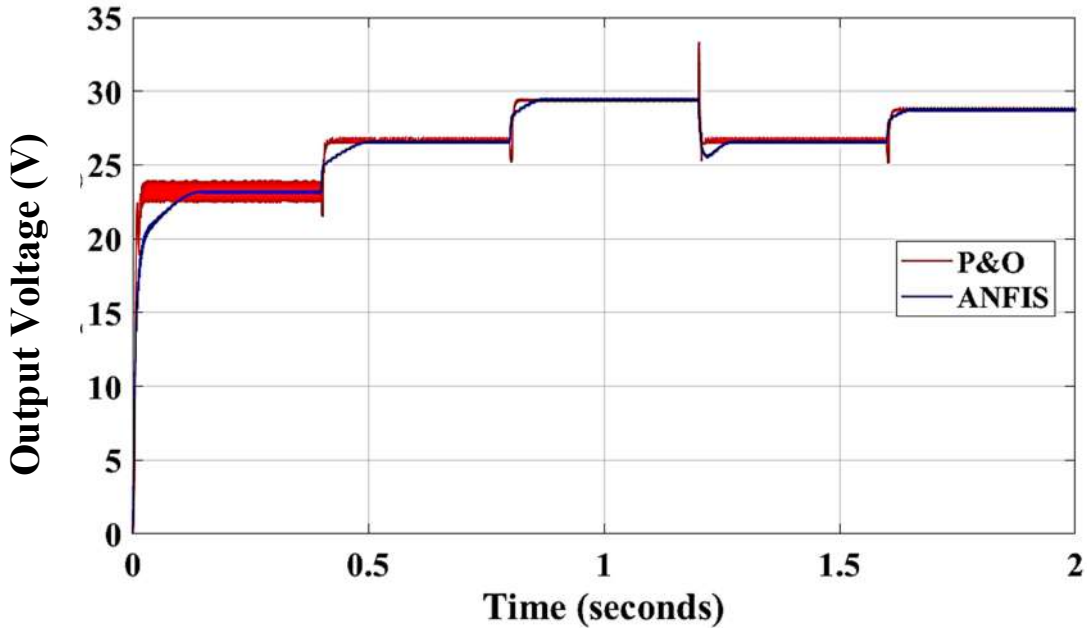


Figure III.19 Output voltage in stand-alone system with variable radiation.

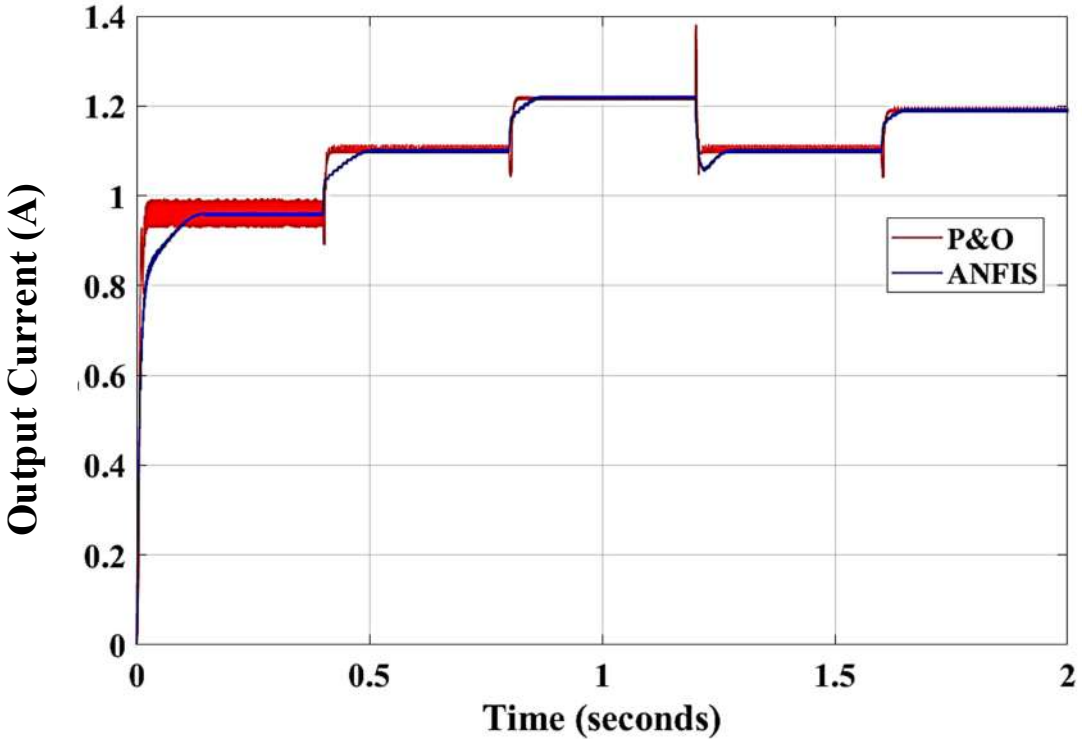


Figure III.20 Output current in stand-alone system with variable radiation.

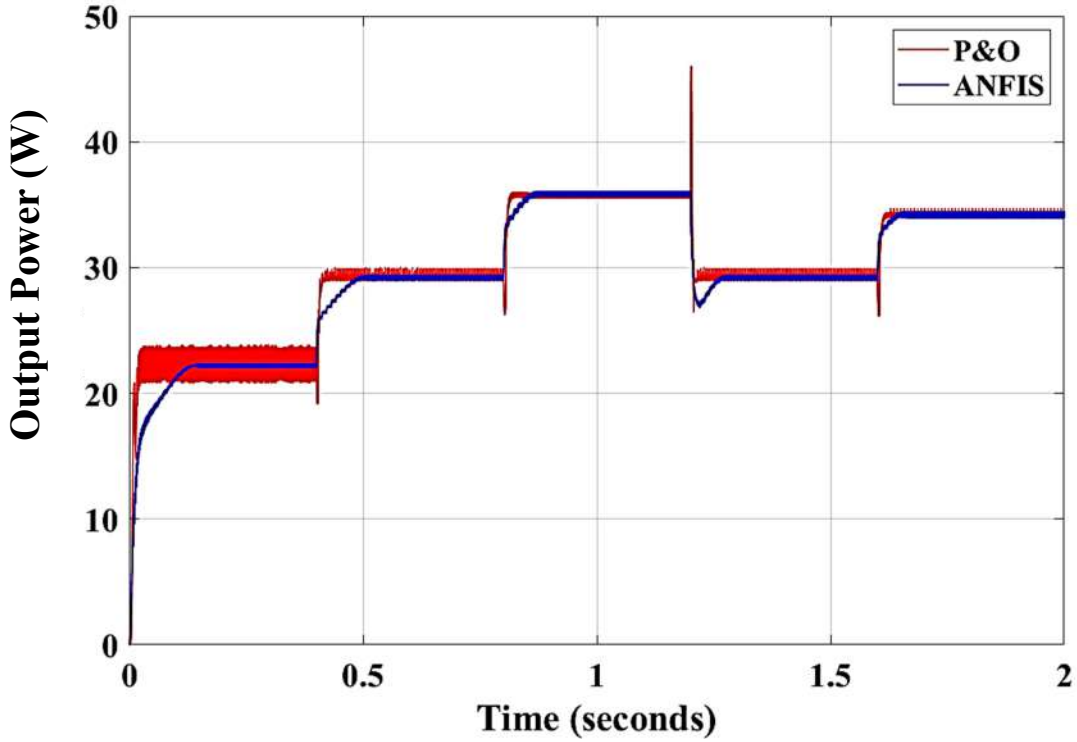


Figure III.21 Output power in stand-alone system with variable radiation.

The Figures (III.16-III.21) depict the simulation results in variable irradiance, where the P&O algorithm faces various problems in solar irradiance varying. The P&O has big oscillations where the changing of radiation levels compared to proposed ANFIS control. In 600, 800, and 950 W/m^2 the ANFIS control has efficiency of 97.34, 98.12, and 99.04 %. In contrary, the P&O algorithm has efficiency of 96.95, 97.88, and 88.98 %.

Table III.3 PV system connectivity to grid parameters.

Description	Value
Maximum power (P_{max})	213.15 W
Maximum voltage (V_{max})	29 V
Peak current (I_{max})	7.35 A
Voltage of open-circuit (V_{oc})	36.3 V
Current of short-circuit (I_{sc})	7.84 A
Number of series cell (N_{ser})	12
Number of parallels cell (N_{par})	42
Switching frequency (fs_boost)	5 KHZ
Grid frequency (f)	50 HZ
Inductance of boost (L)	1000 mH
Capacity of boost (C)	2000 mF
Inductance of filter (L_f)	500 µH
Capacity of filter (C_f)	18.37 µF
Rated power (P)	2.55 W

III.7.2. Simulation with PV system connectivity to grid

In this part, according to Figure III.22 the employing of ANN is the prediction of optimal voltage and current. The main role of FLC method is the control of dc in order to generate an active power of 100KVA in the grid.

Table III.3 gives the datas of considered PV system with connected to grid. The Figures (III.23-III.28) give the simulation results of PV power, output boost voltage, grid voltage and current, active and reactive power in constant radiation respectively.

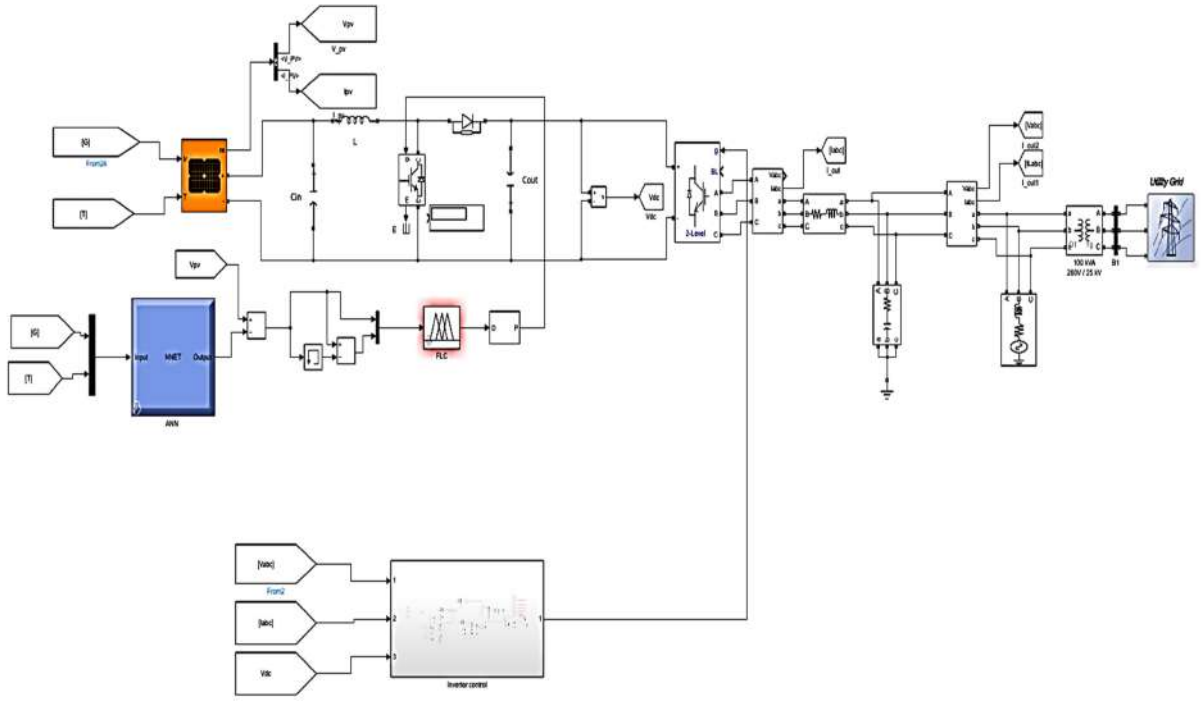


Figure III.22 Grid connected PV system employing MATLAB/Simulink.

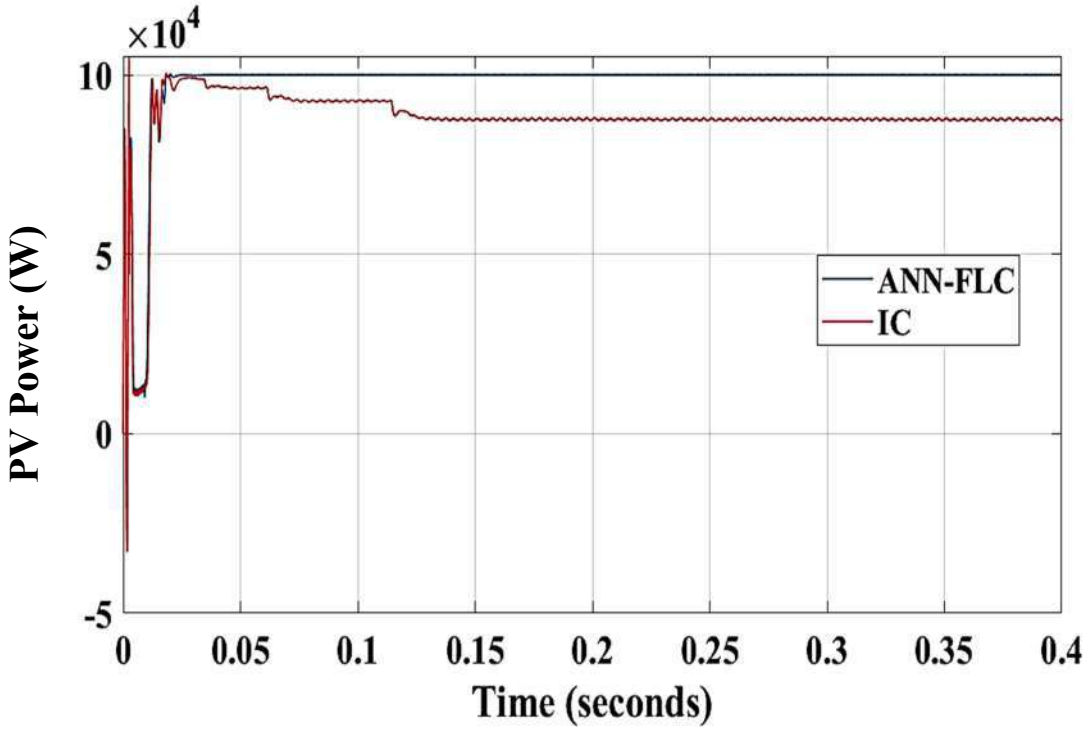


Figure III.23 PV power in PV system connectivity to grid at fixed radiation.

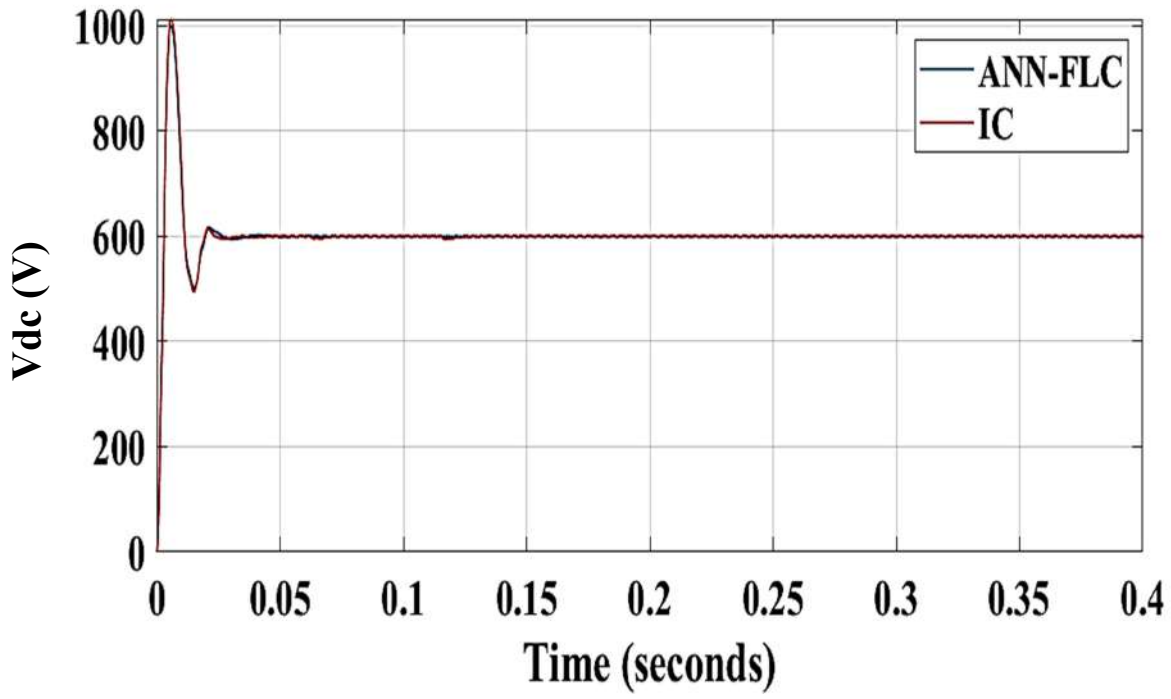


Figure III.24 Output boost voltage at fixed radiation.

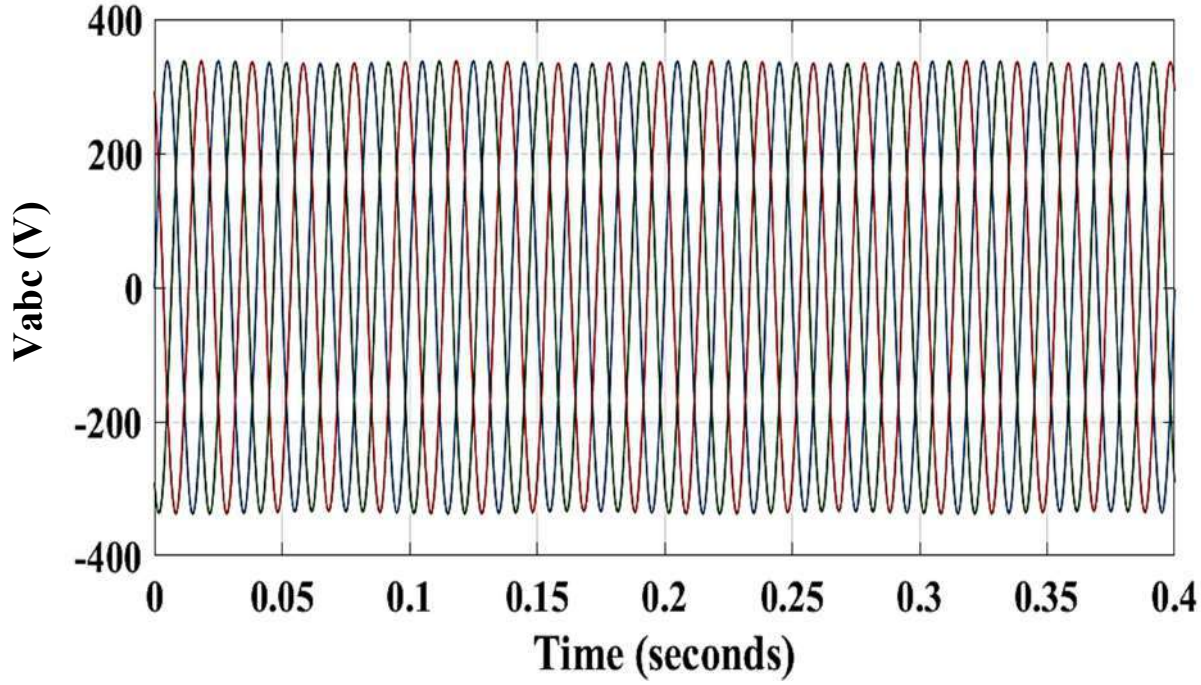


Figure III.25 Grid voltage at fixed radiation.

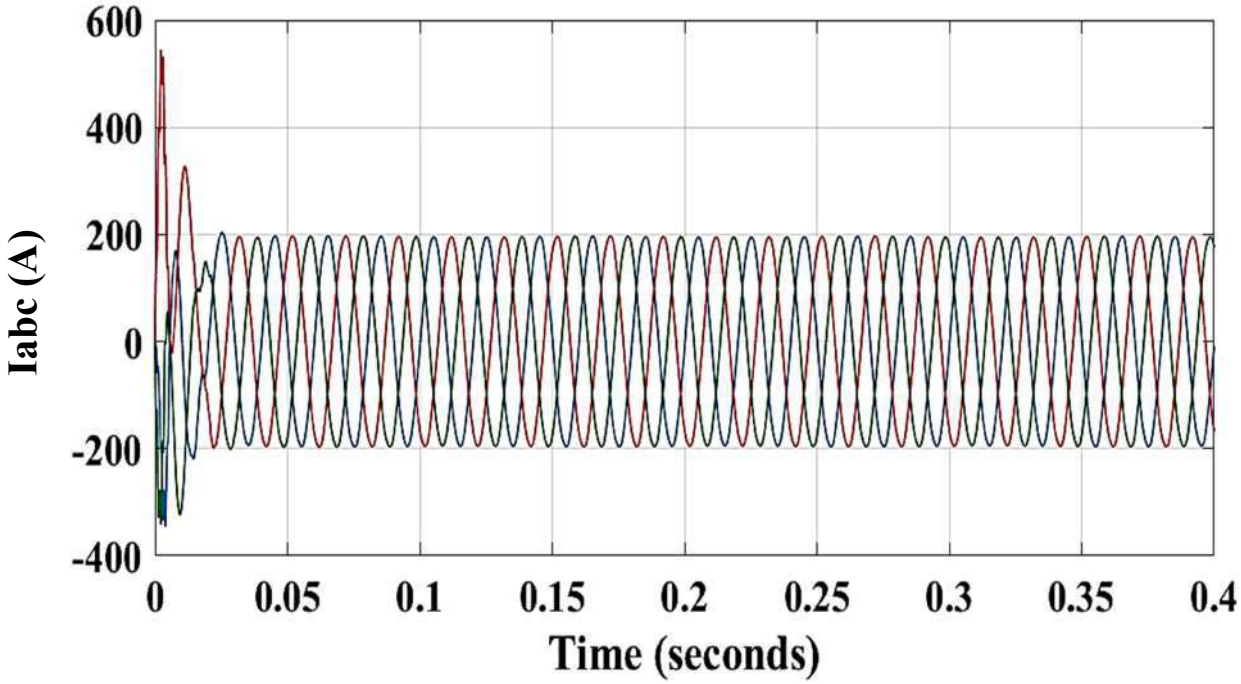


Figure III.26 Grid current at fixed radiation.

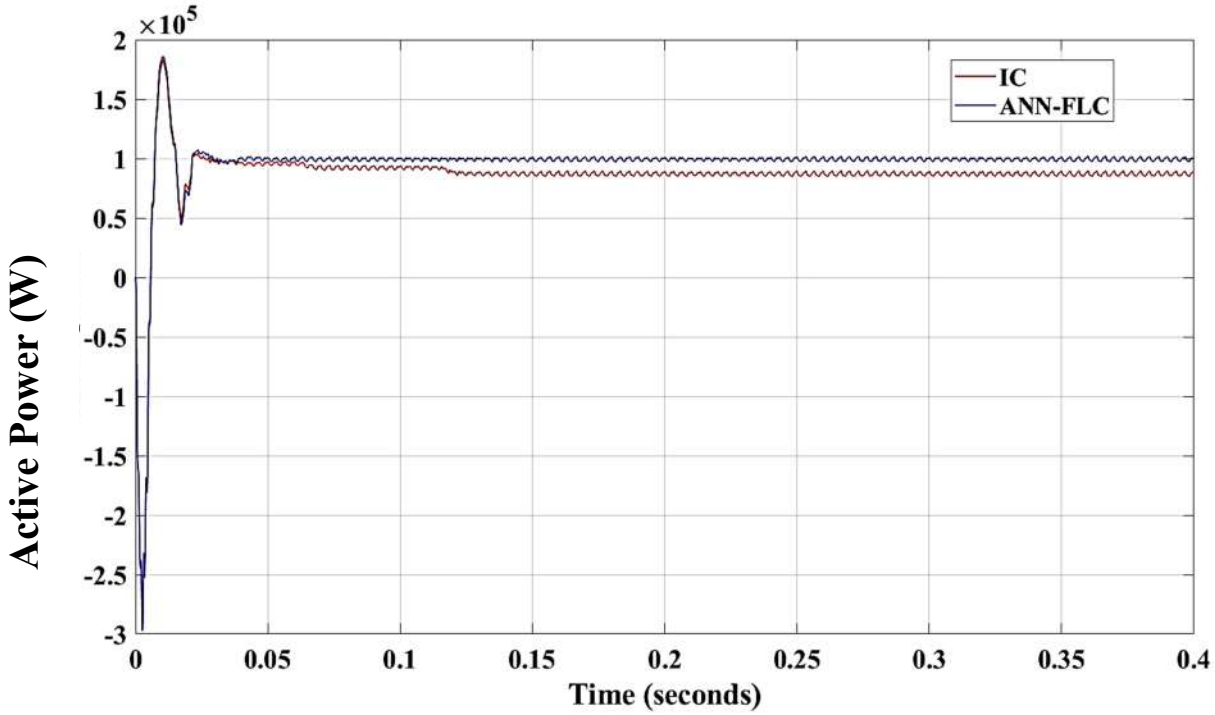


Figure III.27 Active power at fixed radiation.

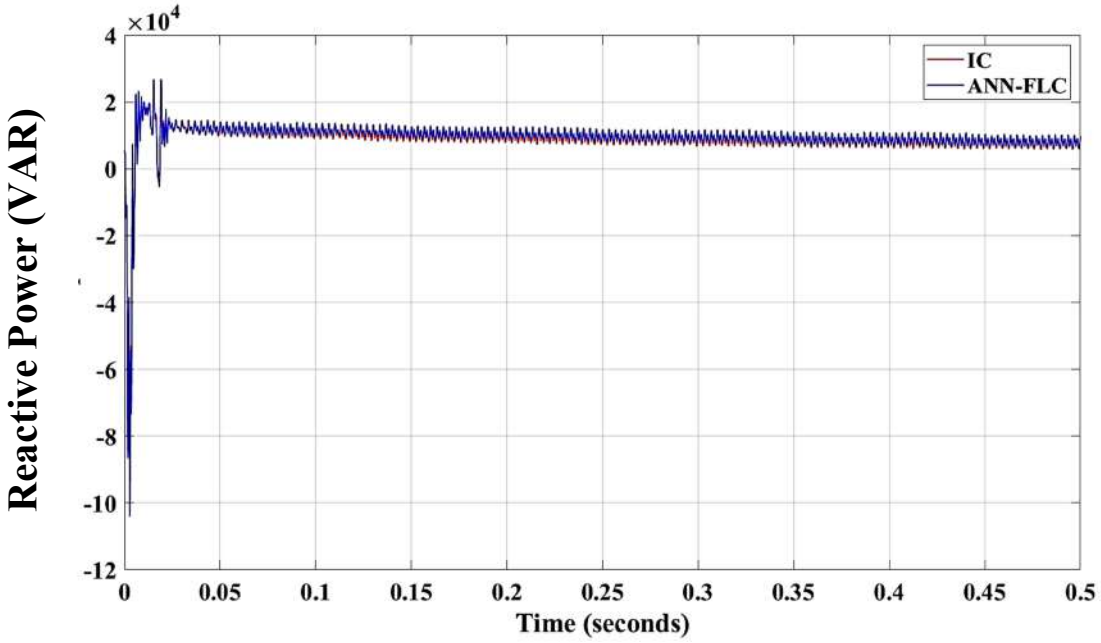


Figure III.28 Reactive power at fixed radiation.

As shown in previous figures, the proposed FLC-ANN give an active power of 100 KVA where the IC gives 89 KVA. In contrary, the reactive power is around 9200 VAR by using two studied MPPT. As shown in Figure III.29, the solar irradiance varies between 300, 700, 950 and 1000 W/m^2. The next Figures (III.30-III.35) depict the simulation results of PV power, output boost voltage, voltage and current in grid, active and reactive power respectively in variable irradiance.

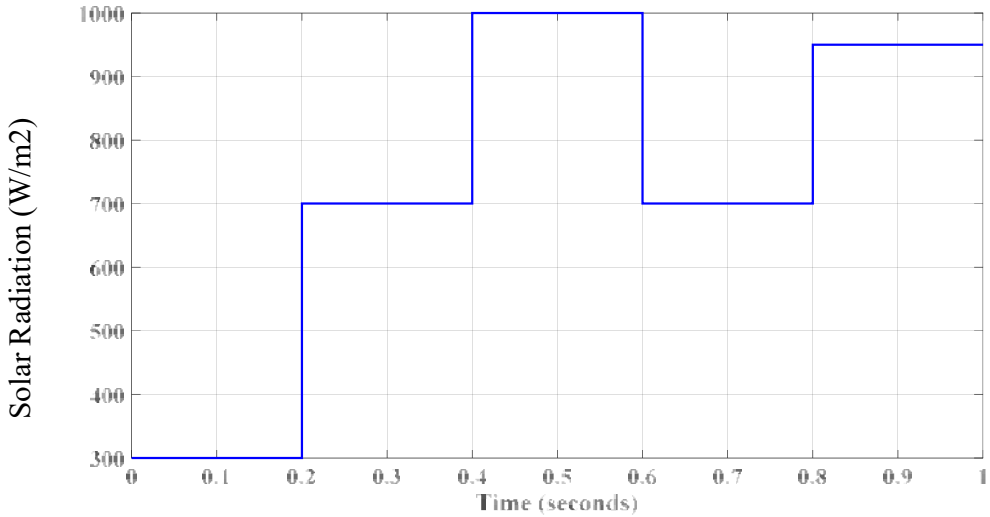


Figure III.29 Solar radiation profile in grid connected PV system.

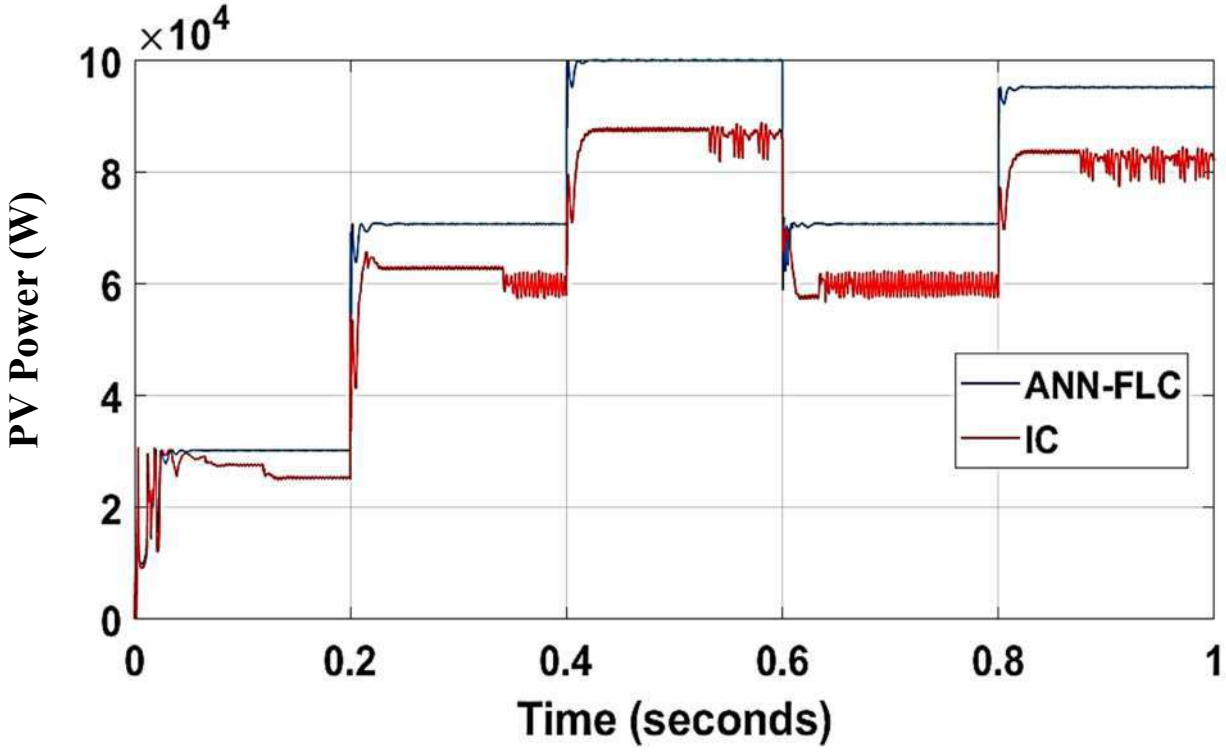


Figure III.30 PV power in PV system connectivity to grid at variable radiation.

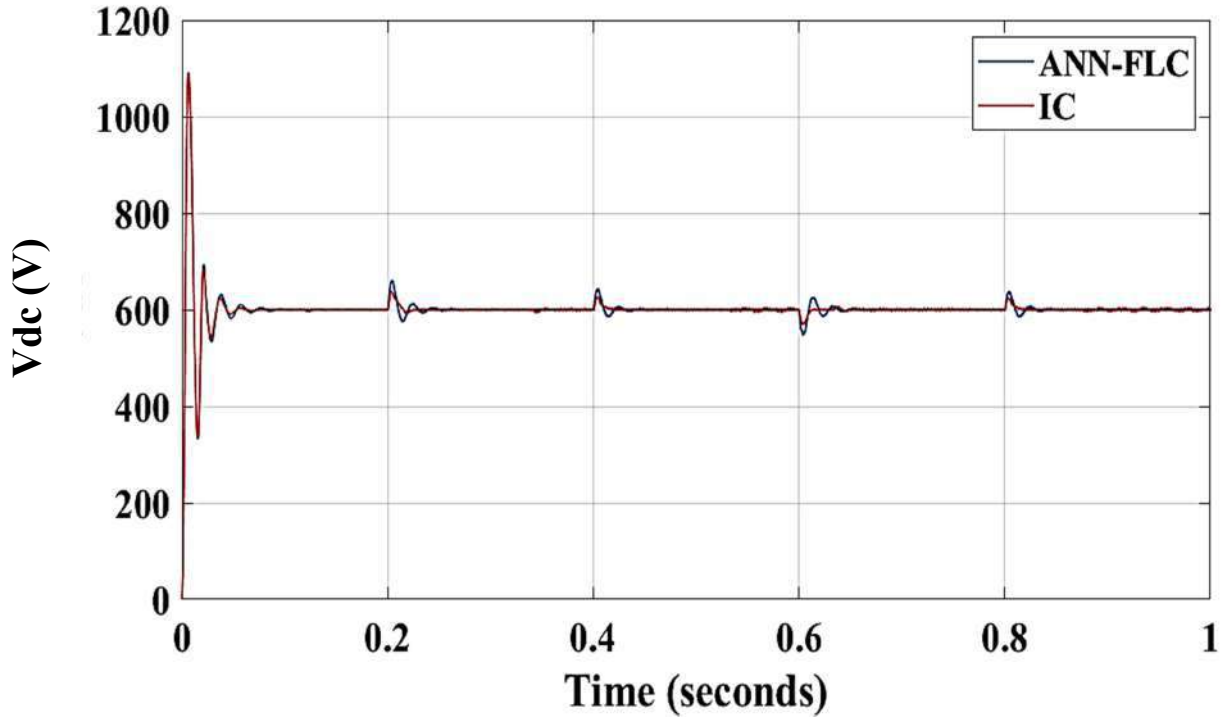


Figure III.31 Output boost voltage at variable radiation.

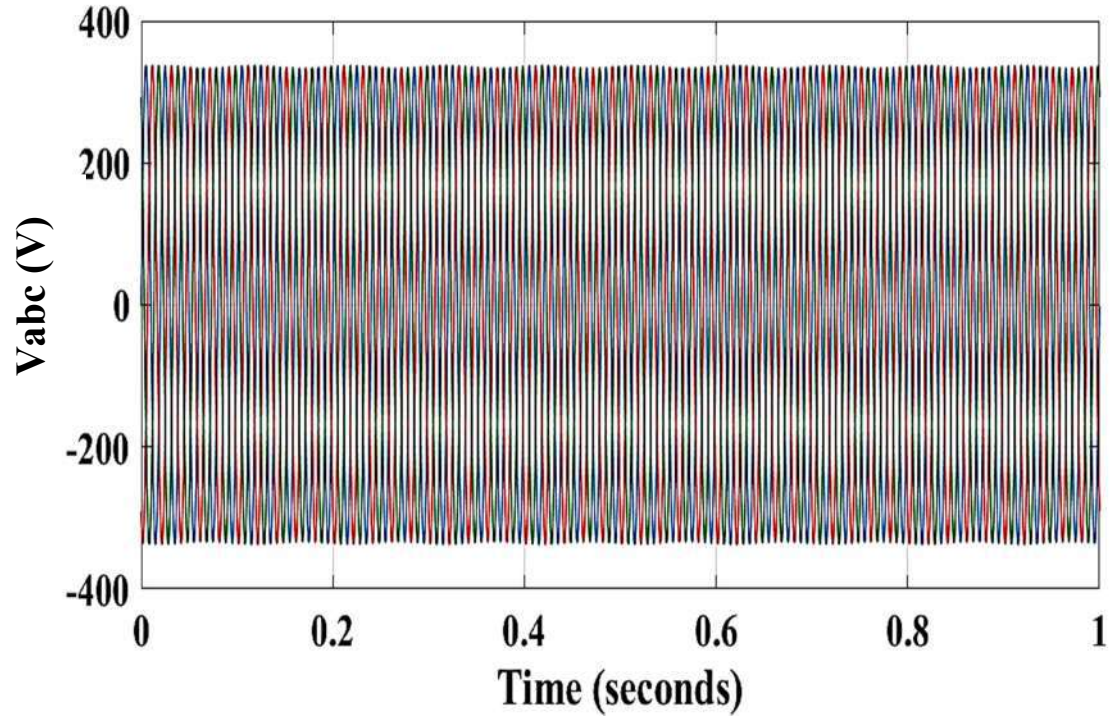


Figure III.32 Grid voltage at variable radiation.

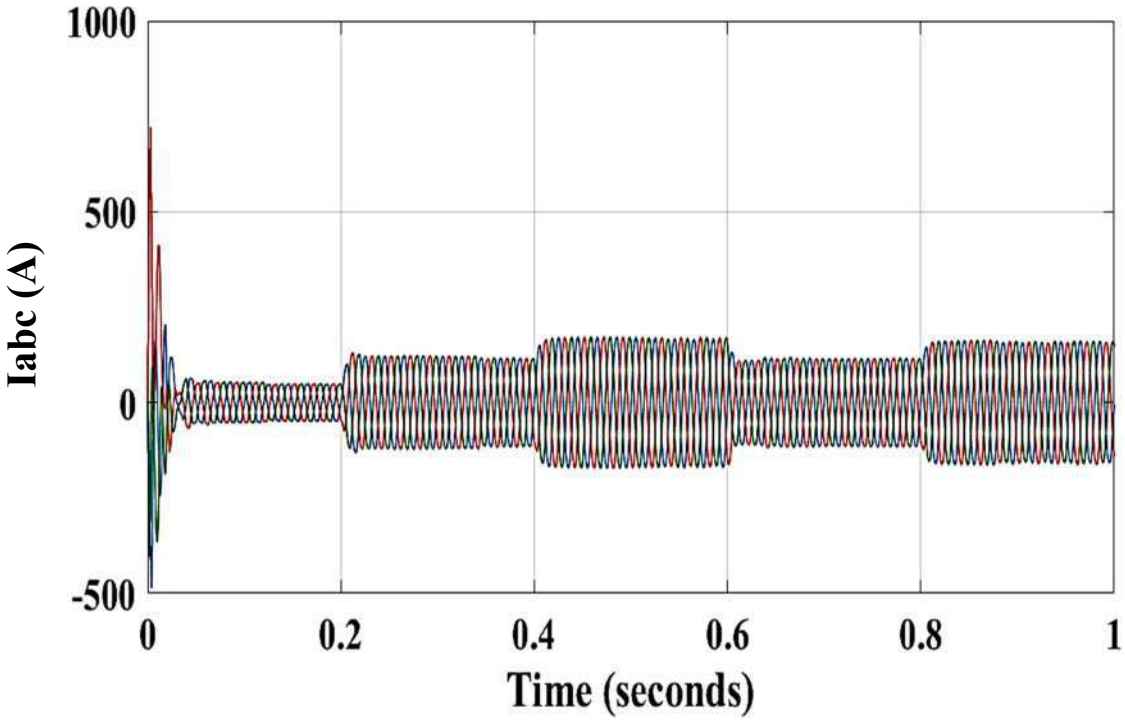


Figure III.33 Grid current at fixed radiation.

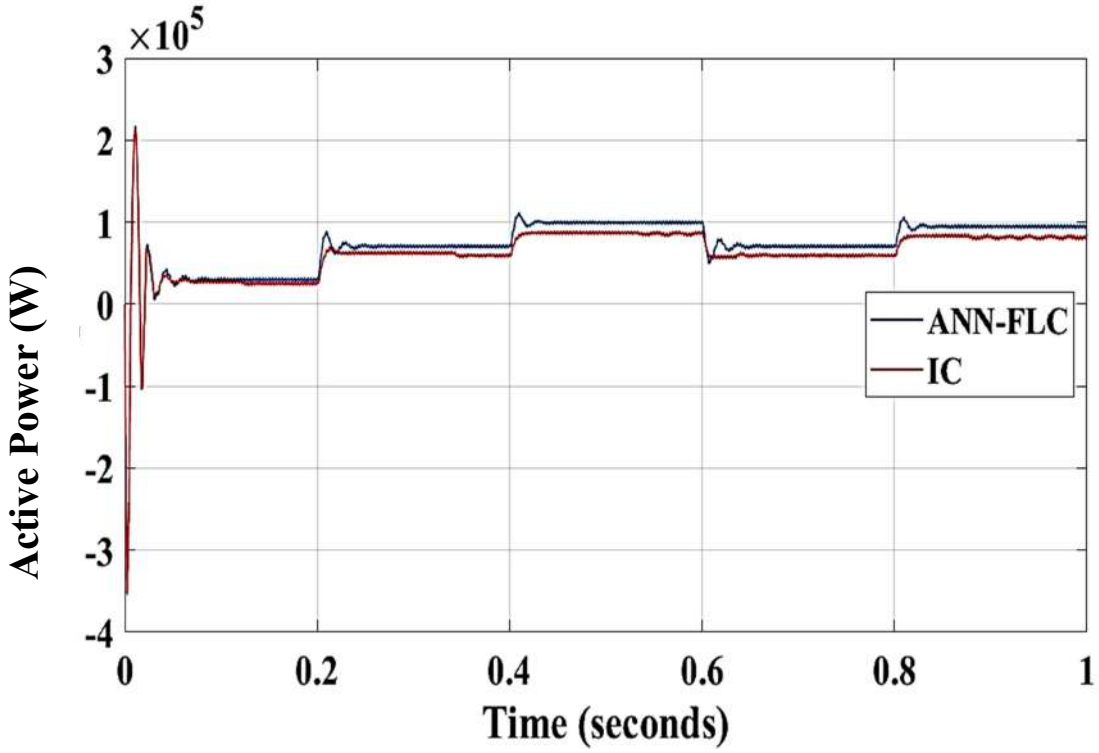


Figure III.34 Active power at fixed radiation.

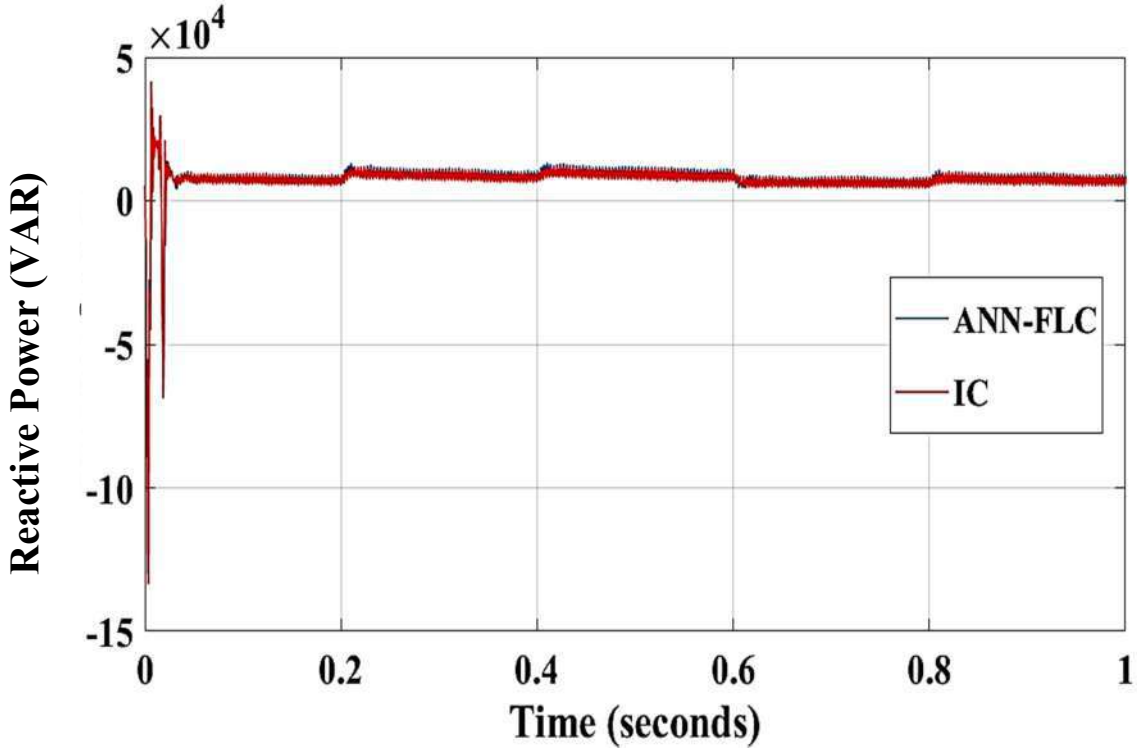


Figure III.35 Reactive power at fixed radiation.

As represented in Figure III.34, where irradiance solar equals 300 W/m^2, the active power is around 31868 VA by employing ANN-FLC comparing to IC which equals around 27305 VA. Where the radiation solar equals 700 W/m^2, by utilizing ANN-FLC based MPPT the active power is 70748 VA where its value is around 61920 VA. The active power values are around 95340 and 82644 VA by utilizing ANN-FLC and IC algorithm respectively at irradiance of 950 W/m^2.

III.8. Conclusion

In this chapter, we described various conventional and intelligent control of PV system and theirs effect in stand-alone system and with connected to grid. In stand-alone PV system, we were simulated and prove the effectiveness of ANFIS method which can follow the MPP smoothly. In contrary, the P&O control has high difficulty at variation in climate, this difficult affect to decreasing of efficiency. In grid connected, where the radiation changes in different levels the active power losses by using IC. By using ANN-FLC control, we can provide higher active power compared to use IC approach. The basic problem where work with FLC, ANN, and ANFIS is the mandatory of selecting precisely of database.

CHAPTER IV

METAHEURISTIC ALGORITHMS BASED MPPT OF A PV SYSTEM UNDER PSC AND MALFUNCTION CONDITIONS

IV.1. Introduction

PV system has many electrical faults, is necessary to proposed methods for detection the fault local. One of these methods based on statistical parameters in feature selection and NN type BP in classification section [186-188]. This chapter focuses on studying MPPT based on various metaheuristic algorithms for PV systems under PSC and the malfunction of the considered system. In contrast to previously studied intelligent controls, these approaches do not require large amounts of system command data. The P.V characteristic in PSC gives various LMPP and one GMPP [198-191]. For that, metaheuristic approaches can search the global solution smoothly compared to ANFIS, ANN, FLC, P&O, and INC techniques using the random selection of best solutions [192]. The GWO depends on the motion of greys in wild during the hunt process [40] [193]. PSO algorithm can find the best solution using by updating the movement and velocity of particles [194] [195]. The APSO has some behavior of PSO technique with adapting of PSO algorithm [196-198].

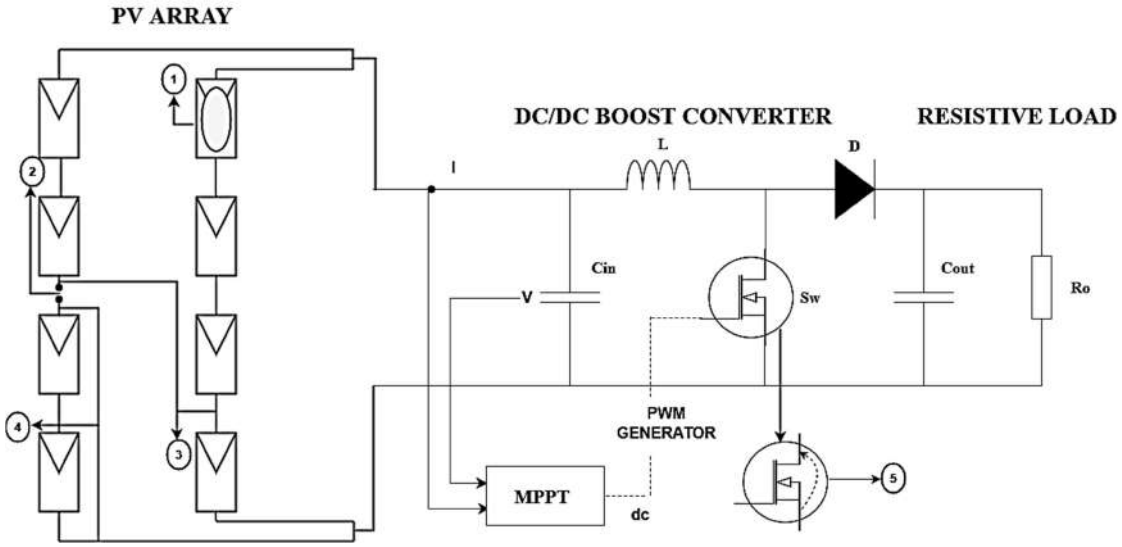


Figure IV.1 Different faults occurring in PV System.

IV.2. Diagnosis method

The studied PV system faces a various electrical fault a causing of varying in atmosphere, or bad implementation or other causes. Figure IV.1 describe five types of faults where (1)

represents SF, (2) is OCF, (3) and (4) present LLF and LGF respectively, (6) depicts converter switch fault [199-201].

As shown in figure IV.2, this work proposed a diagnosis method based on three steps:

- Collection of data from Simulink;
- Feature selection using statistical parameters and the dimension reduction by using PCA;
- Locate of fault using NN type BP.

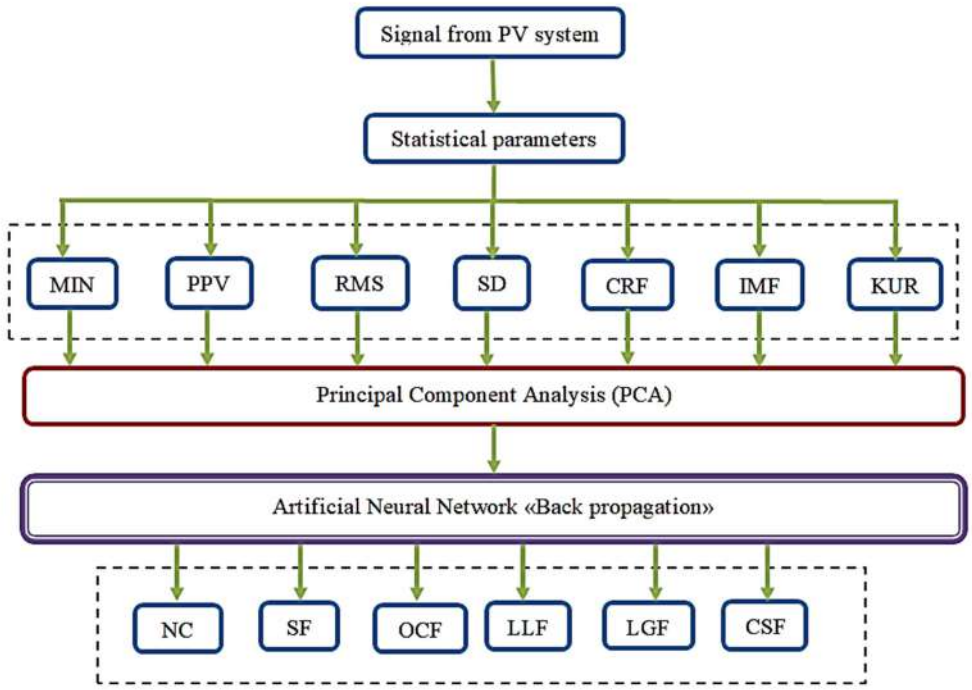


Figure IV.2 Proposed diagnosis method of PV system.

IV.2.1. Collection of data

For data collection 500000 datas of each PV system state (NC, LL fault, LG fault, SF, OCF, switching converter fault (SCF)), each 495000 datas have 99 signals, each signal has 5000 samples.

IV.2.2. Feature selection

In feature selection stage, the statistical parameters considered are given by the following

Equations [202] [203]:

- Minimum:

$$\mathrm{Min} = \min(\mathrm{Xc}) \tag{IV.1}$$

- The peak-to-peak value:

$$\mathrm{PPV} = \frac{1}{2}[\max(\mathrm{Xc}) - \min(\mathrm{Xc})] \tag{IV.2}$$

- The effective value:

$$\mathrm{RMS} = \sqrt{\frac{1}{\mathrm{N}}\sum_{\mathrm{i}=1}^{\mathrm{N}}\left(\mathrm{Xc(i)}\right)^2} \tag{IV.3}$$

- The standard deviation:

$$\mathrm{SD} = \sqrt{\frac{1}{\mathrm{N}}\sum_{\mathrm{i}=1}^{\mathrm{N}}\left(\mathrm{Xc(i)} - \overline{\mathrm{Xc}}\right)^2} \tag{IV.4}$$

- The crest factor:

$$\mathrm{CRF} = \frac{\mathrm{PPV}}{\mathrm{RMS}} \tag{IV.5}$$

- The impulse factor:

$$\mathrm{IMF} = \frac{\mathrm{PPV}}{\frac{1}{\mathrm{N}}\sum_{\mathrm{i}=1}^{\mathrm{N}}|\mathrm{Xc(i)}|} \tag{IV.6}$$

- Kurtosis:

$$\mathrm{KUR} = \frac{\frac{1}{\mathrm{N}}\sum_{\mathrm{i}=1}^{\mathrm{N}}\left(\mathrm{Xc(i)}-\overline{\mathrm{Xc}}\right)^4}{\left[\frac{1}{\mathrm{N}}\sum_{\mathrm{i}=1}^{\mathrm{N}}\left(\mathrm{Xc(i)}-\overline{\mathrm{Xc}}\right)^2\right]^2} \tag{IV.7}$$

With

Xc: Signal;

$\overline{\mathrm{Xc}}$: Mean of signal;

N: Total number of coefficients.

Principal Component Analysis (PCA) is a statistical technique used to reduce the dimensionality of large datasets while retaining the most significant information. It achieves this by transforming the original variables into a smaller set of uncorrelated variables called principal components, which are ranked according to the amount of variance they capture. By focusing on the components with the highest variance, PCA simplifies data interpretation and enhances computational efficiency, making it an effective tool for feature selection in fault diagnosis and other machine learning applications.

V.2.3. Locate of fault

The classification part focuses on used NN type BP is one of the successeful method for classify the fault class [204-206]. In this work, the training process requires 70% of datacollection, 15% in validation part, and 15% for test process. By using MATLAB software, 3 hidden layers is utilized each layer has 10 neurons and a 1000 iterations .

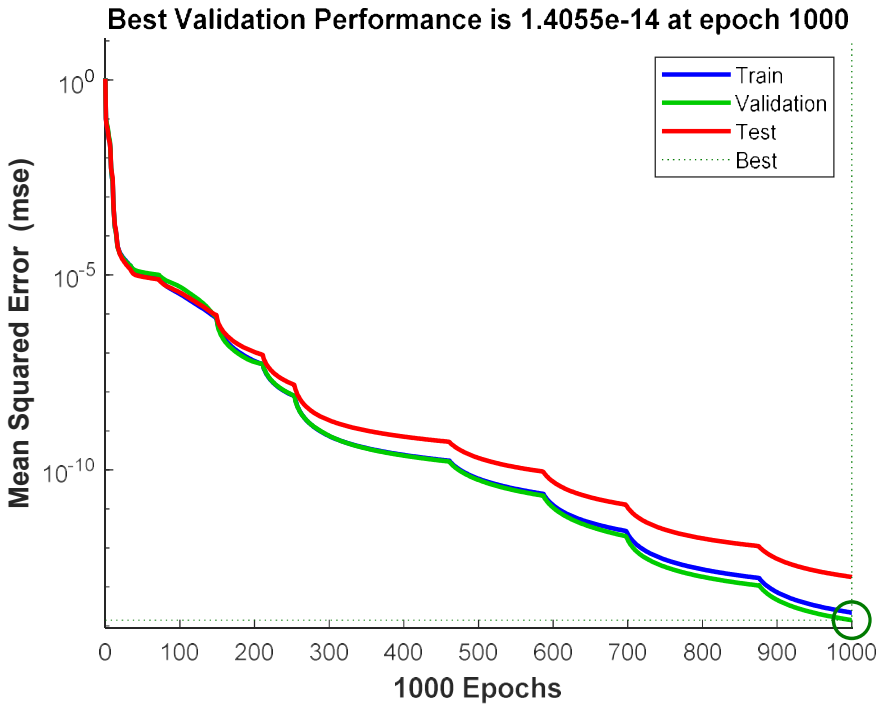


Figure IV.3 NN performance.

Figure IV.3 shows the utilized NN performance where the best MSE is 1.0455*10^(-14). The NN can classifier the locate of fault smoothly with a test accuracy of 98.2% (Figure IV.4).

IV.3. Metaheuristic method based MPPT

In this chapter, three metaheuristic algorithms were proposed in order to follow the MPP under different fault scenarios and variation climatic. The PSO algorithm was used to select the optimal dc under NC and four fault scenarios. The APSO algorithm was proposed to track the MPP under PSC and CSC conditions by a comparative study with a GWO, PSO, ANFIS, FLC and P&O approaches.

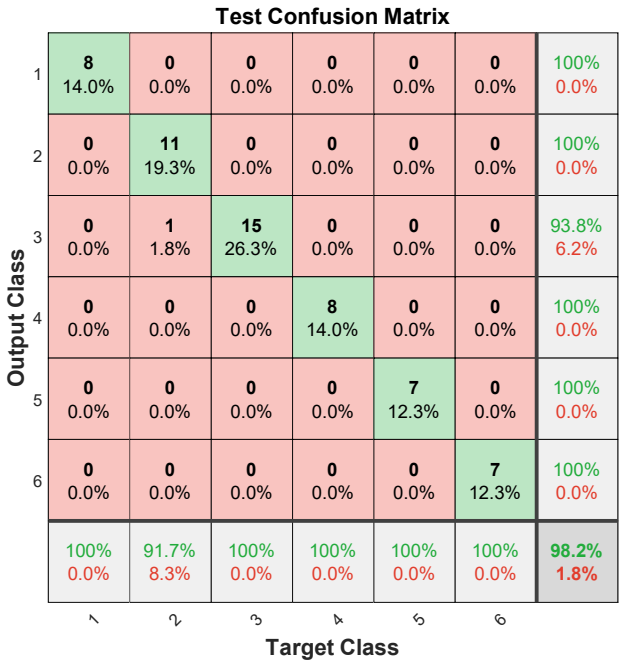


Figure IV.4 Confusion maatrix.

IV.3.1. Grey wolf optimization (GWO)

In 2014, Mirjalili, an academic, presented GWO, a novel meta-heuristic optimization algorithm. It mimics the pack hierarchy and predatory behavior of grey wolves, whereby members follow orders from the pack leader and use techniques including encircling, hunting, and attacking to bring in their prey. Based on the outcomes, this is a massive search algorithm that prioritizes the top three grey wolves [207]. This optimization process is more flexible and has a greater global search capacity since GWO does not have an elimination mechanism. In

other words, if a grey wolf is moving to a worse area than it is now, it still needs to arrive. Generally speaking, it is simple to use, requires few parameters, and can be implemented with ease. Numerous researchers have focused on it, and their efforts have yielded numerous findings. The GWO technique is divided into three stages [207] [208] (Figure IV.5):

IV.3.1.1. Encircling

Finding the prey's location is the primary focus of the first stage of GWO. The method starts by roaming the search space as if the prey's location were unknown, thinking it would be close to the best answer. As part of their hunting strategy, after they pinpoint the location of their prey, they surround it. The area around solutions is scouted by grey wolves [207].

$$D_p = \left|R.G_p(k) - G_{gwo}(k)\right| \quad (IV.12)$$

$$G_{gwo}(k+1) = X_p(k) - H.D_p \quad (IV.13)$$

With

$$H = 2\vec{\alpha}.\overrightarrow{r_1} - \vec{\alpha} \quad (IV.14)$$

$$R = 2.\overrightarrow{r_2} \quad (IV.15)$$

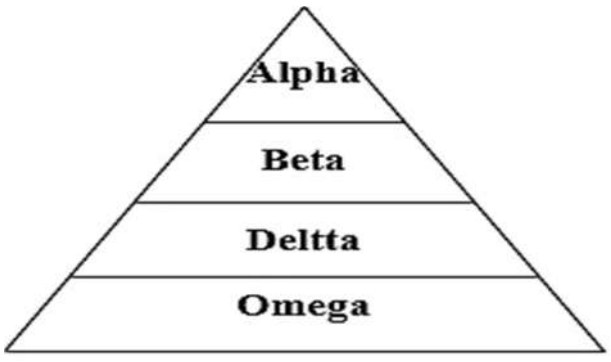


Figure IV.5 Grey wolf's hierarchy (dominance increasing from down to top) [207].

Where the alpha wolves represent the best candidate solutions in the population, the beta serves as a backup leader in the hierarchy, the Deltaa wolves are the third-best solutions, the Omega represent the rest of the population.

IV.3.1.2. Haunting

Mathematically, the wolves' haunting behavior is replicated by supposing that a, β, and δ have a better understanding of the prey's location. Consequently, as shown in Figure IV06, the remaining wolves ʊ follow the best answer provided by a, β, and δ. These equations characterize the wolf pack's hunting behavior [207]:

$$\begin{cases} D_{alpha} = \left|C_{1gwo}G_{alpha} - G_{gwo}(k)\right| \\ D_{beta} = \left|C_{2gwo}G_{beta} - G_{gwo}(k)\right| \\ D_{delta} = \left|C_{3gxo}G_{delta} - G_{gwo}(k)\right| \end{cases} \quad (IV.16)$$

$$\begin{cases} G_{1gwo} = G_{alpha}(k) - H_1 D_{alpha} \\ G_{2gwo} = G_{beta}(k) - H_2 D_{beta} \\ G_{3gwo} = G_{delta}(k) - H_3 D_{delta} \end{cases} \quad (IV.17)$$

$$G_p(t+1) = \frac{G_{1gwo}+G_{2gwo}+Ggwo_3}{3} \quad (IV.18)$$

IV.3.1.3. Attacking

When their prey stops moving, the wolves know it's time to start attacking, marking the conclusion of the hunting phase [207].

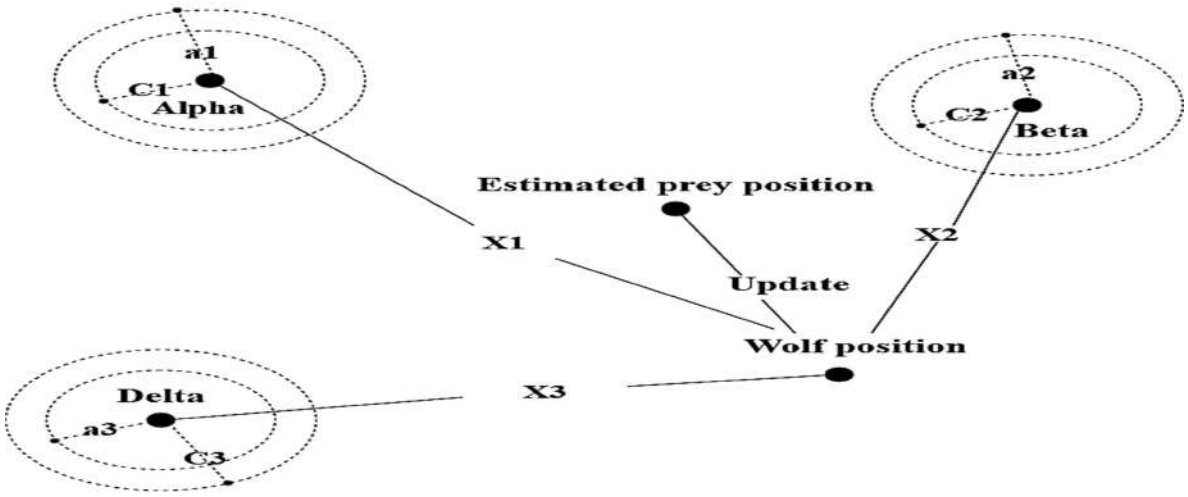


Figure IV.6 Position updating in GWO [207].

In PV system, the dc is characterized as a gray wolf in order to apply the GWO-based MPPT. Thus, may be altered in the manner shown below [40] [209] [210]:

$$dc_i(k+1) = dc_i(k) - H.dc \quad (IV.19)$$

Therefore, the GWO algorithm's fitness function is expressed as after this:

$$P\big(dc_i(k)\big) > P\big(dc_i(k-1)\big) \quad (IV.20)$$

Where P present the power, i is the current wolves number, k is iteration number.

IV.3.2. Particle swarm optimization (PSO)

As an alternative to conventional genetic algorithms, Kennedy and Eberhart created particle swarm optimization (PSO), a parallel optimization method. The coordinated motions of swarms of insects, schools of fish, or flocks of birds serve as an inspiration for these algorithms. Particle swarm algorithms seek for optimization solutions in the same way that these creatures move in swarms to locate food or escape predators [211].

Particles refer to the algorithmic units, whereas swarms denote the population as a whole. Based on its best neighbor and its own experience here, the recollection of the best place it encountered a particle selects its next step in this algorithm. You may describe this neighborhood geographically, like the distance between two particles' places in the real world, or sociometrically, like an individual's position in a swarm. The three inclinations that will determine the particle's new velocity and directions are: the tendency to pursue one's own route, the tendency to return to one's best position obtained, and the tendency to travel towards one's best neighbor. Data that is either discrete or continuous may be processed using particle swarm techniques. Various knowledge extraction tasks have been carried out using particle swarm techniques. The new position and velocity are calculated as follow (Figure IV.7) [212-215]:

$$x_i(k+1) = x_i(k) + v_i(k+1)\,\hat{Y}_i \quad (IV.21)$$

$$v_i(t+1) = w.v_i(t) + C_1 r_1[P_{BST} - x_i(k)] + C_2 r_2[G_{BST} - x_i(k)] \quad (IV.22)$$

With:

w: Inertia weight.

(C_1, C_2): Cognitive and social constants;

$(r_1, r_2) \in [0\ 1]$: Random numbers;

(G_{BST}, P_{BST}): Particles.

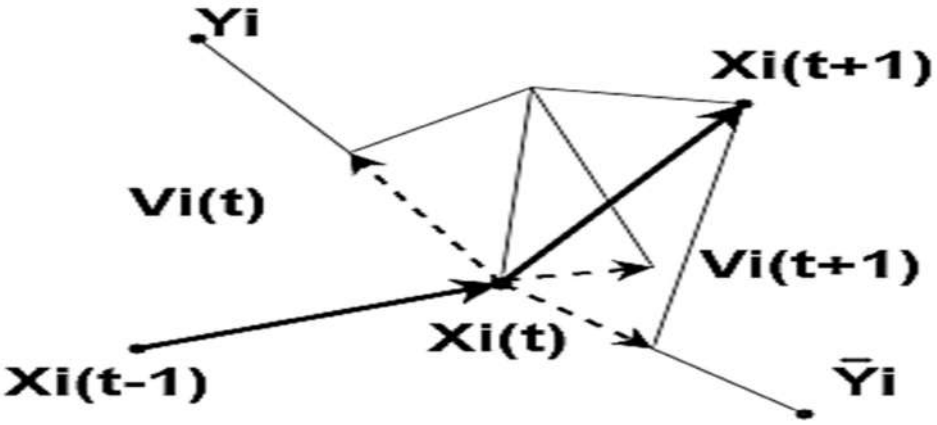


Figure IV.7 Particle motion while optimization.

For utilizing the PSO as a control technique it's necessary to track following step [216] [217]:

- Initialization of the coefficients C_1 and C_2, the inertia coefficient w;
- The formation of the starting population randomly and the computation of the fitness of each particle (P_{besti}): the best location of particle i in the present population; (P_{gbest}): the best position in all populations (the best of the best);
- Calculation of the new speed and new location of each particle;
- Calculation of the best fitness of the original population and compare with the prior one to determine the best of all the populations (P_{gbest});
- Increase of the number of iterations $k = k + 1$;
- If a halting requirements is fulfilled then advance to the next step. Otherwise, move to the 3rd step;
- The location reported in (P_{gbest}) is the ideal solution.

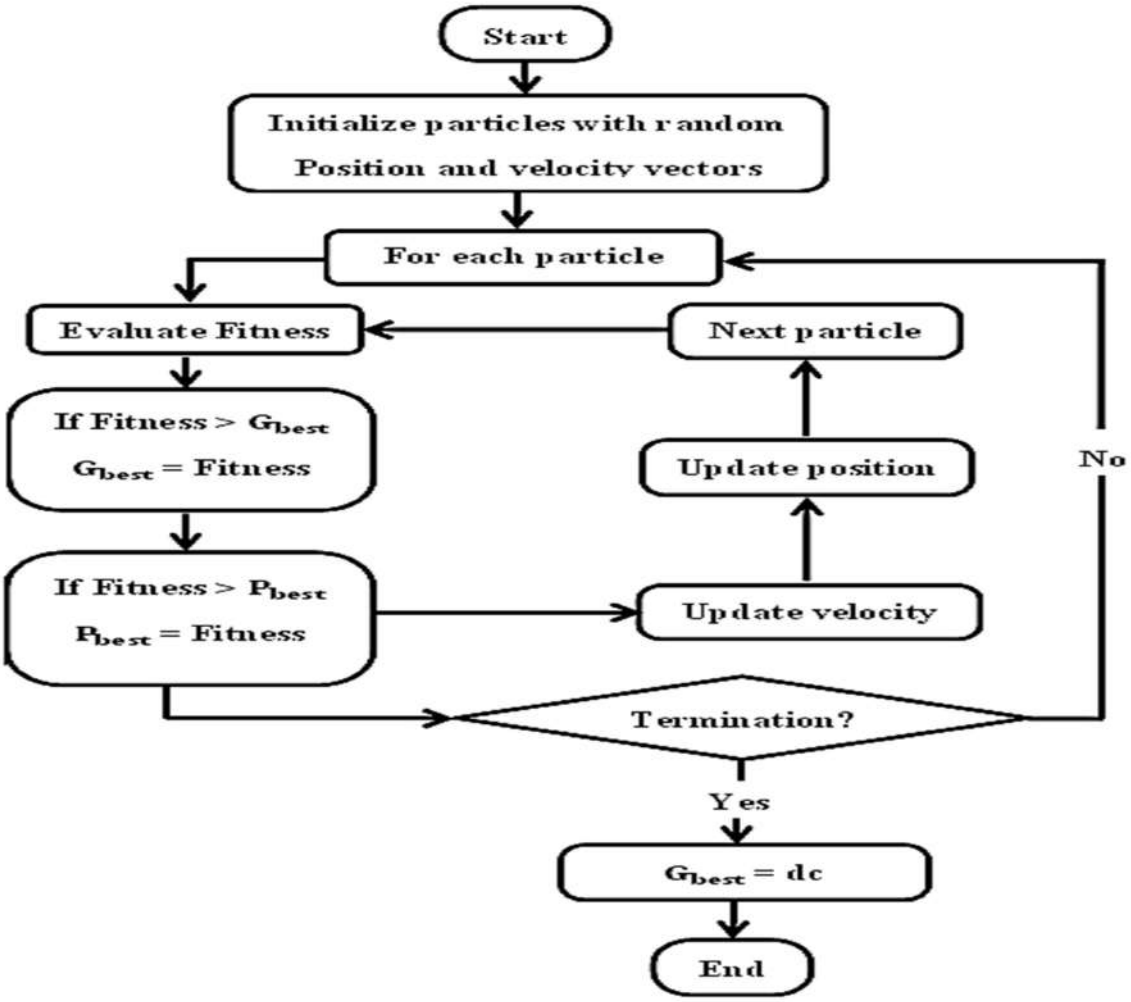


Figure IV.8 PSO flowchart**.**

In PV system, the PSO is widely employed for track the MPP especially in the conditions of partial and complete shading or in presence of any exterior fault. For that, to control the dc is obligatory to utilize its flowchart that is presented in Figure IV.8 [217].

IV.3.3. Adaptive particle swarm optimization (APSO)

When the PSO parameters are inaccurate, the PSO algorithm struggles to find the optimal dc, particularly in the initial state, because these values influence the selection of the next position $x_i(k+1)$ and the required speed of this displacement, $v_i(k+1)$. Following the same basic idea as the PSO approach, the APSO method outperforms both the PSO and MPP methods in terms of weather agnostic performance and robustness to variations in solar radiation [218].

IV.3.3.1. Adaptive inertia weight

The weight of inertia w determines the value of the particle's movement speed, as it is directly proportional to it. The higher the value of w, the greater the speed, and vice versa. But this made it difficult to come up with an accurate global solution. Therefore, the relationship w must be mixed linearly and non-linearly as shown in Equation IV.23 [219] [220].

$$w = \begin{cases} w_{max} & 0 \le \frac{K}{T} \le 0.1, \\ w_{min} + \frac{(w_{max} - w_{min})}{e^{-w_{min} + e^{-1.2 + \frac{20K}{T}}}} & \text{else} \end{cases} \quad (IV.23)$$

Where k and T present current and maximum iteration number.

IV.3.3.2. Adaptive acceleration coefficients

Usually, in traditional PSO the Cognitive and social constants C_1 and C_2 are fixed. Although it is often left constant in most previous work, adaptive adjustment may generally improve algorithm performance by increasing the particles' capacity to find the ideal solution. We use the non-linear approach together to have C_1 progressively fall from 2.5 and C_2 gradually rise from 0.5. This increases search variety, ensures that particles swiftly achieve the global optimum solution, and prevents them from sliding into the local optimal by making it more likely that particles will find the ideal solution based on their own experience in the early iteration phase. In the subsequent iterative process, the particles' high local search capacity and population experience make them more likely to choose the best solution, which allows for finer-grained adjustments to the global optimal solution's accuracy and faster convergence. Equations 4 and 5 demonstrate the particular methods of adjusting the acceleration coefficients C_1 and C_2, respectively [221-223].

$$C_1 = 0.5 * (C_{1max} - C_{1min}) \left(\frac{K}{T}\right)^2 + C_{1min} \quad (IV.24)$$

$$C_2 = 0.5 * (C_{2max} - C_{2min}) \left(\frac{K}{T}\right)^2 + C_{2min} \quad (IV.25)$$

In PV system, the APSO have some behavior like a PSO for selecting the optimal dc but with dynamic values of PSO parameters.

IV.4. Simulation results of studied metaheuristic method

Table IV.1 represents values of all parameters which defines the employed PV array and boost converter in this section. In ANFIS method, 250 epochs is used in this process. For PSO approach, $C_1$and $C_2$are equal 2, w is 0.99. 1000 iterations for the GWO, PSO and APSO techniques.

Table IV.1 Characteristics of PV cell and boost converter.

Description	Value
Maximun power (P_{max})	320.399 W
Voltage at maximun power (V_{max})	40.1 V
Current at maximun power (I_{max})	7.99 A
Voltage of open-circuit (V_{oc})	49.5 V
Current of short-circuit (I_{sc})	*8.6*A
fs_boost	5 KHZ
Inductor boost L	781 µH
Input capacitor C_{in}	25F
Output capacitor C_{out}	118µF

IV.4.1. Simulation under different fault system

In this part, by employing 4 modules in series and 2 in parallel, we were suggested the effectiveness of PSO algorithm to control the required dc compared to ANFIS, ANN and IC algorithms.

IV.4.1.1. Without faults

Figure IV.9 depicts the simulation results of output power where the PV system doesn't face any problem. The PSO algorithm gives a required power near of a 2000 watt, ANFIS and ANN controls also give some value with short problem in theirs curbs. The IC has big oscillations.

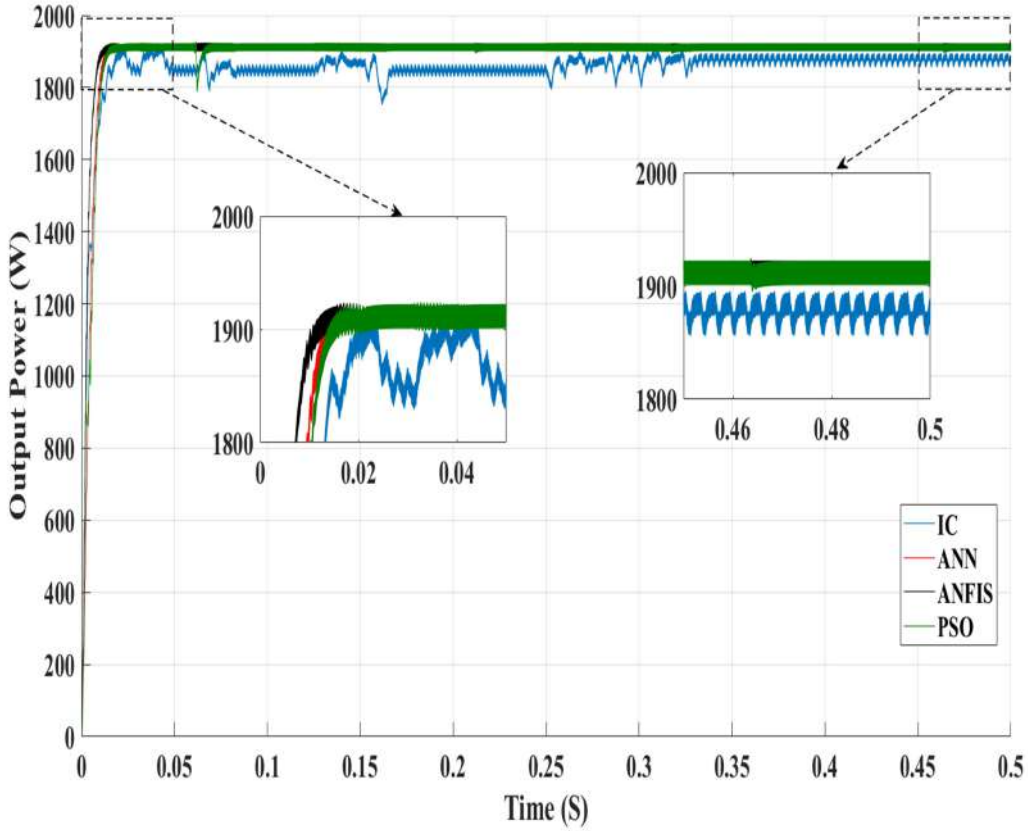


Figure IV.9 Output power without faults.

IV.4.1.2. Shade fault (SF)

Figure IV.10 proves the good behavior of PSO algorithms under SF which gives a value of 1920.7 watts in for output power. The ANFIS and ANN methods give an output power of 1911.4 watts. In contrary, the IC has big oscillations and generates less power in output.

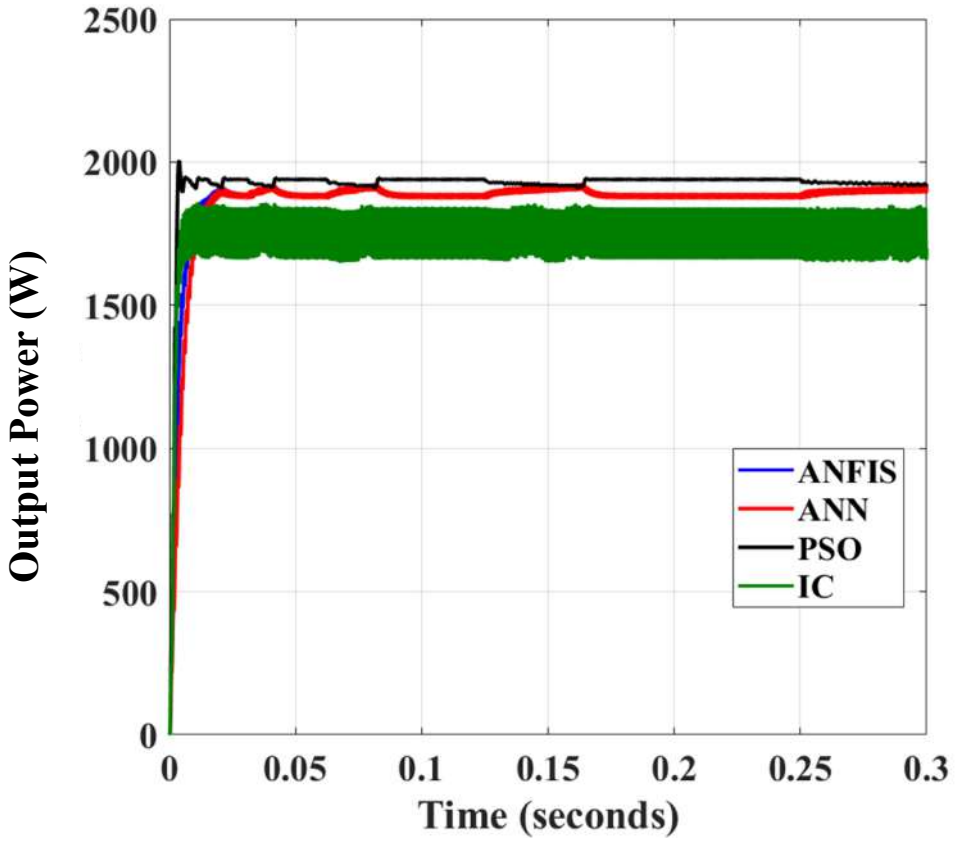


Figure IV.10 Output power under SF.

IV.4.1.3. Open circuit fault (OCF)

In OCF, the PSO approach can give a 1236.6 watt as output power smoothly. The ANSIF control generates 1209 watt compared to ANN which gives power of 1902.8 watt in output. In this state also, the IC algorithm produces the load by less power with oscillations in its curb and an overshoots (see Figure IV.11).

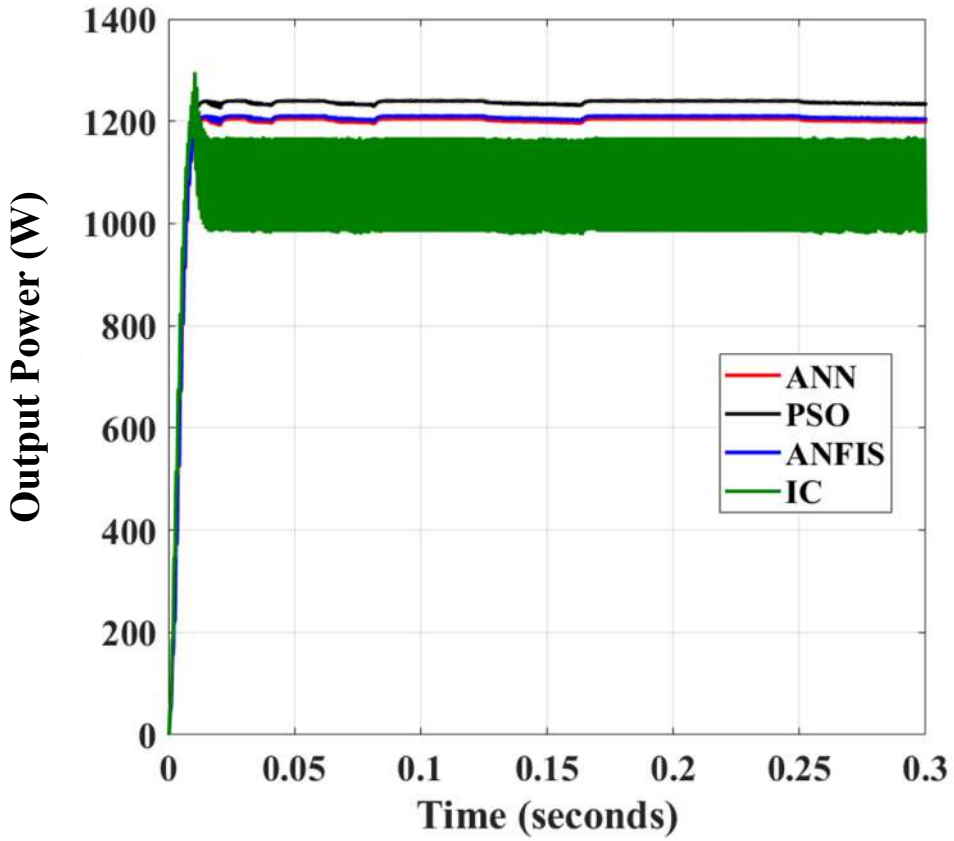


Figure IV.11 Output power under OCF.

IV.4.1.4. Line to line fault (LLF)

As shown in Figure IV.12, where utilized the PSO algorithm based MPPT the output power value is near to 1628 watt. In other hand, the ANFIS and ANN can be generating a 1623 and 1620 watt respectively. Without any variation, the IC approach give the lees power.

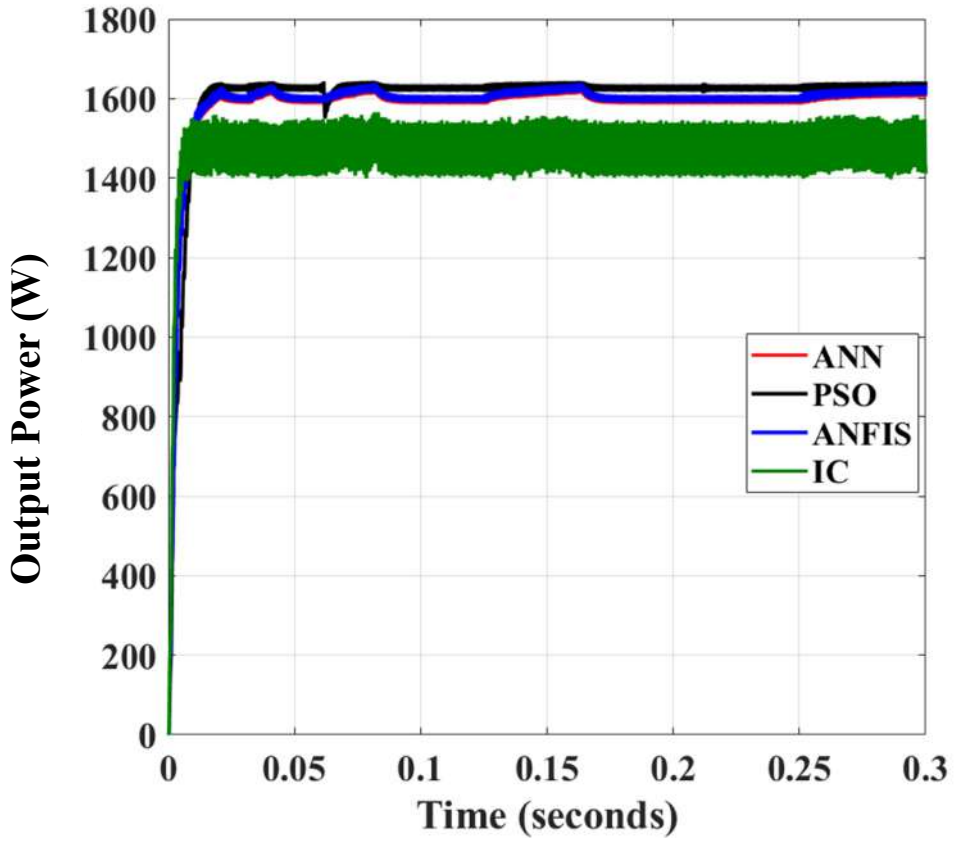


Figure IV.12 Output power under LLF.

IV.4.1.5. Line to ground fault (LGF)

In LGF state, all used approaches based MPPT follow the MPP without any oscillations. The PSO control generates an output power value near to 1212 watt. The ANFIS and ANN techniques produce the load by a power of 1199 and 1194 watt respectively. The IC technique gives an output power of 1154 watt (Figure IV.13).

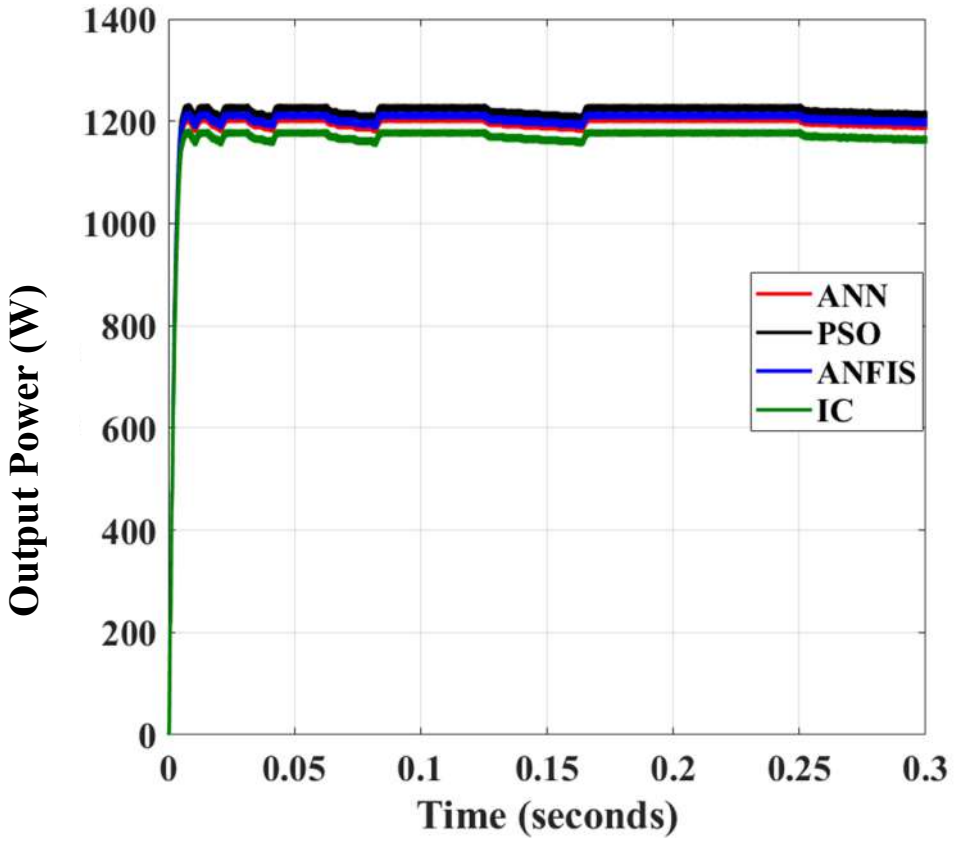


Figure IV.13 Output power under LGF.

IV.5.2. Simulation under PSC

Figure IV.14 describes the four state of studied PV system under PSC and CSC. In this section, we employed the APSO algorithms for selecting the required dc.

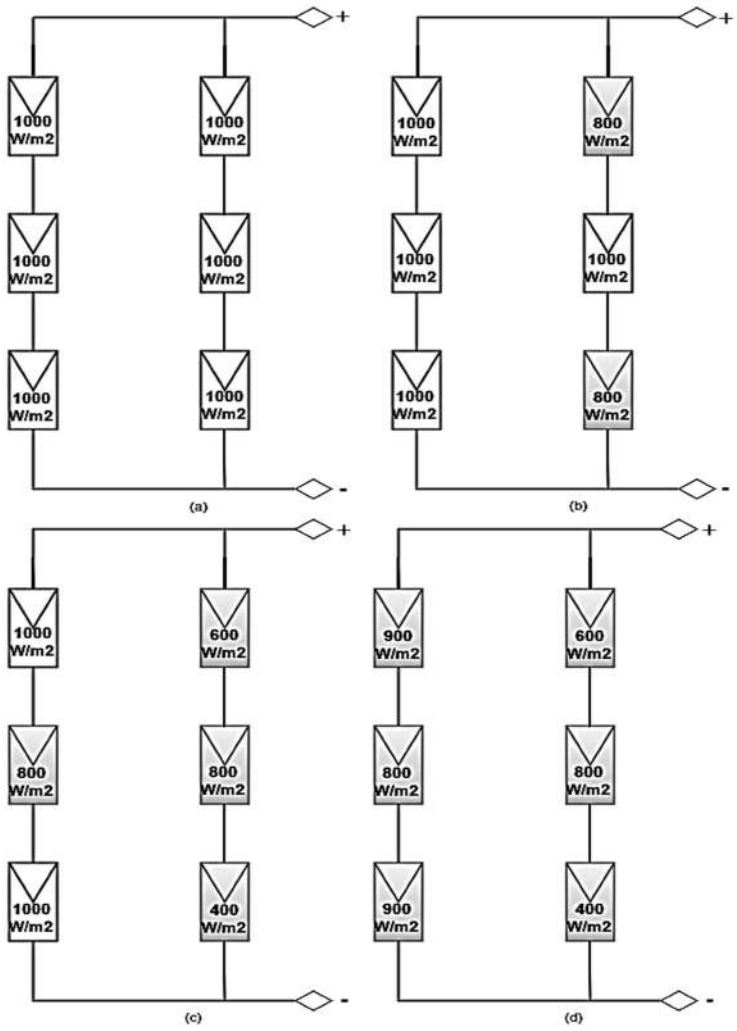


Figure IV.14 State of PV system (a) NC, (b) PSC1, (c) PSC2, (d) CSC.

IV.5.2.1. Normal condition (NC)

While the first solution uses an alternate signal form to provide 1922.5 W, APSO, ANFIS, and FLC easily provide the required power.

Within a time range of 0.05936 to 0.069041 seconds, the PSO method experiences a brief power failure of 133.91 W.

The greatest power loss estimate is 125.3 W, and the oscillation period of GWO is between 0.01412 and 0.17124 seconds.

In contrast to other approaches, P&O has longer oscillation duration of 0.013813 to 0.32988 seconds and a maximum power loss of 120.6 W. A perfect score of 99.97% is achieved by all methods (see Figure IV.15).

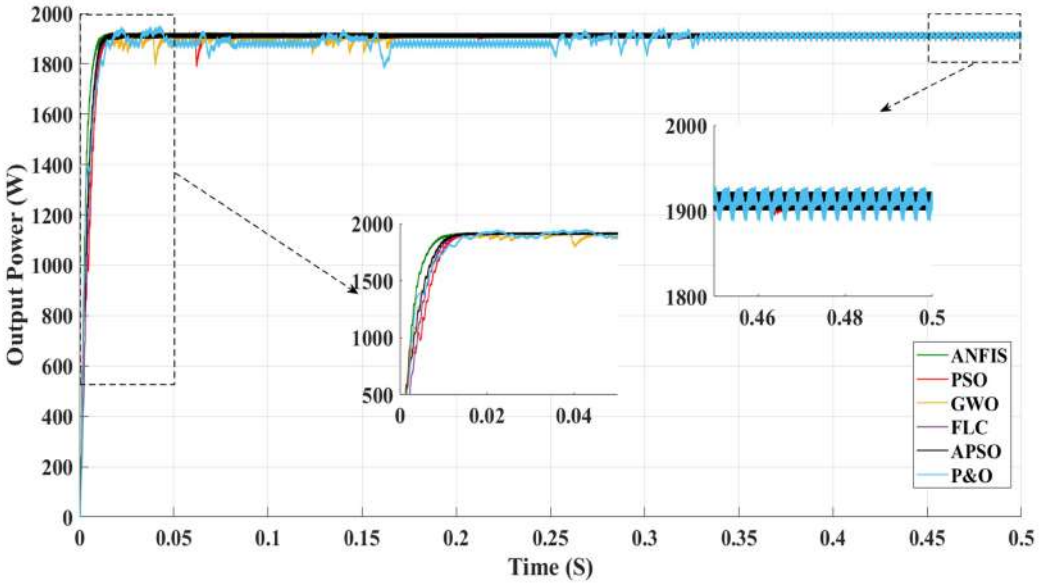


Figure IV.15 Output power under NC.

IV.5.2.2. Partial shading condition 1 (PSC1)

In this mode, the P&O can produce 1662.5 watts with a brief oscillation and mediocre efficiency. FLC and ANFIS also have brief oscillations, and 1690.5 watts may be created. Output power utilizing MPPT based on PSO or GWO comes at 1737 watts, the GWO monitors the MPP with numerous oscillations and a lengthy period of 0.3868 seconds. The ideal option in this scenario is adopting APSO, which operates without oscillation or other difficulties and has improved efficiency. The signal of output power applying current approaches is presented in Figure IV.16.

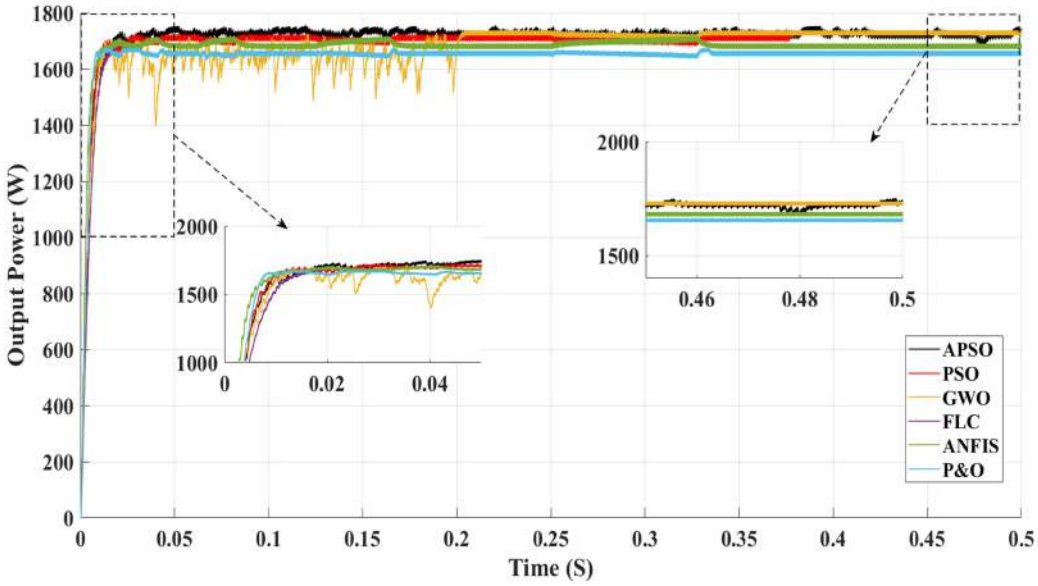


Figure IV.16 Output power under PSC1.

IV.5.2.3. Partial shading condition 2 (PSC2)

The behavior of approaches tested for this situation is depicted in Figure IV.17 The P&O method produces an output power of 1420 watts with a small disturbance before 0.32472 seconds. In addition, the signal of power takes an overshoot of 8.24% at an instant of 0.01364 seconds. When applying the FLC approach, the output power is created with a brief oscillation like a P&O but without overshoot and a value of 1425 watts. ANFIS functions like the FLC, but with an output power of 1443 watts. The next technique is MPPT based on the GWO algorithm, which has oscillations from start to end of 0.09116 seconds and 1451 watts in the output power. The PSO and APSO algorithms produce excellent results, although with a brief oscillation in the beginning with an output power of 1458.5 and 1478 watts, respectively.

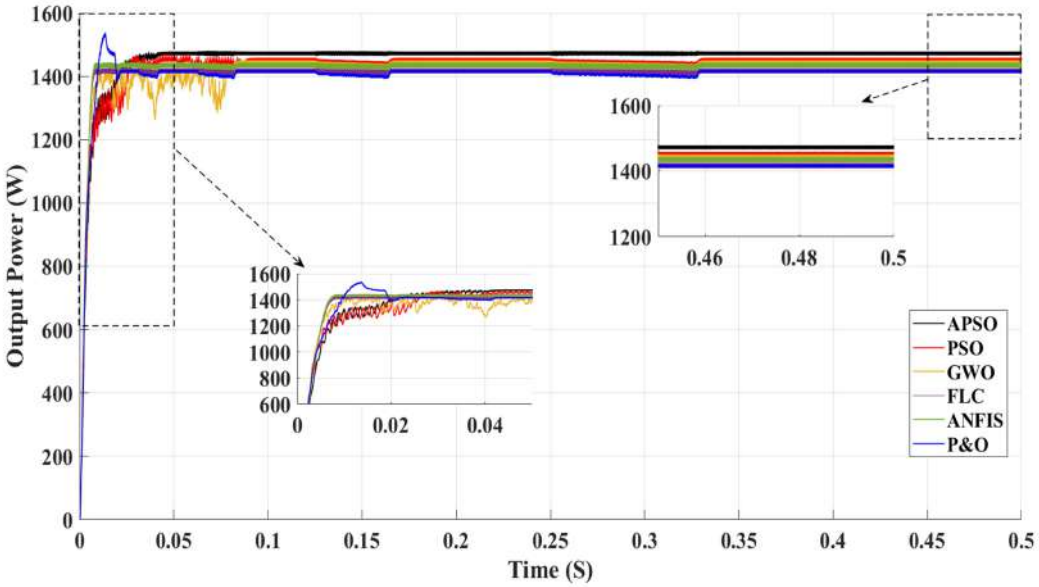


Figure IV.17 Output power under PSC2.

IV.5.2.4. Completely shading condition (CSC)

The P&O in this situation may create 1350 watts with brief overshoot and oscillations with terrible efficiency, after 0.3343 seconds the signal of output power employing P&O starts to settle. The FLC strategy delivers 1370 watts with a brief oscillation in the beginning, The ANFIS technique creates 1380 watts without any overshoot or oscillations but the reaction time may be noticed. The MPPT based on PSO, GWO, and APSO may be supplied 1400 watts but with changes in the form of signals. PSO method has some oscillations compared to APSO, in the time period between 0.009255 and 0.39264 seconds the GWO operates with lengthy oscillations. The APSO algorithm monitors the MPP with excellent results (see Figure IV.18).

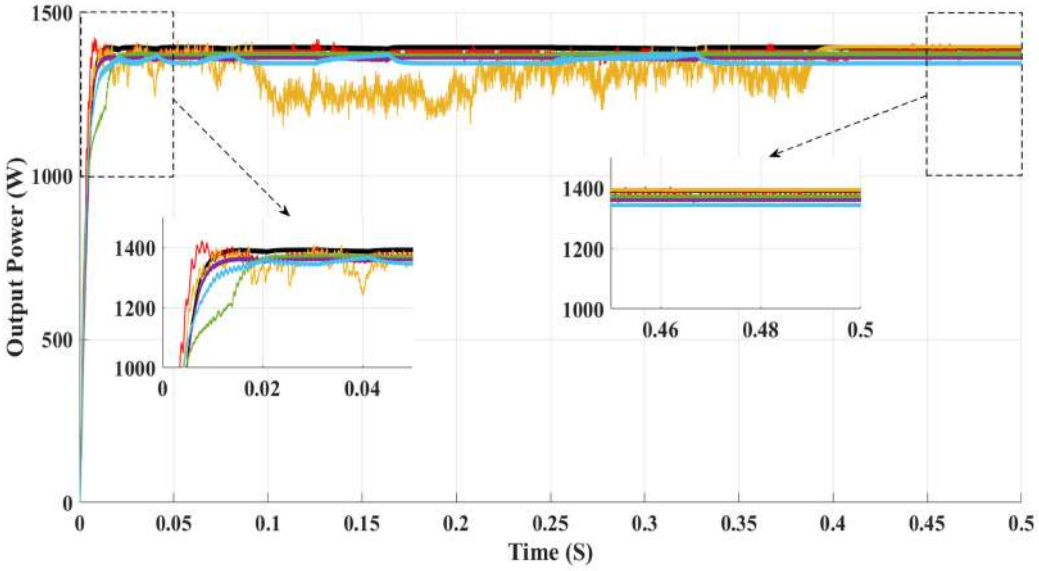


Figure IV.18 Output power under CSC.

The simulation findings validate the usefulness of MPPT based on APSO which has excellent behavior under diverse variable conditions. The PSO and GWO algorithms also may offer output power numbers extremely near when employing APSO but with numerous issues particularly in the beginning. Table IV.2 displays the efficiency of each strategy under various settings.

Table IV.2. Efficiency of different MPPT studied.

Techniques	P&O	FLC	ANFIS	GWO	PSO	APSO
NC	99.97 %	99.97 %	99.97 %	99.97 %	99.97 %	99.97 %
PSC1	98.32 %	98.72 %	98.72 %	99.57 %	99.57 %	99.66 %
PSC2	97.98%	98.46 %	98.48%	98.52 %	98.60 %	98.65 %
CSC	94.88%	95.83 %	95.87 %	95.96 %	95.96 %	95.96

IV.6. Conclusion

In this chapter, we propose firstly an approach based on NN type BP to diagnosis fault of PV system. This approach has successful results for detect and locate the electrical fault in PV system. Secondly, the metaheuristic algorithms can track the MPP under PSC and malfunction system conditions smoothly without need a big system datasets. For that, we were proposed the PSO algorithm based MPPT of PV system under various electrical faults. The APSO control is proposed of PV system under PSC and CSC conditions as comparative study with PSO, GWO, ANFIS, FLC and P&O controls. The obtained results proved the successful and effectiveness of metaheuristic method comared to classical and intelligent techniques.

GENERAL CONCLUSION AND PERSPECTIVE

GENERAL CONCLUSION AND PERSPECTIVE

This thesis highlights the potential of advanced control strategies to improve the efficiency and reliability of photovoltaic (PV) systems, addressing the challenges posed by environmental variations and operational conditions.

Solar energy, as a sustainable resource, has proven to be a viable alternative to fossil fuels, offering simplicity in implementation and compatibility with diverse energy demands. However, issues such as partial shading conditions (PSC) and electrical faults pose significant obstacles to optimal energy generation.

The research presented in this thesis is structured around four key objectives. First, the fundamental components of PV systems were analyzed, emphasizing the impact of environmental factors, particularly PSC, on power generation.

The study demonstrated the superiority of intelligent MPPT techniques, such as ANFIS, over traditional methods like Perturb and Observe (P&O), particularly in stand-alone systems under varying climatic conditions. Second, a combined ANN-FLC control method was proposed for grid-connected systems, effectively predicting optimal voltage and ensuring robust performance compared to incremental conductance (IC) methods.

Third, fault diagnosis in PV systems was addressed through a systematic approach involving data selection, feature extraction using wavelet transform and PCA, and classification via neural networks. This process enabled accurate detection of system faults and informed the implementation of advanced MPPT techniques, such as PSO and APSO, to maintain system performance.

Finally, the effectiveness of metaheuristic algorithms including Grey Wolf Optimization (GWO), particle swarm optimization (PSO), and adaptive PSO was validated through simulations under PSC. Among these, APSO demonstrated the highest efficiency, overcoming the limitations of traditional PSO methods.

The findings of this research were validated using MATLAB/Simulink simulations, showcasing the practical applicability of the proposed techniques. By integrating intelligent and metaheuristic approaches, this work provides a comprehensive framework for enhancing the performance and resilience of PV systems. Future research could explore real-time implementations and the integration of emerging technologies to further advance renewable energy solutions.

REFERENCES

REFERENCES

[1] M. Effendi Amran, M. Nabil Muhtazaruddin, and N. Haron, 'Progress in Energy and Environment Renewable Energy Optimization Review: Variables towards Competitive Advantage in Green Building Development', *Prog. Energy Environ.*, vol. 8, pp. 1–15, 2019.

[2] O. Krishan and S. Suhag, 'An updated review of energy storage systems: Classification and applications in distributed generation power systems incorporating renewable energy resources', *Int. J. Energy Res.*, vol. 43, no. 12, pp. 6171–6210, 2019, doi: 10.1002/er.4285.

[3] C. Jena, J. M. Guerrero, A. Abusorrah, Y. Al-Turki, and B. Khan, 'Multi-Objective Generation Scheduling of Hydro-Thermal System Incorporating Energy Storage With Demand Side Management Considering Renewable Energy Uncertainties', *IEEE Access*, vol. 10, pp. 52343–52357, 2022, doi: 10.1109/ACCESS.2022.3172500.

[4] O. Nematollahi, H. Hoghooghi, M. Rasti, and A. Sedaghat, 'Energy demands and renewable energy resources in the Middle East', *Renew. Sustain. Energy Rev.*, vol. 54, pp. 1172–1181, 2016, doi: 10.1016/j.rser.2015.10.058.

[5] R. Avtar *et al.*, 'Remote Sensing and GIS — A Review', *Resouces*, vol. 8, no. 149, p. 23, 2019.

[6] E. Shahrabi, S. M. Hakimi, A. Hasankhani, G. Derakhshan, and B. Abdi, 'Developing optimal energy management of energy hub in the presence of stochastic renewable energy resources', *Sustain. Energy, Grids Networks*, vol. 26, p. 100428, 2021, doi: 10.1016/j.segan.2020.100428.

[7] A. D. Woldeyohannes, D. E. Woldemichael, and A. T. Baheta, 'Sustainable renewable energy resources utilization in rural areas', *Renew. Sustain. Energy Rev.*, vol. 66, pp. 1–9, 2016, doi: 10.1016/j.rser.2016.07.013.

[8] L. Li *et al.*, 'Review and outlook on the international renewable energy development', *Energy Built Environ.*, vol. 3, no. 2, pp. 139–157, 2022, doi: 10.1016/j.enbenv.2020.12.002.

[9] M. N.S., G. N.A., and A. G.A., 'Role of Renewable Energy Sources in the World', *J. Renew. Energy, Electr. Comput. Eng.*, vol. 2, no. 2, p. 63, 2022, doi: 10.29103/jreece.v2i2.8779.

[10] D. Maradin, 'Advantages and disadvantages of renewable energy sources utilization', *Int. J. Energy Econ. Policy*, vol. 11, no. 3, pp. 176–183, 2021, doi: 10.32479/ijeep.11027.

[11] S. Y. Abujarad, M. W. Mustafa, and J. J. Jamian, 'Recent approaches of unit commitment in the presence of intermittent renewable energy resources: A review', *Renew. Sustain. Energy Rev.*, vol. 70, no. October 2015, pp. 215–223, 2017, doi: 10.1016/j.rser.2016.11.246.

[12] F. M. Guangul and G. T. Chala, 'Solar energy as renewable energy source: SWOT analysis', *2019 4th MEC Int. Conf. Big Data Smart City, ICBDSC 2019*, pp. 1–5, 2019, doi: 10.1109/ICBDSC.2019.8645580.

[13] I. Akhtar, S. Kirmani, M. Jameel, and F. Alam, 'Feasibility Analysis of Solar Technology Implementation in Restructured Power Sector with Reduced Carbon Footprints', *IEEE Access*, vol. 9, pp. 30306–30320, 2021, doi: 10.1109/ACCESS.2021.3059297.

[14] N. Kannan and D. Vakeesan, 'Solar energy for future world: - A review', *Renew. Sustain. Energy Rev.*, vol. 62, pp. 1092–1105, 2016, doi: 10.1016/j.rser.2016.05.022.

[15] M. Malinowski, J. I. Leon, and H. Abu-Rub, 'Solar Photovoltaic and Thermal Energy Systems: Current Technology and Future Trends', *Proc. IEEE*, vol. 105, no. 11, pp. 2132–2146, 2017, doi: 10.1109/JPROC.2017.2690343.

[16] N. Hashim, Z. Salam, D. Johari, and N. F. N. Ismail, 'DC-DC boost converter design for fast and accurate MPPT algorithms in stand-alone photovoltaic system', *Int. J. Power Electron. Drive Syst.*, vol. 9, no. 3, pp. 1038–1050, 2018, doi: 10.11591/ijpeds.v9.i3.pp1038-1050.

[17] A. Amir, A. Amir, H. S. Che, A. Elkhateb, and N. A. Rahim, 'Comparative analysis of high voltage gain DC-DC converter topologies for photovoltaic systems', *Renew. Energy*, vol. 136, pp. 1147–1163, 2019, doi: 10.1016/j.renene.2018.09.089.

[18] T. Khatib, W. Elmenreich, and A. Mohamed, 'Simplified I-V characteristic tester for

photovoltaic modules using a DC-DC boost converter', *Sustain.*, vol. 9, no. 4, pp. 1–12, 2017, doi: 10.3390/su9040657.

[19] N. H. Baharudin, T. M. N. T. Mansur, F. A. Hamid, R. Ali, and M. I. Misrun, 'Topologies of DC-DC converter in solar PV applications', *Indones. J. Electr. Eng. Comput. Sci.*, vol. 8, no. 2, pp. 368–374, 2017, doi: 10.11591/ijeecs.v8.i2.pp368-374.

[20] M. Zhioua *et al.*, 'Modeling, Dynamics, Bifurcation Behavior and Stability Analysis of a DC-DC Boost Converter in Photovoltaic Systems', *Int. J. Bifurc. Chaos*, vol. 26, no. 10, pp. 1–16, 2016, doi: 10.1142/S0218127416501662.

[21] P. Sathyanarayana, R. Ballal, L. S. P. S, and G. Kumar, 'Effect of Shading on the Performance of Solar PV Panel', vol. 5, pp. 1–4, 2015, doi: 10.5923/c.ep.201501.01.

[22] S. A. Zaki, J. Yao, H. Zhu, M. Al Fakih, and A. R. Sayed, 'Deep-learning – based method for faults classification of PV system', no. May 2020, pp. 193–205, 2021, doi: 10.1049/rpg2.12016.

[23] G. A. Raiker, U. Loganathan, and S. B. Reddy, 'Current Control of Boost Converter for PV Interface with Momentum-Based Perturb and Observe MPPT', IEEE Trans. Ind. Appl., vol. 57, no. 4, pp. 4071–4079, 2021, doi: 10.1109/TIA.2021.3081519.

[24] A. K. Gupta et al., 'Effect of Various Incremental Conductance MPPT Methods on the Charging of Battery Load Feed by Solar Panel', IEEE Access, vol. 9, pp. 90977–90988, 2021, doi: 10.1109/ACCESS.2021.3091502.

[25] U. Yilmaz, A. Kircay, and S. Borekci, 'PV system fuzzy logic MPPT method and PI control as a charge controller', Renew. Sustain. Energy Rev., vol. 81, no. April 2016, pp. 994–1001, 2018, doi: 10.1016/j.rser.2017.08.048.

[26] R. Bisht and A. Sikander, 'An improved method based on fuzzy logic with beta parameter for PV MPPT system', Optik (Stuttg)., vol. 259, no. March, p. 168939, 2022, doi: 10.1016/j.ijleo.2022.168939.

[27] S. Ahmed and T. Nasserdine, 'A sliding mode control and artificial neural network based MPPT for a direct grid - connected photovoltaic source', no. May 2018, pp. 1–14, 2019, doi: 10.1002/asjc.2007.

[28] S. Messalti, A. Harrag, and A. Loukriz, ‘crossmark’, Renew. Sustain. Energy Rev., vol. 68, no. August 2015, pp. 221–233, 2017, doi: 10.1016/j.rser.2016.09.131.

[29] A. Brahim, Y. Soufi, D. Ounnas, and D. Guiza, ‘Stand alone photovoltaic system control based on Artificial neural network and fuzzy logic’, no. March, pp. 29–31, 2022.

[30] A. A. Aldair, A. A. Obed, and A. F. Halihal, ‘Design and implementation of ANFIS-reference model controller based MPPT using FPGA for photovoltaic system’, Renew. Sustain. Energy Rev., vol. 82, no. July 2016, pp. 2202–2217, 2018, doi: 10.1016/j.rser.2017.08.071.

[31] D. S. Pillai, F. Blaabjerg, and N. Rajasekar, ‘A Comparative Evaluation of Advanced Fault Detection Approaches for PV Systems’, IEEE J. Photovoltaics, vol. 9, no. 2, pp. 513–527, 2019, doi: 10.1109/JPHOTOV.2019.2892189.

[32] Z. Chen et al., ‘Random forest based intelligent fault diagnosis for PV arrays using array voltage and string currents’, Energy Convers. Manag., vol. 178, no. August, pp. 250–264, 2018, doi: 10.1016/j.enconman.2018.10.040.

[33] F. Harrou, B. Taghezouit, and Y. Sun, ‘Improved k NN-Based Monitoring Schemes for Detecting Faults in PV Systems’, vol. 9, no. 3, pp. 811–821, 2019.

[34] M. Mao, L. Cui, Q. Zhang, K. Guo, L. Zhou, and H. Huang, ‘Classification and summarization of solar photovoltaic MPPT techniques: A review based on traditional and intelligent control strategies’, Energy Reports, vol. 6, no. 174, pp. 1312–1327, 2020, doi: 10.1016/j.egyr.2020.05.013.

[35] R. B. Bollipo, S. Mikkili, and P. K. Bonthagorla, ‘Critical Review on PV MPPT Techniques: Classical, Intelligent and Optimisation’, IET Renew. Power Gener., vol. 14, no. 9, pp. 1433–1452, 2020, doi: 10.1049/iet-rpg.2019.1163.

[36] A. Ali et al., ‘Investigation of MPPT Techniques under Uniform and Non-Uniform Solar Irradiation Condition-A Retrospection’, IEEE Access, vol. 8, pp. 127368–127392, 2020, doi: 10.1109/ACCESS.2020.3007710.

[37] H. Chaieb and A. Sakly, 'A novel MPPT method for photovoltaic application under partial shaded conditions', Sol. Energy, vol. 159, no. October 2017, pp. 291–299, 2018, doi: 10.1016/j.solener.2017.11.001.

[38] N. Priyadarshi, S. Padmanaban, S. Member, and J. B. Holm-nielsen, 'An Experimental Estimation of Hybrid ANFIS – PSO-Based MPPT for PV Grid Integration Under Fluctuating Sun Irradiance', IEEE Syst. J., vol. PP, pp. 1–12, 2019, doi: 10.1109/JSYST.2019.2949083.

[39] T. Imtiaz, B. H. Khan, and N. Khanam, 'Fast and improved PSO (FIPSO)-based deterministic and adaptive MPPT technique under partial shading conditions', IET Renew. Power Gener., vol. 14, no. 16, pp. 3164–3171, 2020, doi: 10.1049/iet-rpg.2020.0039.

[40] S. Mohanty, B. Subudhi, and P. K. Ray, 'A new MPPT design using grey Wolf optimization technique for photovoltaic system under partial shading conditions', IEEE Trans. Sustain. Energy, vol. 7, no. 1, pp. 181–188, 2016, doi: 10.1109/TSTE.2015.2482120.

[41] A. M. Eltamaly, M. S. Al-Saud, A. G. Abokhalil, and H. M. H. Farh, 'Simulation and experimental validation of fast adaptive particle swarm optimization strategy for photovoltaic global peak tracker under dynamic partial shading', Renew. Sustain. Energy Rev., vol. 124, no. January, p. 109719, 2020, doi: 10.1016/j.rser.2020.109719.

[42] Q. Akhter et al., 'Efficient Energy Management for Household: Optimization-Based Integration of Distributed Energy Resources in Smart Grid', IEEE Access, vol. 11, no. August, pp. 85716–85727, 2023, doi: 10.1109/ACCESS.2023.3303204.

[43] F. Z. Peng, C.-C. Liu, Y. Li, A. K. Jain, and D. Vinnikov, 'Envisioning the Future Renewable and Resilient Energy Grids—A Power Grid Revolution Enabled by Renewables, Energy Storage, and Energy Electronics', IEEE J. Emerg. Sel. Top. Ind. Electron., vol. 5, no. 1, pp. 8–26, 2023, doi: 10.1109/jestie.2023.3343291.

[44] Erdiwansyah, Mahidin, H. Husin, Nasaruddin, M. Zaki, and Muhibbuddin, 'A critical review of the integration of renewable energy sources with various technologies', Prot.

Control Mod. Power Syst., vol. 6, no. 1, 2021, doi: 10.1186/s41601-021-00181-3.

[45] J. Hu, X. Liu, M. Shahidehpour, and S. Xia, 'Optimal operation of energy hubs with large-scale distributed energy resources for distribution network congestion management', IEEE Trans. Sustain. Energy, vol. 12, no. 3, pp. 1755–1765, 2021, doi: 10.1109/TSTE.2021.3064375.

[46] A. Qazi et al., 'Towards Sustainable Energy: A Systematic Review of Renewable Energy Sources, Technologies, and Public Opinions', IEEE Access, vol. 7, pp. 63837–63851, 2019, doi: 10.1109/ACCESS.2019.2906402.

[47] E. Kabir, P. Kumar, S. Kumar, A. A. Adelodun, and K. H. Kim, 'Solar energy: Potential and future prospects', *Renew. Sustain. Energy Rev.*, vol. 82, no. September 2016, pp. 894–900, 2018, doi: 10.1016/j.rser.2017.09.094.

[48] C. Ye, C. Tai, Y. Huang, and J. Chen, 'Dispersed partial shading effect and reduced power loss in a PV array using a complementary SuDoKu puzzle topology', *Energy Convers. Manag.*, vol. 246, no. May, p. 114675, 2021, doi: 10.1016/j.enconman.2021.114675.

[49] R. Hariharan, M. Chakkarapani, G. Saravana Ilango, and C. Nagamani, 'A Method to Detect Photovoltaic Array Faults and Partial Shading in PV Systems', IEEE J. Photovoltaics, vol. 6, no. 5, pp. 1278–1285, 2016, doi: 10.1109/JPHOTOV.2016.2581478.

[50] A. Echevarria et al., 'Unleashing Sociotechnical Imaginaries to Advance Just and Sustainable Energy Transitions: The Case of Solar Energy in Puerto Rico', IEEE Trans. Technol. Soc., vol. 4, no. 3, pp. 255–268, 2022, doi: 10.1109/tts.2022.3191542.

[51] A. Shahsavari and M. Akbari, 'Potential of solar energy in developing countries for reducing energy-related emissions', Renew. Sustain. Energy Rev., vol. 90, no. March, pp. 275–291, 2018, doi: 10.1016/j.rser.2018.03.065.

[52] O. Höhn et al., 'Impact of Irradiance Data on the Energy Yield Modeling of Dual-Junction Solar Module Stacks for One-Sun Applications', vol. 11, no. 3, pp. 692–698, 2021, doi: 10.1109/JPHOTOV.2021.3064562.

[53] N. Aouchiche, 'Conception d ' une commande MPPT optimale à base d ' intelligence

artificielle d ’ un système photovoltaïque . Nedjma Aouchiche To cite this version : HAL Id : tel-02902953’, 2020.

[54] S. Y. Alsadi and Y. F. Nassar, ‘Estimation of Solar Irradiance on Solar Fields: An Analytical Approach and Experimental Results’, IEEE Trans. Sustain. Energy, vol. 8, no. 4, pp. 1601–1608, 2017, doi: 10.1109/TSTE.2017.2697913.

[55] P. Espinet-Gonzalez et al., ‘Nanowire Solar Cells: A New Radiation Hard PV Technology for Space Applications’, IEEE J. Photovoltaics, vol. 10, no. 2, pp. 502–507, 2020, doi: 10.1109/JPHOTOV.2020.2966979.

[56] B. M. Karambasti, M. Naghashzadegan, M. Ghodrat, G. Ghorbani, R. B. V. B. Simorangkir, and A. Lalbakhsh, ‘Optimal Solar Greenhouses Design Using Multiobjective Genetic Algorithm’, IEEE Access, vol. 10, no. June, pp. 73728–73742, 2022, doi: 10.1109/ACCESS.2022.3189348.

[57] M. K. Boutahir, Y. Farhaoui, M. Azrour, I. Zeroual, and A. El Allaoui, ‘Effect of Feature Selection on the Prediction of Direct Normal Irradiance’, Big Data Min. Anal., vol. 5, no. 4, pp. 309–317, 2022, doi: 10.26599/BDMA.2022.9020003.

[58] H. Jiang, Y. Yang, Y. Bai, and H. Wang, ‘Evaluation of the Total, Direct, and Diffuse Solar Radiations from the ERA5 Reanalysis Data in China’, IEEE Geosci. Remote Sens. Lett., vol. 17, no. 1, pp. 47–51, 2020, doi: 10.1109/LGRS.2019.2916410.

[59] R. Nunez et al., ‘Spectral Impact on Multijunction Solar Cells Obtained by Means of Component Cells of a Different Technology’, IEEE J. Photovoltaics, vol. 8, no. 2, pp. 646–653, 2018, doi: 10.1109/JPHOTOV.2017.2782561.

[60] P. K. Enaganti, ‘Underwater Analysis of Solar Photovoltaic Cells with Filtered Solar Spectrum’, pp. 2219–2223.

[61] Y. Zeng et al., ‘Review on Metallization Approaches for High - Efficiency Silicon Heterojunction Solar Cells’, Trans. Tianjin Univ., vol. 28, no. 5, pp. 358–373, 2022, doi: 10.1007/s12209-022-00336-9.

[62] G. S. Thirunavukkarasu et al., ‘Optimization of mono-crystalline silicon solar cell devices

using pc1d simulation', Energies, vol. 14, no. 16, pp. 1–13, 2021, doi: 10.3390/en14164986.

[63] B. Raillani, H. A. L. Ouali, S. Amraqui, M. A. Moussaoui, and A. Mezrhab, 'Analyze and Study on Photovoltaic Parameters of Mono-Crystalline Silicon Solar Cell', Proc. - 2019 Int. Conf. Intell. Syst. Adv. Comput. Sci. ISACS 2019, pp. 1–5, 2019, doi: 10.1109/ISACS48493.2019.9068923.

[64] F. Haase et al., 'Interdigitated back contact solar cells with polycrystalline silicon on oxide passivating contacts for both polarities', Jpn. J. Appl. Phys., vol. 56, no. 8, pp. 1–5, 2017, doi: 10.7567/JJAP.56.08MB15.

[65] K. ElKhamisy, H. Abdelhamid, E. S. M. El-Rabaie, and N. Abdel-Salam, 'A Comprehensive Survey of Silicon Thin-film Solar Cell: Challenges and Novel Trends', Plasmonics, vol. 19, no. 1, pp. 1–20, 2024, doi: 10.1007/s11468-023-01905-x.

[66] A. Romeo and E. Artegiani, 'Cdte-based thin film solar cells: Past, present and future', Energies, vol. 14, no. 6, 2021, doi: 10.3390/en14061684.

[67] I. M. Dharmadasa, A. E. Alam, A. A. Ojo, and O. K. Echendu, 'Scientific complications and controversies noted in the field of CdS/CdTe thin film solar cells and the way forward for further development', J. Mater. Sci. Mater. Electron., vol. 30, no. 23, pp. 20330–20344, 2019, doi: 10.1007/s10854-019-02422-6.

[68] N. Rezaei, P. Procel, M. Simor, Z. Vroon, M. Zeman, and O. Isabella, 'Interdigitated back-contacted structure: A different approach towards high-efficiency ultrathin copper indium gallium (di)selenide solar cells', Prog. Photovoltaics Res. Appl., vol. 28, no. 9, pp. 899–908, 2020, doi: 10.1002/pip.3296.

[69] X. Sun, T. Silverman, R. Garris, C. Deline, and M. A. Alam, 'An Illumination-and Temperature-Dependent Analytical Model for Copper Indium Gallium Diselenide (CIGS) Solar Cells', IEEE J. Photovoltaics, vol. 6, no. 5, pp. 1298–1307, 2016, doi: 10.1109/JPHOTOV.2016.2583790.

[70] J. Ramanujam and U. P. Singh, 'Copper indium gallium selenide based solar cells - A

review', Energy Environ. Sci., vol. 10, no. 6, pp. 1306–1319, 2017, doi: 10.1039/c7ee00826k.

[71] Y. He, L. Xu, C. Yang, X. Guo, and S. Li, 'Design and numerical investigation of a lead-free inorganic layered double perovskite cs4cusb2cl12 nanocrystal solar cell by scaps-1d', Nanomaterials, vol. 11, no. 9, pp. 1–19, 2021, doi: 10.3390/nano11092321.

[72] W. M. M. Lin, D. Bozyigit, O. Yarema, and V. Wood, 'Transient Photovoltage Measurements in Nanocrystal-Based Solar Cells', J. Phys. Chem. C, vol. 120, no. 23, pp. 12900–12908, 2016, doi: 10.1021/acs.jpcc.6b03695.

[73] H. Sun et al., 'High-Performance All-Polymer Solar Cells Enabled by an n-Type Polymer Based on a Fluorinated Imide-Functionalized Arene', Adv. Mater., vol. 31, no. 15, pp. 1–8, 2019, doi: 10.1002/adma.201807220.

[74] S. HAYASE, 'Dye-Sensitized Solar Cells -Present and Future-', J. Adhes. Soc. Japan, vol. 45, no. 8, pp. 313–320, 2009, doi: 10.11618/adhesion.45.313.

[75] Y. Xing et al., 'A review of concentrator silicon solar cells', Renew. Sustain. Energy Rev., vol. 51, pp. 1697–1708, 2015, doi: 10.1016/j.rser.2015.07.035.

[76] A. Kabbani and M. S. Honnurvali, 'PV Cell Parameters Modeling and Temperature Effect Analysis', vol. 353731643, no. August, 2021.

[77] Y. Emre, K. Vardar, and M. Ali, 'Modeling and Simulation of PV Systems Modeling and Simulation of PV Systems', no. April, 2018, doi: 10.9790/1676-1302030111.

[78] P. Dwivedi, K. Sudhakar, A. Soni, and E. Solomin, 'Case Studies in Thermal Engineering Advanced cooling techniques of P . V . modules : A state of art', Case Stud. Therm. Eng., vol. 21, no. May, p. 100674, 2020, doi: 10.1016/j.csite.2020.100674.

[79] M. Al-addous, Z. Dalala, F. Alawneh, and C. B. Class, 'Modeling and quantifying dust accumulation impact on PV module performance', Sol. Energy, vol. 194, no. September, pp. 86–102, 2019, doi: 10.1016/j.solener.2019.09.086.

[80] R. Kumar and S. K. Singh, 'Solar photovoltaic modeling and simulation : As a renewable energy solution', Energy Reports, vol. 4, pp. 701–712, 2018, doi: 10.1016/j.egyr.2018.09.008.

[81] A. Bouraiou, M. Hamouda, A. Chaker, M. Sadok, M. Mostefaoui, and S. Lachtar, 'Modeling and Simulation of Photovoltaic Module and Array Based on One and Two Diode Model Using Matlab/Simulink', Energy Procedia, vol. 74, pp. 864–877, 2015, doi: 10.1016/j.egypro.2015.07.822.

[82] G. P. R. Engineering, I. Andri, A. Pina, P. Ferrão, and M. Vijaya, 'ScienceDirect ScienceDirect ScienceDirect ScienceDirect 1st International Conference A MATLAB based PV Module Models analysis under Conditions of A MATLAB PV Module Models analysis under Conditions of The based Nonuniform Irradiance Nonuniform Irradiance ', Energy Procedia, vol. 117, pp. 974–983, 2017, doi: 10.1016/j.egypro.2017.05.218.

[83] H. Bellia, R. Youcef, and M. Fatima, 'A detailed modeling of photovoltaic module using MATLAB', NRIAG J. Astron. Geophys., vol. 3, no. 1, pp. 53–61, 2014, doi: 10.1016/j.nrjag.2014.04.001.

[84] E. Elibol, Ö. T. Özmen, N. Tutkun, and O. Köysal, 'Outdoor performance analysis of different PV panel types', Renew. Sustain. Energy Rev., vol. 67, pp. 651–661, 2017, doi: 10.1016/j.rser.2016.09.051.

[85] A. R. Amelia, Y. M. Irwan, W. Z. Leow, M. Irwanto, I. Safwati, and M. Zhafarina, 'Investigation of the effect temperature on photovoltaic (PV) panel output performance', Int. J. Adv. Sci. Eng. Inf. Technol., vol. 6, no. 5, pp. 682–688, 2016, doi: 10.18517/ijaseit.6.5.938.

[86] M. Kasper, D. Bortis, and J. W. Kolar, 'Classification and comparative evaluation of PV panel-integrated DC-DC converter concepts', IEEE Trans. Power Electron., vol. 29, no. 5, pp. 2511–2526, 2014, doi: 10.1109/TPEL.2013.2273399.

[87] S. Sajwan, M. K. Singh, and S. Urooj, 'Physical relocation of PV panel for optimization of power under PSC in PV array', 2018 IEEMA Eng. Infin. Conf. eTechNxT 2018, no. 1, pp. 1–6, 2018, doi: 10.1109/ETECHNXT.2018.8385322.

[88] C. Saiprakash, A. Mohapatra, and B. Nayak, 'An A TT Array Configuration for Performance Enhancement of PV system under PSC', ICPEE 2021 - 2021 1st Int. Conf. Power Electron. Energy, no. 2, 2021, doi: 10.1109/ICPEE50452.2021.9358645.

[89] C. Ye, C. Tai, Y. Huang, and J. Chen, 'Dispersed partial shading effect and reduced power loss in a PV array using a complementary SuDoKu puzzle topology', Energy Convers. Manag., vol. 246, no. May, p. 114675, 2021, doi: 10.1016/j.enconman.2021.114675.

[90] P. Sathyanarayana, R. Ballal, L. S. P. S, and G. Kumar, 'Effect of Shading on the Performance of Solar PV Panel', vol. 5, pp. 1–4, 2015, doi: 10.5923/c.ep.201501.01.

[91] A. Haque, K. V. S. Bharath, M. A. Khan, I. Khan, and Z. A. Jaffery, 'Fault diagnosis of Photovoltaic Modules', Energy Sci. Eng., vol. 7, no. 3, pp. 622–644, 2019, doi: 10.1002/ese3.255.

[92] Q. Liu et al., 'Asynchronous Decentralized Federated Learning for Collaborative Fault Diagnosis of PV Stations', IEEE Trans. Netw. Sci. Eng., vol. 9, no. 3, pp. 1680–1696, 2022, doi: 10.1109/TNSE.2022.3150182.

[93] X. Wang, B. Yang, Q. Liu, T. Jin, and C. Chen, 'Collaboratively Diagnosing IGBT Open-circuit Faults in Photovoltaic Inverters: A Decentralized Federated Learning-based Method', IECON Proc. (Industrial Electron. Conf., vol. 2021-October, 2021, doi: 10.1109/IECON48115.2021.9589794.

[94] K. Kasar and P. P. C. Tapre, 'A New Fast Detection Module for Short-circuit Current Detection in PV Grid system', no. Icisc, pp. 468–472, 2018.

[95] X. Lu et al., 'Fault diagnosis for photovoltaic array based on convolutional neural network and electrical time series graph', Energy Convers. Manag., vol. 196, no. February, pp. 950–965, 2019, doi: 10.1016/j.enconman.2019.06.062.

[96] W. Miao, X. Liu, K. H. Lam, and P. W. T. Pong, 'Arc-Faults Detection in PV Systems by Measuring Pink Noise With Magnetic Sensors', vol. 55, no. 7, 2019.

[97] S. A. M. Abdelwahab, A. M. Hamada, and W. S. E. Abdellatif, 'Comparative Analysis of the Modified Perturb & Observe with Different MPPT Techniques for PV Grid Connected Systems', no. March 2020, 2021.

[98] I. Aboudrar et al., ‘Robust Control of 5 hree 1 hase Grid Connected PV 4 ystem # ased on ADRC and Fuzzy’.

[99] M. Das, S. Member, and V. Agarwal, ‘Novel High Performance Stand Alone Solar PV System with High Gain , High Efficiency DC-DC Converter Power Stages’, vol. 9994, no. c, 2015, doi: 10.1109/TIA.2015.2454488.

[100] E. Mattos, A. M. S. S. Andrade, G. V Hollweg, J. R. Pinheiro, and M. L. S. Martins, ‘A Review of Boost Converter Analysis and Design in Aerospace Applications’, vol. 16, no. 2, 2018.

[101] A. M. Parimi and U. M. Rao, ‘Performance Evaluation of DC Grid Connected Solar PV System for Hybrid Control of DC-DC Boost Converter’.

[102] A. Chauhan, ‘Frequency estimation in Power Systems : A brief comparison of Phase locked loops and its derivatives’, 2018 3rd IEEE Int. Conf. Recent Trends Electron. Inf. Commun. Technol., pp. 915–919, 2018.

[103] Z. Li, A. Jiang, P. Shen, and Y. Han, ‘Resonance Damping and Parameter Design Method Photovoltaic Inverters’, 2016.

[104] A. Pradhan and B. Panda, ‘A Simplified Design and Modeling of Boost Converter for Photovoltaic Sytem’, vol. 8, no. 1, pp. 141–149, 2018, doi: 10.11591/ijece.v8i1.pp141-149.

[105] H. Fathabadi, ‘ScienceDirect Novel high efficiency DC / DC boost converter for using in photovoltaic systems’, Sol. ENERGY, vol. 125, pp. 22–31, 2016, doi: 10.1016/j.solener.2015.11.047.

[106] A. Alisson et al., ‘High-voltage gain dc – dc boost converter with coupled inductors for photovoltaic systems’, vol. 8, pp. 1885–1892, 2015, doi: 10.1049/iet-pel.2014.0520.

[107] S. S. M. N. Arjun, ‘Mathematical Modeling of Power Electronic Converters’, SN Comput. Sci., 2021, doi: 10.1007/s42979-021-00637-1.

[108] H. A. Mohamed, H. A. Khattab, A. Mobarka, and G. A. Morsy, ‘Design, control and performance analysis of DC-DC boost converter for stand-alone PV system’, 2016 18th Int. Middle-East Power Syst. Conf. MEPCON 2016 - Proc., pp. 101–106, 2017, doi: 10.1109/MEPCON.2016.7836878.

[109] R. Ayop and C. W. Tan, 'Design of boost converter based on maximum power point resistance for photovoltaic applications', Sol. Energy, vol. 160, no. November 2017, pp. 322–335, 2018, doi: 10.1016/j.solener.2017.12.016.

[110] M. M. Garg, Y. V. Hote, and M. K. Pathak, 'Design and Performance Analysis of a PWM dc–dc Buck Converter Using PI–Lead Compensator', Arab. J. Sci. Eng., vol. 40, no. 12, pp. 3607–3626, 2015, doi: 10.1007/s13369-015-1838-z.

[111] P. Falkowski, M. Korzeniewski, A. Ruszczyk, and K. Kóska, 'Analiza i projektowanie wysokiej sprawności przekształtnika DC/DC typu buck', Prz. Elektrotechniczny, vol. 92, no. 5, pp. 156–161, 2016, doi: 10.15199/48.2016.05.29.

[112] A. W. Cristri and R. F. Iskandar, 'Analysis and Design of Dynamic Buck Converter with Change in Value of Load Impedance', Procedia Eng., vol. 170, pp. 398–403, 2017, doi: 10.1016/j.proeng.2017.03.064.

[113] Z. Iqbal, U. Nasir, M. T. Rasheed, and K. Munir, 'A comparative analysis of synchronous buck, isolated buck and buck converter', 2015 IEEE 15th Int. Conf. Environ. Electr. Eng. EEEIC 2015 - Conf. Proc., pp. 992–996, 2015, doi: 10.1109/EEEIC.2015.7165299.

[114] M. Junaid and B. Singh, 'Analysis and design of buck-boost converter for power quality improvement in high frequency on/off-line UPS system', 2014 IEEE Int. Conf. Power Electron. Drives Energy Syst. PEDES 2014, 2014, doi: 10.1109/PEDES.2014.7042008.

[115] X. Weng et al., 'Comprehensive comparison and analysis of non-inverting buck boost and conventional buck boost converters', J. Eng., vol. 2019, no. 16, pp. 3030–3034, 2019, doi: 10.1049/joe.2018.8373.

[116] M. Veerachary and V. Khubchandani, 'Analysis, Design, and Control of Switching Capacitor Based Buck-Boost Converter', IEEE Trans. Ind. Appl., vol. 55, no. 3, pp. 2845–2857, 2019, doi: 10.1109/TIA.2018.2889848.

[117] K. C. Wu, H. H. Wu, and C. L. Wei, 'Analysis and Design of Mixed-Mode Operation for Noninverting Buck-Boost DC-DC Converters', IEEE Trans. Circuits Syst. II Express Briefs, vol. 62, no. 12, pp. 1194–1198, 2015, doi: 10.1109/TCSII.2015.2469032.

[118] H. S. Son, J. K. Kim, J. B. Lee, S. S. Moon, J. H. Park, and S. H. Lee, 'A New Buck-Boost Converter with Low-Voltage Stress and Reduced Conducting Components', IEEE Trans. Ind. Electron., vol. 64, no. 9, pp. 7030–7038, 2017, doi: 10.1109/TIE.2017.2686300.

[119] J. Li and J. Liu, 'A Novel Buck-Boost Converter with Low Electric Stress on Components', IEEE Trans. Ind. Electron., vol. 66, no. 4, pp. 2703–2713, 2019, doi: 10.1109/TIE.2018.2847646.

[120] B. R. Kiran and G. A. Ezhilarasi, 'Design and analysis of soft-switched Buck-Boost Converter for PV applications', 12th IEEE Int. Conf. Electron. Energy, Environ. Commun. Comput. Control (E3-C3), INDICON 2015, no. 1, pp. 1–5, 2016, doi: 10.1109/INDICON.2015.7443509.

[121] M. R. Banaei, H. A. F. Bonab, and N. T. Kalantari, 'Analysis and design of a new single switch non-isolated buck-boost DC-DC converter', J. Oper. Autom. Power Eng., vol. 8, no. 2, pp. 116–127, 2020, doi: 10.22098/joape.2019.5363.1403.

[122] K. Lu, F. Lin, and B. Yang, 'Profit Optimization-Based Power Compensation Control Strategy for Grid-Connected PV System', no. 1, pp. 1–1, 2017, doi: 10.1109/nsyss.2017.7885812.

[123] J. Jana, H. Saha, and K. Das Bhattacharya, 'A review of inverter topologies for single-phase grid-connected photovoltaic systems', Renew. Sustain. Energy Rev., vol. 72, no. October 2016, pp. 1256–1270, 2017, doi: 10.1016/j.rser.2016.10.049.

[124] D. Kolantla, S. Mikkili, S. R. Pendem, and A. A. Desai, 'Critical review on various inverter topologies for PV system architectures', vol. 14, pp. 3418–3438, 2021, doi: 10.1049/iet-rpg.2020.0317.

[125] S. P. V Inverters, I. Vairavasundaram, V. Varadarajan, and P. J. Pavankumar, 'A Review on Small Power Rating PV Inverter Topologies and', 2021.

[126] R. Dogga and M. K. Pathak, 'Recent trends in solar PV inverter topologies', Sol. Energy, vol. 183, no. February, pp. 57–73, 2019, doi: 10.1016/j.solener.2019.02.065.

[127] S. Bouguerra, S. Member, M. R. Yaiche, O. Gassab, and S. Member, 'The Impact of PV Panel Positioning and Degradation on the PV Inverter Lifetime and Reliability', vol. 6777, no. c, pp. 1–14, 2020, doi: 10.1109/JESTPE.2020.3006267.

[128] K. Zeb et al., 'A comprehensive review on inverter topologies and control strategies for grid connected photovoltaic system', vol. 94, no. June, pp. 1120–1141, 2018, doi: 10.1016/j.rser.2018.06.053.

[129] C. J. O. Rourke, M. M. Qasim, M. R. Overlin, and J. L. Kirtley, 'A Geometric Interpretation of Reference Frames and Transformations: dq0, Clarke and Park', IEEE Trans. Energy Convers., vol. PP, no. c, p. 1, 2019, doi: 10.1109/TEC.2019.2941175.

[130] Q. Zhang, M. Mao, G. Ke, L. Zhou, and B. Xie, 'Stability problems of PV inverter in weak grid : a review', pp. 2165–2174, 2020, doi: 10.1049/iet-pel.2019.1049.

[131] D. Lauria and M. Coppola, 'ScienceDirect Design and control of an advanced PV inverter', Sol. Energy, vol. 110, pp. 533–542, 2014, doi: 10.1016/j.solener.2014.09.040.

[132] B. Saleh et al., 'Environmental Effects Performance Analysis of Maximum Power Point Tracking for Two Techniques with Direct Control of Photovoltaic Grid -Connected Systems Performance Analysis of Maximum Power Point Tracking for Two Techniques with Direct Control of Photovoltaic Grid -Connected', Energy Sources, Part A Recover. Util. Environ. Eff., vol. 00, no. 00, pp. 1–23, 2021, doi: 10.1080/15567036.2021.1898496.

[133] Y. Xu and Z. Gu, 'Stability Analysis and Control of Two-Stage Three-Phase Photovoltaic Grid-Connected System with Phase-Locked Loop', 2018 2nd IEEE Conf. Energy Internet Energy Syst. Integr., pp. 1–6, 2018.

[134] P. G. Student, 'interfaced with grid connected solar PV', 2018 Natl. Power Eng. Conf., no. 1, pp. 1–6, 2018.

[135] P. Jain, V. Agarwal, B. Prasad, and M. Bhel, 'Hybrid Phase Locked Loop for Controlling Centralized Inverters in Large Solar Photovoltaic Power Plants'.

[136] H. Athari, M. Niroomand, and M. Ataei, 'Review and Classification of Control Systems in Grid-tied Inverters', Renew. Sustain. Energy Rev., no. October, pp. 0–1, 2016, doi: 10.1016/j.rser.2016.10.030.

[137] T. K. Roy, M. A. Mahmud, and S. N. Islam, 'Nonlinear Backstepping Controller Design for Grid-Connected Photovoltaic Systems with Output LC Filters to Improve Dynamic Stability and Power Quality', pp. 1–5, 2020.

[138] R. Juntunen, J. Korhonen, and T. Musikka, 'Identification of Resonances in Parallel Connected Grid Inverters with LC - and LCL - filters', pp. 2–7.

[139] K. Abd and E. Wahid, 'LCL filter design with passive damping for photovoltaic grid connected systems', IREC2015 Sixth Int. Renew. Energy Congr., no. October 2019, pp. 1–4, 2015, doi: 10.1109/IREC.2015.7110945.

[140] X. Li, S. Member, R. S. Balog, and S. Member, 'PLL-less Robust Active and Reactive Power Controller for Single Phase Grid-Connected Inverter with LCL Filter', pp. 2154–2159, 2015.

[141] P. Gakhar, 'Harmonic Mitigation in a Transformer Less Grid Connected Solar PV System Using Modified LCL Filter', 2018 3rd Int. Conf. Work. Recent Adv. Innov. Eng., vol. 2018, no. November, pp. 1–4, 2018.

[142] M. Ben Sa, M. W. Naouar, I. S. Belkhodja, and E. Monmasson, 'ScienceDirect Simple and systematic LCL filter design for three-phase grid-connected power converters', 2015, doi: 10.1016/j.matcom.2015.09.011.

[143] R. B. Bollipo, S. Mikkili, S. Member, and P. K. Bonthagorla, 'Hybrid , Optimal , Intelligent and Classical PV MPPT Techniques : A Review', vol. 7, no. 1, pp. 9–33, 2021, doi: 10.17775/CSEEJPES.2019.02720.

[144] S. Cities, Lecture Notes in Networks and Systems 102 Smart Energy Empowerment in Smart and Resilient Cities.

[145] S. B. Kjær, 'Evaluation of the " Hill Climbing " and the " Incremental Conductance " Maximum Power Point Trackers for Photovoltaic Power Systems', vol. 27, no. 4, pp. 922–929, 2012.

[146] A. K. Abdelsalam, A. M. Massoud, S. Ahmed, and P. N. Enjeti, 'High-Performance Adaptive Perturb and Observe MPPT Technique for Photovoltaic-Based Microgrids', vol. 26, no. 4, pp. 1010–1021, 2011.

[147] Y. Yang and H. Wen, 'Adaptive perturb and observe maximum power point tracking with current predictive and decoupled power control for grid- connected photovoltaic inverters', J. Mod. Power Syst. Clean Energy, vol. 7, no. 2, pp. 422–432, 2019, doi: 10.1007/s40565-018-0437-x.

[147] B. Bendib, F. Krim, H. Belmili, M. F. Almi, and S. Boulouma, 'Advanced Fuzzy MPPT Controller for a stand-alone PV system', Energy Procedia, vol. 50, pp. 383–392, 2014, doi: 10.1016/j.egypro.2014.06.046.

[148] F. Yahiaoui et al., 'An Experimental Testing of Optimized Fuzzy Logic-Based MPPT for a Standalone PV System Using Genetic Algorithms', vol. 2023, 2023.

[149] R. Divyasharon, 'Artificial Neural Network based MPPT with CUK Converter Topology for PV Systems Under Varying Climatic Conditions', 2019 IEEE Int. Conf. Intell. Tech. Control. Optim. Signal Process., pp. 1–6, 2019, doi: 10.1109/INCOS45849.2019.8951321.

[150] S. Ahmed and T. Nasserdine, 'A sliding mode control and artificial neural network based MPPT for a direct grid - connected photovoltaic source', no. May 2018, pp. 1–14, 2019, doi: 10.1002/asjc.2007.

[151] M. Fathi and J. A. Parian, 'Intelligent MPPT for photovoltaic panels using a novel fuzzy logic and artificial neural networks based on evolutionary algorithms', Energy Reports, vol. 7, pp. 1338–1348, 2021, doi: 10.1016/j.egyr.2021.02.051.

[152] M. M. Elymany, M. A. Enany, and N. A. Elsonbaty, 'Hybrid optimized-ANFIS based MPPT for hybrid microgrid using zebra optimization algorithm and artificial gorilla troops optimizer Supercapacitor Energy Storage system', Energy Convers. Manag., vol. 299, no. October 2023, p. 117809, 2024, doi: 10.1016/j.enconman.2023.117809.

[153] R. Kahani, M. Jamil, and M. T. Iqbal, 'An Improved Perturb and Observed Maximum Power Point Tracking Algorithm for Photovoltaic Power Systems', vol. 11, no. 4, pp. 1165–1175, 2023, doi: 10.35833/MPCE.2022.000245.

[154] P. String-integrated-converters and O. Mppt, 'Assessment of Cross-coupling Effects in PV Algorithm Under Various Partial Shading Patterns', vol. 8, no. 4, pp. 1013–1028, 2022, doi: 10.17775/CSEEJPES.2019.03330.

[155] M. Killi and S. Samanta, 'Modified Perturb and Observe MPPT Algorithm for Drift Avoidance in Photovoltaic Systems', vol. 62, no. 9, pp. 5549–5559, 2015.

[156] M. A. Elgendy, B. Zahawi, S. Member, and D. J. Atkinson, 'Assessment of the Incremental Conductance Maximum Power Point Tracking Algorithm', pp. 1–10, 2012.

[157] N. Kumar, M. Ieee, I. Hussain, B. Singh, F. Ieee, and B. Ketan, 'Self-Adaptive Incremental Conductance Algorithm for Swift and Ripple Free Maximum Power Harvesting from PV Array', vol. 3203, no. c, pp. 1–10, 2017, doi: 10.1109/TII.2017.2765083.

[158] T. T. Yetayew, 'Evaluation of Incremental Conductance and Firefly Algorithm for PV MPPT Application under Partial Shade condition', pp. 1–6, 2016.

[159] D. C. Huynh and M. W. Dunnigan, 'Development and Comparison of an Improved Incremental Conductance Algorithm for Tracking the MPP of a Solar PV Panel', vol. 3029, no. c, 2016, doi: 10.1109/TSTE.2016.2556678.

[160] L. Shang, H. Guo, and W. Zhu, 'An improved MPPT control strategy based on incremental conductance algorithm', 2020.

[161] M. Fannakh, M. L. Ehafyani, and S. Zouggar, 'Hardware implementation of the fuzzy logic MPPT in an Arduino card using a Simulink support package for PV application', IET Renew. Power Gener., vol. 13, no. 3, pp. 510–518, 2019, doi: 10.1049/iet-rpg.2018.5667.

[162] M. N. Ali, K. Mahmoud, M. Lehtonen, and M. M. F. Darwish, 'An Efficient Fuzzy-Logic Based Variable-Step Incremental Conductance MPPT Method for Grid-Connected PV Systems', IEEE Access, vol. 9, pp. 26420–26430, 2021, doi: 10.1109/ACCESS.2021.3058052.

[163] M. Dabboussi, A. Hmidet, and O. Boubaker, 'An efficient fuzzy logic MPPT control approach for solar PV system: A comparative analysis with the conventional perturb and observe technique', 6th IEEE Int. Energy Conf. ENERGYCon 2020, pp. 366–371, 2020, doi: 10.1109/ENERGYCon48941.2020.9236503.

[164] H. Rezk, M. Aly, M. Al-Dhaifallah, and M. Shoyama, 'Design and Hardware Implementation of New Adaptive Fuzzy Logic-Based MPPT Control Method for Photovoltaic Applications', IEEE Access, vol. 7, pp. 106427–106438, 2019, doi: 10.1109/ACCESS.2019.2932694.

[165] V. Subramanian, V. Indragandhi, R. Kuppusamy, and Y. Teekaraman, 'Modeling and analysis of pv system with fuzzy logic mppt technique for a dc microgrid under variable atmospheric conditions', Electron., vol. 10, no. 20, 2021, doi: 10.3390/electronics10202541.

[166] T. U. Hassan et al., 'A novel algorithm for MPPT of an isolated PV system using push pull converter with fuzzy logic controller', Energies, vol. 13, no. 15, pp. 1–21, 2020, doi: 10.3390/en13154007.

[167] S. Tang, Y. Sun, Y. Chen, Y. Zhao, Y. Yang, and W. Szeto, 'An Enhanced MPPT Method Combining Fractional-Order and Fuzzy Logic Control', IEEE J. Photovoltaics, vol. 7, no. 2, pp. 640–650, 2017, doi: 10.1109/JPHOTOV.2017.2649600.

[168] X. Li, H. Wen, Y. Hu, and L. Jiang, 'A novel beta parameter based fuzzy-logic controller for photovoltaic MPPT application', Renew. Energy, vol. 130, pp. 416–427, 2019, doi: 10.1016/j.renene.2018.06.071.

[169] S. Farajdadian and S. M. H. Hosseini, 'Optimization of fuzzy-based MPPT controller via metaheuristic techniques for stand-alone PV systems', Int. J. Hydrogen Energy, vol. 44, no. 47, pp. 25457–25472, 2019, doi: 10.1016/j.ijhydene.2019.08.037.

[170] A. Brahim, Y. Soufi, D. Ounnas, and D. Guiza, 'Fuzzy logic control of a photovoltaic system connected to grid', Proc. - 2022 5th Int. Conf. Power Electron. their Appl. ICPEA 2022, no. March, pp. doi:10.1109/ICPEA51060.2022.9791172.

[171] M. Nour Ali, 'Improved Design of Artificial Neural Network for MPPT of Grid-Connected PV Systems', 2018 20th Int. Middle East Power Syst. Conf. MEPCON 2018 - Proc., pp. 97–102, 2018, doi: 10.1109/MEPCON.2018.8635202.

[172] R. B. Roy et al., 'A Comparative Performance Analysis of ANN Algorithms for MPPT Energy Harvesting in Solar PV System', IEEE Access, vol. 9, pp. 102137–102152, 2021, doi: 10.1109/ACCESS.2021.3096864.

[173] S. Duman, N. Yorukeren, and I. H. Altas, 'A novel MPPT algorithm based on optimized artificial neural network by using FPSOGSA for standalone photovoltaic energy systems', Neural Comput. Appl., vol. 29, no. 1, pp. 257–278, 2018, doi: 10.1007/s00521-016-2447-9.

[174] H. A. Attia, 'High performance PV system based on artificial neural network MPPT with PI controller for direct current water pump applications', Int. J. Power Electron. Drive Syst., vol. 10, no. 3, pp. 1329–1338, 2019, doi: 10.11591/ijpeds.v10.i3.pp1329-1338.

[175] A. M. Farayola, A. N. Hasan, and A. Ali, 'Efficient photovoltaic mppt system using coarse gaussian support vector machine and artificial neural network techniques', Int. J. Innov. Comput. Inf. Control, vol. 14, no. 1, pp. 323–339, 2018, doi: 10.24507/ijicic.14.01.323.

[176] L. P. N. Jyothy and M. R. Sindhu, 'An Artificial Neural Network based MPPT Algorithm for Solar PV System', Proc. 4th Int. Conf. Electr. Energy Syst. ICEES 2018, pp. 375–380, 2018, doi: 10.1109/ICEES.2018.8443277.

[177] S. Kumar Roy, S. Hussain, and M. A. Bazaz, 'Implementation of MPPT technique for solar PV system using ANN', 2017 Recent Dev. Control. Autom. Power Eng. RDCAPE 2017, vol. 3, pp. 338–342, 2018, doi: 10.1109/RDCAPE.2017.8358293.

[178] C. G. Villegas-mier, J. Rodriguez-resendiz, and J. M. Álvarez-alvarado, 'Micromachines-12-01260-V2.Pdf', pp. 1–19, 2021.

[179] Y. E. A. Idrissi, K. Assalaou, L. Elmahni, and E. Aitiaz, 'New improved MPPT based on artificial neural network and PI controller for photovoltaic applications', Int. J. Power Electron. Drive Syst., vol. 13, no. 3, pp. 1791–1801, 2022, doi: 10.11591/ijpeds.v13.i3.pp1791-1801.

[180] K. J. Reddy et al., 'A stochastic variance reduction gradient-based GSO-ANFIS optimized method for maximum power extraction of proton exchange membrane fuel cell', Energy Convers. Manag. X, vol. 21, no. December 2023, p. 100505, 2024, doi: 10.1016/j.ecmx.2023.100505.

[181] S. Padmanaban, N. Priyadarshi, M. S. Bhaskar, J. B. Holm-Nielsen, V. K. Ramachandaramurthy, and E. Hossain, 'A Hybrid ANFIS-ABC Based MPPT Controller for PV System with Anti-Islanding Grid Protection: Experimental Realization', IEEE Access, vol. 7, pp. 103377–103389, 2019, doi: 10.1109/ACCESS.2019.2931547.

[182] H. Tao, M. Ghahremani, F. W. Ahmed, W. Jing, M. S. Nazir, and K. Ohshima, 'A novel MPPT controller in PV systems with hybrid whale optimization-PS algorithm based ANFIS

under different conditions', Control Eng. Pract., vol. 112, no. August 2020, p. 104809, 2021, doi: 10.1016/j.conengprac.2021.104809.

[183] M. Lasheen and M. Abdel-Salam, 'Maximum power point tracking using Hill Climbing and ANFIS techniques for PV applications: A review and a novel hybrid approach', Energy Convers. Manag., vol. 171, no. March, pp. 1002–1019, 2018, doi: 10.1016/j.enconman.2018.06.003.

[184] C. G. Villegas-Mier, J. Rodriguez-Resendiz, J. M. Álvarez-Alvarado, H. Rodriguez-Resendiz, A. M. Herrera-Navarro, and O. Rodríguez-Abreo, 'Artificial neural networks in mppt algorithms for optimization of photovoltaic power systems: A review', Micromachines, vol. 12, no. 10, 2021, doi: 10.3390/mi12101260.

[185] K. Amara et al., 'Improved Performance of a PV Solar Panel with Adaptive Neuro Fuzzy Inference System ANFIS based MPPT', 7th Int. IEEE Conf. Renew. Energy Res. Appl. ICRERA 2018, vol. 5, pp. 1098–1101, 2018, doi: 10.1109/ICRERA.2018.8566818.

[186] Q. Liu, B. Yang, Z. Wang, X. Wang, D. Zhu, and X. Guan, 'A PV Fault Diagnosis Framework Based on Asynchronous Federated Learning', ASCC 2022 - 2022 13th Asian Control Conf. Proc., no. Ascc, pp. 494–499, 2022, doi: 10.23919/ASCC56756.2022.9828106.

[187] D. S. Pillai and N. Rajasekar, 'An MPPT-based sensorless line-line and line-ground fault detection technique for pv systems', IEEE Trans. Power Electron., vol. 34, no. 9, pp. 8646–8659, 2019, doi: 10.1109/TPEL.2018.2884292.

[188] S. Liu, L. Dong, X. Liao, X. Cao, X. Wang, and B. Wang, 'Application of the Variational Mode Decomposition-Based Time and Time-Frequency Domain Analysis on Series DC Arc Fault Detection of Photovoltaic Arrays', IEEE Access, vol. 7, pp. 126177–126190, 2019, doi: 10.1109/ACCESS.2019.2938979.

[189] M. A. M. Ramli, S. Twaha, K. Ishaque, and Y. A. Al-Turki, 'A review on maximum power point tracking for photovoltaic systems with and without shading conditions', Renew. Sustain. Energy Rev., vol. 67, pp. 144–159, 2017, doi: 10.1016/j.rser.2016.09.013.

[190] A. F. Mirza, M. Mansoor, Q. Ling, B. Yin, and M. Y. Javed, 'A Salp-Swarm Optimization based MPPT technique for harvesting maximum energy from PV systems under

partial shading conditions', Energy Convers. Manag., vol. 209, no. February, p. 112625, 2020, doi: 10.1016/j.enconman.2020.112625.

[191] N. Kumar, I. Hussain, B. Singh, and B. K. Panigrahi, 'Rapid MPPT for Uniformly and Partial Shaded PV System by Using JayaDE Algorithm in Highly Fluctuating Atmospheric Conditions', IEEE Trans. Ind. Informatics, vol. 13, no. 5, pp. 2406–2416, 2017, doi: 10.1109/TII.2017.2700327.

[192] Y. H. Liu, J. H. Chen, and J. W. Huang, 'A review of maximum power point tracking techniques for use in partially shaded conditions', Renew. Sustain. Energy Rev., vol. 41, pp. 436–453, 2015, doi: 10.1016/j.rser.2014.08.038.

[193] B. Laxman, A. Annamraju, and N. V. Srikanth, 'A grey wolf optimized fuzzy logic based MPPT for shaded solar photovoltaic systems in microgrids', Int. J. Hydrogen Energy, vol. 46, no. 18, pp. 10653–10665, 2021, doi: 10.1016/j.ijhydene.2020.12.158.

[194] S. Javed and K. Ishaque, 'A comprehensive analyses with new findings of different PSO variants for MPPT problem under partial shading', Ain Shams Eng. J., vol. 13, no. 5, p. 101680, 2022, doi: 10.1016/j.asej.2021.101680.

[195] D. M. Djanssou, A. Dadjé, A. Tom, and N. Djongyang, 'Improvement of the Dynamic Response of Robust Sliding Mode MPPT Controller-Based PSO Algorithm for PV Systems under Fast-Changing Atmospheric Conditions', Int. J. Photoenergy, vol. 2021, 2021, doi: 10.1155/2021/6671133.

[196] A. M. Eltamaly, M. S. Al-Saud, A. G. Abokhalil, and H. M. H. Farh, 'Simulation and experimental validation of fast adaptive particle swarm optimization strategy for photovoltaic global peak tracker under dynamic partial shading', Renew. Sustain. Energy Rev., vol. 124, no. January, p. 109719, 2020, doi: 10.1016/j.rser.2020.109719.

[197] A. M. Eltamaly, H. M. H. Farh, and A. G. Abokhalil, 'A novel PSO strategy for improving dynamic change partial shading photovoltaic maximum power point tracker', Energy Sources, Part A Recover. Util. Environ. Eff., 2020, doi: 10.1080/15567036.2020.1769774.

[198] A. M. Eltamaly, M. S. Al-Saud, A. G. Abokhalil, and H. M. H. Farh, 'Photovoltaic maximum power point tracking under dynamic partial shading changes by novel adaptive

particle swarm optimization strategy', Trans. Inst. Meas. Control, vol. 42, no. 1, pp. 104–115, 2020, doi: 10.1177/0142331219865627.

[199] X. Wang, B. Yang, Q. Liu, T. Jin, and C. Chen, 'Collaboratively Diagnosing IGBT Open-circuit Faults in Photovoltaic Inverters: A Decentralized Federated Learning-based Method', IECON Proc. (Industrial Electron. Conf., vol. 2021-Octob, 2021, doi: 10.1109/IECON48115.2021.9589794.

[200] A. Adouni, K. Elmellah, D. Chariag, and L. Sbita, 'DC-DC converter fault diagnostic in PV system', Int. Conf. Green Energy Convers. Syst. GECS 2017, 2017, doi: 10.1109/GECS.2017.8066136.

[201] D. S. Pillai and N. Rajasekar, 'A comprehensive review on protection challenges and fault diagnosis in PV systems', Renew. Sustain. Energy Rev., vol. 91, no. July 2017, pp. 18–40, 2018, doi: 10.1016/j.rser.2018.03.082.

[202] P. K. Ray, A. Mohanty, B. K. Panigrahi, and P. K. Rout, 'Modified wavelet transform based fault analysis in a solar photovoltaic system', Optik (Stuttg)., vol. 168, pp. 754–763, 2018, doi: 10.1016/j.ijleo.2018.03.131.

[203] C. Souaidia, T. Thelaidjia, and S. Chenikher, 'Independent vector analysis based on binary grey wolf feature selection and extreme learning machine for bearing fault diagnosis', J. Supercomput., vol. 79, no. 6, pp. 7014–7036, 2023, doi: 10.1007/s11227-022-04931-4.

[204] Syafaruddin, E. Karatepe, and T. Hiyama, 'Controlling of artificial neural network for fault diagnosis of photovoltaic array', 2011 16th Int. Conf. Intell. Syst. Appl. to Power Syst. ISAP 2011, pp. 1–6, 2011, doi: 10.1109/ISAP.2011.6082219.

[205] M. Marweni, R. Fezai, M. Hajji, and M. Mansouri, 'Deep Learning for Fault Detection and Diagnosis: Application to Photovoltaic System', 2022 19th IEEE Int. Multi-Conference Syst. Signals Devices, SSD 2022, pp. 829–834, 2022, doi: 10.1109/SSD54932.2022.9955680.

[206] P. Xi et al., 'Online Fault Diagnosis for Photovoltaic Arrays Based on Fisher Discrimination Dictionary Learning for Sparse Representation', IEEE Access, vol. 9, pp. 30180–30192, 2021, doi: 10.1109/ACCESS.2021.3059431.

[207] P. Niu, S. Niu, N. liu, and L. Chang, 'The defect of the Grey Wolf optimization algorithm and its verification method', Knowledge-Based Syst., vol. 171, pp. 37–43, 2019, doi: 10.1016/j.knosys.2019.01.018.

[208] J. Liu, X. Wei, and H. Huang, 'An Improved Grey Wolf Optimization Algorithm and its Application in Path Planning', IEEE Access, vol. 9, pp. 121944–121956, 2021, doi: 10.1109/ACCESS.2021.3108973.

[209] A. M. Eltamaly and H. M. H. Farh, 'Dynamic global maximum power point tracking of the PV systems under variant partial shading using hybrid GWO-FLC', Sol. Energy, vol. 177, no. October 2018, pp. 306–316, 2019, doi: 10.1016/j.solener.2018.11.028.

[210] M. V. Da Rocha, L. P. Sampaio, and S. A. O. Da Silva, 'Comparative analysis of ABC, Bat, GWO and PSO algorithms for MPPT in PV systems', 8th Int. Conf. Renew. Energy Res. Appl. ICRERA 2019, pp. 347–352, 2019, doi: 10.1109/ICRERA47325.2019.8996520.

[211] F. Marini and B. Walczak, 'Particle swarm optimization (PSO). A tutorial', Chemom. Intell. Lab. Syst., vol. 149, pp. 153–165, 2015, doi: 10.1016/j.chemolab.2015.08.020.

[212] S. K. Gopalakrishnan, S. Kinattingal, and S. P. Simon, 'MPPT in PV Systems Using PSO Appended with Centripetal Instinct Attribute', Electr. Power Components Syst., vol. 48, no. 9–10, pp. 881–891, 2020, doi: 10.1080/15325008.2020.1825552.

[213] F. M. de Oliveira, S. A. Oliveira da Silva, F. R. Durand, L. P. Sampaio, V. D. Bacon, and L. B. G. Campanhol, 'Grid-tied photovoltaic system based on PSO MPPT technique with active power line conditioning', IET Power Electron., vol. 9, no. 6, pp. 1180–1191, 2016, doi: 10.1049/iet-pel.2015.0655.

[214] O. Ben Belghith, L. Sbita, and F. Bettaher, 'MPPT Design Using PSO Technique for Photovoltaic System Control Comparing to Fuzzy Logic and P&O Controllers', Energy Power Eng., vol. 08, no. 11, pp. 349–366, 2016, doi: 10.4236/epe.2016.811031.

[215] W. Hayder, E. Ogliari, A. Dolara, A. Abid, M. Ben Hamed, and L. Sbita, 'Improved PSO: A comparative study in MPPT algorithm for PV system control under partial shading conditions', Energies, vol. 13, no. 8, 2020, doi: 10.3390/en13082035.

[216] T. Wei, D. Liu, and C. Zhang, 'An improved Particle Swarm Optimization (PSO)-Based MPPT strategy for PV system', MATEC Web Conf., vol. 139, 2017, doi: 10.1051/matecconf/201713900052.

[217] K. P. Panda, A. Anand, P. R. Bana, and G. Panda, 'Novel PWM Control with Modified PSO-MPPT Algorithm for Reduced Switch MLI Based Standalone PV System', Int. J. Emerg. Electr. Power Syst., vol. 19, no. 5, pp. 1–17, 2018, doi: 10.1515/ijeeps-2018-0023.

[218] M. Hu, T. Wu, and J. D. Weir, 'An Adaptive Particle Swarm Optimization with Multiple Adaptive Methods', no. c, 2011.

[219] B. Ayeb, Y. Soufi, D. Ounnas, A. Kouzou, and D. Guiza, 'Adaptive Particle Swarm Optimization of a Photovoltaic System under Partial Shading', EEA - Electroteh. Electron. Autom., vol. 72, no. 1, pp. 30–38, 2024, doi: 10.46904/eea.24.72.1.1108004.

[220] N. Pragallapati, T. Sen, and V. Agarwal, 'Adaptive Velocity PSO for Global Maximum Power Control of a PV Array under Nonuniform Irradiation Conditions', IEEE J. Photovoltaics, vol. 7, no. 2, pp. 624–639, 2017, doi: 10.1109/JPHOTOV.2016.2629844.

[221] M. Merchaoui, M. Hamouda, A. Sakly, and M. F. Mimouni, 'Fuzzy logic adaptive particle swarm optimisation based MPPT controller for photovoltaic systems', IET Renew. Power Gener., vol. 14, no. 15, pp. 2933–2945, 2020, doi: 10.1049/iet-rpg.2019.1207.

[222] Y. Duan, N. Chen, L. Chang, Y. Ni, S. V. N. S. Kumar, and P. Zhang, 'CAPSO: Chaos Adaptive Particle Swarm Optimization Algorithm', IEEE Access, vol. 10, pp. 29393–29405, 2022, doi: 10.1109/ACCESS.2022.3158666.

[223] X. Yuan, D. Yang, and H. Liu, 'MPPT of PV system under partial shading condition based on adaptive inertia weight particle swarm optimization algorithm', 2015 IEEE Int. Conf. Cyber Technol. Autom. Control Intell. Syst. IEEE-CYBER 2015, pp. 729–733, 2015, doi: 10.1109/CYBER.2015.7288032.